Dissertação de Mestrado

Inatel

Photonics-based Radio Frequency Amplification in Radio over Fiber Systems with CAP modulation

April 2015

Estrada, Natalia Cañas
E821p

Photonics-based radio frequency amplification in radio over fiber systems with CAP modulation. / Natalia Cañas Estrada. – Santa Rita do Sapucaí, 2015.

116p.

Orientador: Prof. Dr. Arismar Cerqueira Sodré.

Dissertação de Mestrado – Engenharia de Telecomunicações – Instituto Nacional de Telecomunicações – INATEL.

Inclui bibliografia.

1. Comunicações ópticas 2. Rádio sobre fibra 3. FWM – Four wave mixing 4. Óptica não linear 5. Engenharia de Telecomunicações. I. Sodré, Arismar Cerqueira. II. Instituto Nacional de Telecomunicações – INATEL. III. Título.

CDU 621.39

Photonics-based Radio Frequency Amplification in Radio over Fiber Systems with CAP modulation

NATALIA CAÑAS ESTRADA

Dissertação apresentada ao Instituto Nacional de Telecomunicações, como parte dos requisitos para obtenção do Título de Mestre em Telecomunicações.

ORIENTADOR: Prof. Dr. Arismar Cerqueira Sodré Junior

Santa Rita do Sapucaí
2015

FOLHA DE APROVAÇÃO

Dissertação defendida e aprovada em _____ /_____ /_____ , pela comissão julgadora:

_____

Prof. Dr. Arismar Cerqueira Sodré Junior

INATEL

_____

Prof. Dr. Carmelo José Albanez Bastos Filho

Universidade de Pernambuco

_____

Prof. Dr. José Antônio Justino Ribeiro

INATEL

_____

Coordenador do Curso de Mestrado

Prof. Dr. José Marcos Camara Brito

“Live as if you were to die tomorrow. Learn as if you were to live forever.”

– Mahatma Gandhi

Acknowledgements

I can finally say I finished this master thanks to the help and support of many people. First, I want to thank my family for supporting me on every decision I make, for the courage and company you have given me through the years, and for the love I receive from you no matter how far we are from each other. To Neil, who gave me the idea of enrolling into this master degree, and who supported me with his wise words, love and patience during these two last years. All of you are very important to me.

I want to thank Professor Arismar Cerqueira Sodré Jr. for giving me the opportunity to learn about telecommunications, work with his group and to meet the best colleagues one can ask for. All meetings were important, and I really appreciate the time, patience and disposition you had during this master degree. This dissertation is the result of hard work you encouraged and the advices you gave me.

To the WOCA colleagues, who were always available to teach me Portuguese and telecommunications, who always had a smile and a great attitude no matter how much work they had. It was great to meet you, I really appreciate your friendship and I will have great memories forever. Specially, I want to thank Dionísio and Ramon, who were my colleagues at CPqD, for all the knowledge you shared with me; I learnt a lot from you and wish you the best on your lives. Moreover, I would like to thank André Luiz, who helped me, weekends included, to make the final simulations.

Thanks to Gisele, Aline, and all the people that works at the SRA and the finance office at Inatel, your help and assistance made everything easier. I specially want to thank Andreia, who not only helped me with my scholarship documents, but also offered me her friendship and a place to live in Santa Rita. Moreover, I want to thank Julio Cesar Rodrigues Fernandes de Oliveira and his team at CPqD because of the opportunity they gave us to use their lab for experimental work; conducting experiments in the Lasor laboratory was an enriching experience, I am grateful for the knowledge and training I acquired at the CPqD facilities.

I want to thank Inatel for giving me the opportunity to do this course. I enjoyed learning from great teachers such as Prof. Arismar Cequeira, Prof. Justino, and Prof. Carlinhos; Thanks to the knowledge they shared with me, I could finish this master degree. And finally, thanks to Fundação Instituto Nacional de Telecomunicações (Finatel) for the financial support.

Table of Content

List of Figures

List of Tables

Acronyms

1G	*First Generation*
2G	*Second Generation*
3G	*Third Generation*
AM	*Amplitude modulator*
ASE	*Amplified Spontaneous Emission*
B2B	*Back-to-Back*
BB	*Baseband*
BER	*Bit Error Rate*
BS	*Base Station*
CAP	*Carrierless Amplitude Phase*
CW	*Continuous Wave*
CNR	*Carrier to Noise Ratio*
CO	*Central Office*
CS	*Central Station*
DAC	*Digital-Analog Converter*
dB	*Decibel*
DDF	*Dispersion Distributed Fibers*
DMT	*Discrete Multitone*
EDFA	*Erbium Doped Fiber Amplifier*

ESA	*Electrical Spectrum Analyzer*
FBG	*Fiber Bragg Grating*
FDMA	*Frequency Division Multiple Access*
FEC	*Forward Error Correction*
FPC	*Fiber Polarization Controller*
FWM	*Four-Wave Mixing*
GSM	*Global System for Mobile Communications*
GVD	*Group Velocity Dispersion*
HNLF	*Highly Non-Linear Fiber*
ICT	*Information and Communication Technology*
IF	*Intermediate Frequency*
IM	*Intensity Modulator*
IR	*Infrared*
ISI	*Intersymbol Interference*
MFWM	*Multiple Four-Wave Mixing*
MZM	*Mach-Zehnder Modulator*
NRZ	*Non-return to Zero*
OFDM	*Orthogonal Frequency Division Multiplexing*
OIL	*Optical Injection Locking*
OIPL	*Optical Injection Phase-Locking*
OPLL	*Optical Phase-Locked Loop*
OSA	*Optical Spectrum Analyzer*
OSNR	*Optical Signal-to-Noise Ratio*
PC	*Polarization Controller*

PM	*Phase Modulator*
PMD	*Polarization Mode Dispersion*
QAM	*Quadrature Amplitude Modulation*
RAU	*Remote Antenna Unit*
RF	*Radio Frequency*
RoF	*Radio over Fiber*
SBS	*Stimulated Brillouin Scattering*
SMF	*Single-mode Fiber*
SNR	*Signal-to-Noise Radio*
SPM	*Self-Phase Modulation*
SRRC	*Square Root Rise Cosine*
SSB-SC	*Single-Side Band Suppressed Carrier*
TDMA	*Time Division Multiple Access*
TLS	*Tunable Laser Source*
UMTS	*Universal Mobile Telecommunications System*
UWB	*Ultrawideband*
VCSEL	*Vertical Cavity Surface Emitting Laser*
VHT	*Very High Troughput*
VSG	*Vectorial Signal Generator*
WDM	*Wavelength Division Multiplexing*
Wi-Fi	*Wireless-Fidelity*
Wi-Max	*Worldwide Interoperability for Microwave Access*
WLAN	*Wireless Local Area Network*
XPM	*Cross-Phase Modulation*

List of Publications

1. N. Cañas-Estrada, Neil Guerrero Gonzalez, Arismar Cerqueira S. Jr., "*Performance Analysis of a Novel Photonically Amplified 10Gbit/s Radio over Fiber System"*, in conference proceedings of IEEE LatinCom workshop, November 2014, pp. 1-4, Cartagena (Colombia).

2. Arismar Cerqueira S. Jr., N. Cañas-Estrada, D.F. Noque, R. M. Borges, S. A. S. Melo, Neil G. González, and J. C. R. F. Oliveira, "*Photonic-Assisted Microwave Amplification Using Multiple Four-Wave Mixing*", IET Optoelectronics, *submitted* in December 2014.

3. M.M. Bontempo, D. Mazzer, N. Cañas Estrada, Arismar Cerqueira S. Jr., "*Implementation of an ARM-based Wi-Fi Cognitive Network*", IEEE International Microwave and Optoelectronics Conference (IMOC), submitted in May 2015.

4. N. Cañas-Estrada, Arismar Cerqueira S. Jr., D.F. Noque, R. M. Borges, Neil G. González and J. C. R. F. Oliveira, "*Implementation of a Photonic-Assisted RF Amplifier"*, IEEE International Microwave and Optoelectronics Conference (IMOC), submitted in April 2015.

Resumo

Este trabalho tem por objetivo a implementação de um amplificador de radiofrequência (RF) baseado no efeito não-linear mistura de quatro ondas aplicado a um sistema de rádio sobre fibra (RoF) com modulação CAP (modulação de amplitude e fase sem portadora). Tal sistema viabiliza o transporte da informação utilizando um backhaul óptico, no qual a fibra óptica é utilizada como canal de comunicação e como meio ativo de ganho de RF. O ganho de RF é definido com a diferença entre a potencia elétrica fotodetectada utilizando o produto de FWM e aquela do sistema RoF convencional. Este ganho depende fortemente dos parâmetros elétricos e ópticos do sistema, tais como separação dos laseres, estado de polarização, frequência da portadora de RF e tensão de polarização do modulador óptico.

O trabalho baseou-se em simulações numéricas, utilizando OptiSystem ® da Optiwave Inc., e resultados experimentais obtidos em parceria com o laboratório Lasor do Centro de Pesquisa e Desenvolvimento em Telecomunicações (CPqD) de Campinas. Obteve-se experimentalmente amplificação de RF baseada em tecnologia fotônica na faixa de 4,0 a 19,0 GHz, relação sinal-ruído (SNR) de até 51 dB e ganhos de até 26 dB.

Palavras-chave: Comunicações Ópticas, Fibras Altamente Não-Lineares, Fotônica de Micro-ondas, Modulação em amplitude e fase, Mistura de Quatro-Ondas, Rádio sobre fibra e Amplificação de RF.

Abstract

The objective of this work is the implementation of a radio-frequency (RF) amplifier based on the four-wave mixing nonlinear effect applied to a radio over fiber (RoF) system with CAP (Carrierless Amplitude Phase modulation). Such system enables the transmission of information using an optical backhaul, wherein the optical fiber is used as the communication channel and as an active medium for RF gain. The RF gain is defined as the difference between the photodetected electrical power in the FWM product and that of the conventional RoF system. This gain strongly depends on the electrical and optical parameters of the system, such as separation of lasers, state of the light polarization, frequency of the RF carrier and the bias voltage of the optical modulator.

The work is based on numerical simulations using OptiSystem ®, by Optiwave Inc., and experimental results obtained in cooperation with the Lasor laboratory from the research and development center (CPqD) of Campinas-SP, Brazil. Experiments results demonstrate photonics-based RF amplification from 4.0 to 19.0 GHz, signal-to-noise ratio (SNR) up to 51 dB and electrical gains up to 26 dB.

Keywords: Optical Communications, Highly Non-Linear Fibers, Microwave Photonics, Carrierless Amplitude Phase modulation, Multiple Four-Wave Mixing, Radio over Fiber and RF amplification.

Chapter 1

1. Introduction

Over the past years, the world has seen a remarkable growth in the usage and acceptance of information and communication technology (ICT); moreover, by the end of 2014 approximately three billion people were using the internet. Due to the uptake in mobile and fixed-broadband subscribers, appropriate infrastructure for broadband internet access is a priority for telecommunication service providers and governments over the world [1]. Fig. 1 shows a chart of the mobile-broadband growth and penetration percentage in the world from 2005 to year 2014, and the percentage of subscribers in specific regions of the world in 2014. It is worth mentioning that in Europe, the fixed-broadband penetration is much higher than in other regions (27.7%), it is almost three times as high as the world average (9.8%).

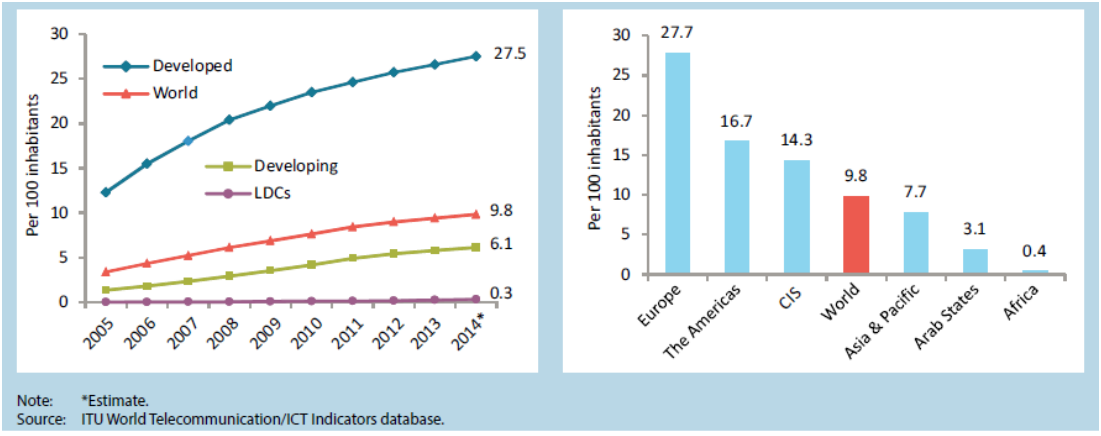

Fig. 1 - Wired-broadband subscriptions by country development level between 2005 and 2014 (left), and estimated subscribers by region in 2014 (right). LDC: Least developed countries. Figure taken from [1].

During the past years, broadband subscriptions around the world have increased along with the growth of backbone infrastructure, capacity and internet bandwidth. In 2001 it was estimated that the average international internet bandwidth was of approximately 1600 Gbit/s, in 2010 it increased to around 60400 Gbit/s, and more than 140000 Gbit/s in year 2014 [1], as shown in Fig. 2. The growth in international bandwidth reflects a development in infrastructure to provide internet services in all the regions of the world.

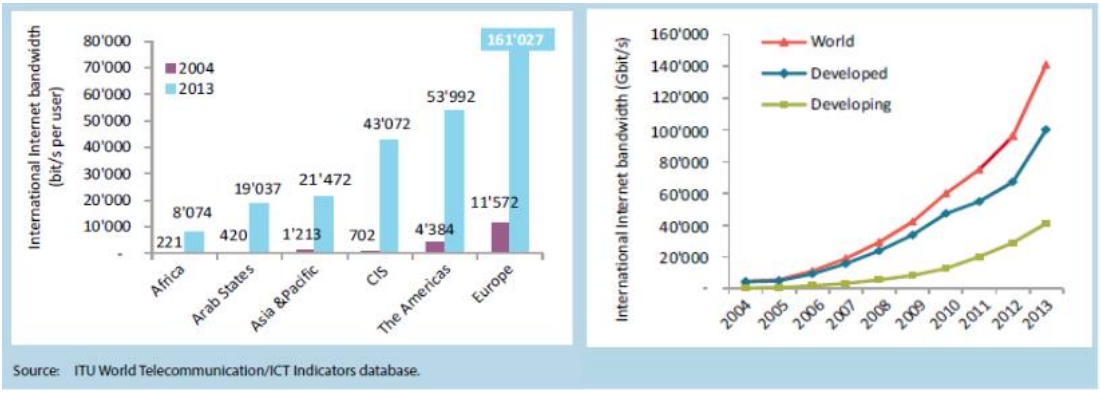

Fig. 2 - International internet bandwidth per internet user by region. Figure taken from [1].

Fixed broadband is a critical characteristic for high speed, capacity and consistent internet services. Households and offices are its main subscribers. By the end of 2014, it was estimated that approximately a 44% of the world's households had internet access. In contrast, 78% of the households in developed countries had access to the internet by the end of the same year [1]. Moreover, data capacity has increased due to Dense Wavelength Division Multiplexing (DWDM), which enables the simultaneous transmission of multiple wavelengths for several different services and traffic types over the same network [2]. One of the DWDM advantages is that data capacity has increased to around 10 Tb/s per fiber. The 10 Tb/s could be allocated to one million subscribers, each one of them with 10 Mb/s; however, the problem is to provide the mentioned data rate to each one of the subscribers. Fiber networks are connected to telephone companies, which use switching stations to provide users with internet access. Users usually do not have direct access to the fiber network because service providers use twisted-pair wiring with data rates from 128 kb/s to 2.3 Mb/s, or cable modems to provide shared access at a rate of about 30

Mb/s. The high cost of laying optical fiber to each household is the main reason to look for alternatives other than optical fibers to connect users to the network; this is referred as the last-mile problem [3].

Optical wireless communications is a complementary technology for Radio Frequency (RF) and optical fiber that combines the advantages of both transmission media in a unique one: flexibility and mobility from wireless systems with wide bandwidth and absence of electromagnetic interference from optical fibers. This technology is an attractive solution for the last-mile problem in dense populated areas. The service can be provided by demand without any special infrastructure: Optical receivers can be installed in windows or rooftops of buildings, where they can communicate with a local communication node that sends independent optical signals to each subscriber; then, only paying subscribers receive the optical wireless service [3]. Moreover, optical wireless communications has the potential of transmitting data at a high rate for short distance indoor and outdoor applications in short haul. It is an attractive wireless broadband technology for providing internet access in different places including public facilities; in some countries, libraries and post offices offer free internet access using optical wireless. For indoor applications, Infrared (IR) and visible light communication systems are preferred; on the other hand, outdoor applications mainly use semiconductor lasers with broad bandwidths and high power [4]. However, optical wireless communications may present performance impairments in indoor systems due to dispersion, and in outdoor systems due to atmospheric conditions. Thus, suitable mitigation techniques are required to maintain the link operation [5].

Mobile communications have shown a constant evolution since first generation, a change of generation occurs approximately every ten years. In the early 1980's, at the beginning of first generation (1G), systems were intended to provide voice services and low rate circuit switched data services, the mobile devices were large in size, and the employed technologies were analog frequency modulation along with Frequency Division Multiple Access (FDMA). The critical problems of 1G included capacity bottlenecks and incompatible standards [6] [7]. Mobile technology had a second boost in the 1990's with 2G digital technology standards, including Global System for Mobile Communications (GSM), IS-136 (Time-division

multiple access, TDMA), IS-95 (code division multiple access, CDMA), and Personal Digital Cellular (PDC), which were designed to improve voice quality, higher capacity and a continental system with full international roaming and handoff [8]. Digital technology not only enhanced voice quality and services, but also significantly reduced the cost of handsets and infrastructure systems [9]. Furthermore, 3G systems improved spectral efficiency, costs, and data capacity; Third generation cellular systems rates can reach up to 2Mb/s in indoor, and 144kb/s in vehicular environments [10].

The mobile generation evolution has influenced in the upgrade of mobile networks worldwide, in order to support new technologies. As seen in Fig. 3, in 2010 the number of 3G subscriptions surpassed those of 2G in developed countries, even though the growth of 3G seems to be slowing down in the following years due to the uptake of 4G technology. In developing countries, a large majority of subscriptions is 2G, but the number of 3G users is increasing rapidly. The difference between technology acceptance between developed and developing countries is due the fact that fixed and mobile broadband technologies entered earlier in the market of developed countries than in other countries.

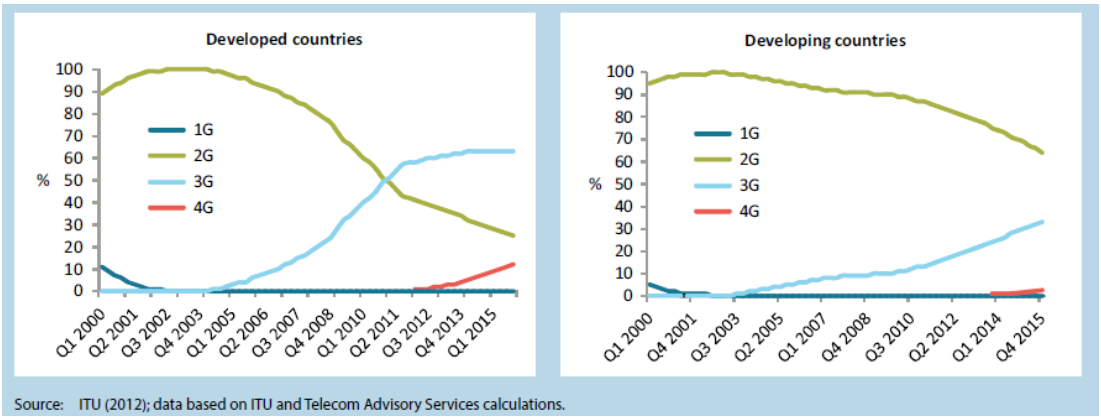

Fig. 3 - Mobile subscriptions by technologies between years 2000 and 2015 in developed countries (left) and developing countries (right). Figure taken from [1].

Current cellular networks provide services that were not available before, such as e-mail, internet access and video exchange; next generation devices and

applications may demand faster internet speeds and an increase in data capacity. In addition, it is estimated the global IP traffic will reach 1.6 zettabytes per year in 2018 [1]. Higher data capacity can be achieved through advanced transmission techniques with efficient speech coding, codes for error correction, and band efficient modulation [8]. Besides high-speed, symmetric, and guaranteed bandwidth demands for future internet connection technologies, next generation access networks are driving the needs for the convergence of wired and wireless services.

Broadband communications is a solution that offers high-speed internet access, mobile voice and data services. Fig. 4 shows the most widely used communication technologies for broadband communications. Optical communication systems can support Tb/s capacities over many thousand kilometers; consequently, it is an ideal technology for high-capacity landline networking. Growing capacities and bandwidth demand of data services can be satisfied by a wavelength division multiplexing (WDM) systems. Furthermore, a system cost reduction is achieved by sharing optical components among all WDM channels, such as optical fiber, used for transport and dispersion management, and optical amplifiers, placed along the transmission path for WDM channel re-amplification [11].

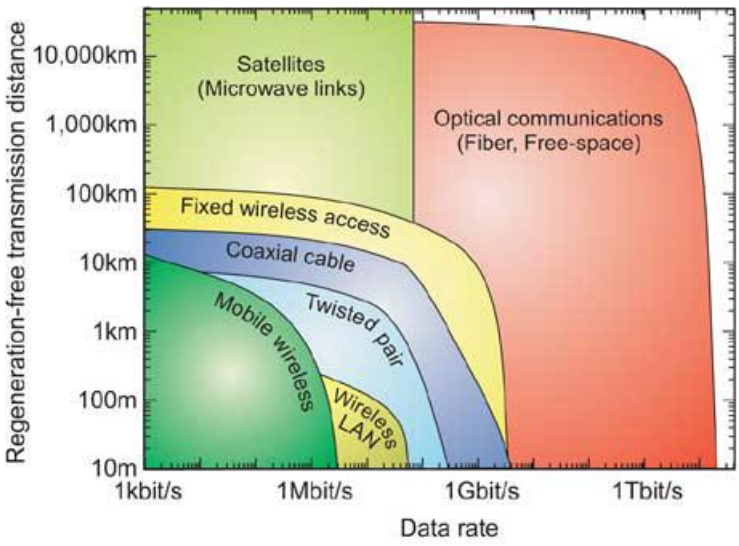

Fig. 4 - Broadband communication technologies [11].

The need to exploit optical bandwidth more efficiently, while employing advanced modulation formats can satisfy reducing cost per bit. Multilevel formats

enable the reduction of symbol rate in the system, nevertheless as a counterpart, there is an increase in the transmitter and receiver complexity. Multilevel signaling consists on encoding $log_2 M$ data bits on M symbols that are transmitted at a reduced symbol rate of $R/log_2 M$, where R is the bit rate; this technique offers high spectral efficiencies at the cost of a reduced tolerance to noise [12] [13]. According to Shannon's theory if the constellation size increases, so does the spectral efficiency, and in contrast the Euclidean space between two constellations points decreases, thereby requiring a higher signal-to-noise ratio (SNR) [14].

Multilevel formats reduce the channel optical bandwidth consumption and enables WDM transmission with narrow bandwidths. In addition, by increasing the symbol rate per channel and/or the size of symbols constellation, higher optical signal power that can be launched into the fiber without generating excessive nonlinear distortions for the same bit rate [15]. Several multilevel modulation formats have been studied for multi-gigabit transmission, including multilevel intensity modulation [16][17], multilevel phase modulation [18][19], and also hybrid multilevel intensity/phase modulation [20][21]. However, multilevel optical phase and amplitude have complex transmitters and receivers because optical phase is lost upon detection; only the envelope of the signal is received, thereby requiring coherent detection [22]. Thus, from this point of view it is attractive to consider different modulation methods.

Other techniques that have been used for advanced modulation in short-range communications are discrete multitone (DMT) [23] [24], Quadrature amplitude phase modulation [25][26] and carrierless amplitude phase modulation (CAP) [27][28][29][30]. CAP is technique that outstands between the others due to its high data rate, spectral efficiency and flexibility; it is a multidimensional and multilevel modulation scheme that was proposed in the 70's by Bell Labs [31]. CAP has been included in few communication standards including 155Mbps ATM-LAN transmission [32], and high-bitrate digital subscriber line (HSDL) [33]. If CAP is compared to other modulation schemes, such as Quadrature Amplitude Modulation (QAM) and Orthogonal Frequency Division Multiplexing (OFDM), no electrical or optical complex-to-real-value conversion is necessary; neither requires discrete

Fourier transform used in OFDM demodulation. For high-speed transmission, CAP has been demonstrated to have less complex transmitter and receiver design, and a better performance than DMT [34]. CAP is similar to QAM, but employs a different way to generate two orthogonal components of the signal; in QAM two sinusoidal waves are generated, but CAP employs two digital filters with orthogonal impulse responses.

This work presents contributions in the research areas of microwave photonics, optical-wireless communications and CAPS modulation, which was chosen as the modulation format due to its high capacity. We present numerical and experimental results on photonics-based RF amplification in radio over fiber systems using CAP modulation. The RF amplification is based on the non-linear effect of Multiple Four-wave Mixing (MFWM). We use HNLF to increase the FWM efficiency and generate new wavelengths for optical transmission. The optical spectrum at the output of the fiber consists of optical carriers and sidebands equally spaced between them, and generated from various combinations of interacting signals. The high RF powers of the generated idler frequencies suggest that these wavelengths are more suitable for transmission than the optical carriers. In other words, we propose a novel CAP modulated radio over fiber scheme with a HNLF to produce photonic amplification using FWM.

To study the feasibility of the proposed scheme, several numerical and experimental analyses were carried out starting with the multiple four-wave mixing techniques on a radio over fiber scheme using highly nonlinear fiber. Then, MATLAB was used as a tool for CAP modulation algorithm design and simulation of the transmitter and receptor block diagrams. Finally, the RoF scheme is simulated using OptiSystem ® in order to study the feasibility of using CAP as the modulation format, and therefore achieving a photonic assisted amplification of a CAP modulated signal on a radio over fiber scheme. This document presents contributions in the following areas of microwave photonics: i) a novel optical signal generation scheme of amplified microwave carriers based on controlled generation of optical nonlinear effects, ii) a high capacity radio over fiber system for intermediate reach applications, iii) an optical signal generation scheme based on CAP modulation and RoF architecture for high capacity transmission.

The dissertation is structured as follows: chapter 2 is a short review of Microwave photonics, multiple four-wave mixing and carrierless amplitude phase modulation, which are the main techniques used in this research project. Secondly, chapter 3 treats on radio over fiber systems including CAP modulation; the first part includes a short introduction to radio over fiber systems; then, details of the implementation of the radio over fiber system with CAP modulation are presented, including numeric simulations. Chapter 4 provides information regarding radio frequency amplification using multiple four-wave mixing, along with simulations using OptiSystem ® software and results of the experiments carried out at the *Centro de Pesquisa e Desenvolvimento* (CPqD) in Campinas - SP. Chapter 5 is intended as a revision of the work, and a set of conclusions and future works is presented.

Chapter 2

2. Theoretical Background

In this chapter, three main topics are explained for providing a theoretical background on the main research area of this Dissertation. First, we describe the generation of microwaves and millimeter waves using different optical generation methods. Then, the nonlinear phenomenon of four-wave mixing is defined; this phenomenon allows to obtain the photonic amplification we propose in our experimental setup. Finally, the modulation format used in our research, Carrierless Amplitude Phase modulation, is explained step by step including simulations and results obtained with MATLAB for CAP-16, CAP-32, CAP-64 and CAP-128.

2.1. Microwave Photonics

Microwave photonics has been proposed as an area concerning the interaction between microwave and optical signals [59]. Its applications of microwave photonics in telecommunication engineering include broadband communications, design of broadband and more sensitive radar systems, satellite communications, high capacity wireless signal transmission, optical signal processing [60] and remote sensing [61]. At first, optical signal generation of microwave carriers has been widely reported due to physical advantages of optical devices such as lower optical power attenuation compared to conventional electrical components for RF applications and broader bandwidth compared to RF sources, modulators and amplifiers [62].

2.1.1. Optical signal generation of microwave signals

Many applications require low-phase noise and frequency tunable sources of microwave and millimeter-wave signals, as well as distribution of generated signals to remote areas. Optical fibers represent a potential solution for microwave signal distribution due to its broad bandwidth and low loss characteristics; hence, the generation of optical microwave and millimeter-wave signals represent an advantage in signal distribution via optical fiber from a central office to remote areas [59].

The first method to generate microwave and millimeter-wave signals in the optical domain are called optical heterodyning, depicted in Fig. 5 [62]. This method consists of two optical waves of different wavelengths that beat into a photodetector (PD). The optical waves are given by

$$E_1 = E_{01}\cos(\omega_1 t + \phi_1) \tag{1}$$

$$E_2 = E_{02}\cos(\omega_2 t + \phi_2) \tag{2}$$

where E_{01} and E_{02} represent the amplitude, ω_1 and ω_2 are the angular frequency, and ϕ_1 and ϕ_2 are phase terms of the optical signals. The resulting electrical field (E_0) is the sum of the wavelength's input fields $E_0 = E_1 + E_2$. The intensity at the output (I_{RF}) of the light beam at the output of the photodetector is proportional to the square of E_0. The square of the resulting electrical field is expressed as follows

$$|E_0|^2 = |E_1 + E_2|^2 = |E_1|^2 + |E_2|^2 + E_1{E_2}^* + {E_1}^* E_2 \tag{3}$$

$$|E_0|^2 = |E_1|^2 + |E_2|^2 + 2|E_1||E_2|\cos\big((\omega_2 - \omega_1)t - (\phi_2 - \phi_1)\big) \tag{4}$$

The current at the output of the photodetector is given by

$$I_{RF} = I_1 + I_2 + 2(I_1 I_2)^{1/2}\cos\big((\omega_2 - \omega_1)t - (\phi_2 - \phi_1)\big) \tag{5}$$

$$I_{RF} = A\cos[(\omega_1 - \omega_2) + (\phi_1 - \phi_2)] \tag{6}$$

where the terms I_1 and I_2 represent currents produced at the photodiode by the optical waves. The term $2(I_1 I_2)^{1/2} \cos\big((\omega_2 - \omega_1)t - (\phi_2 - \phi_1)\big)$ is a cosine varying intensity at the beat frequency given by the frequency difference of the two light beams [100]. The generated RF frequency is equal to the difference of the optical waves` frequencies. This technique allows electrical signal generation with frequencies of up to the THz band, and the only limitation depends on the bandwidth of the photodetector.

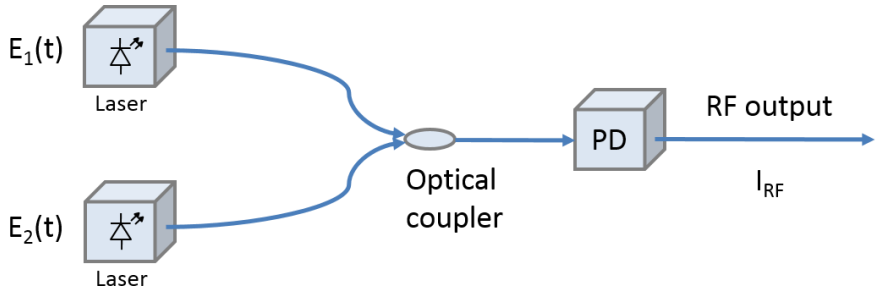

Fig. 5 – Block diagram for the optical heterodyning technique. PD: Photodetector.

However, two different laser sources generate the optical waves, E_1 and E_2; since it is not possible to guarantee phase correlation between them, it is probable to have high phase noise. To avoid this problem, different techniques have been proposed. The first one is optical injection locking (OIL) [62][63]. This technique consists of a master laser directly modulated by a RF signal reference and two slave lasers (see Fig. 6). At the output of the master laser, frequency modulation generates optical sidebands of different orders. Then, this signal is injected into the slave lasers, whose free-running wavelengths are close to two sidebands. If the free-running wavelengths are close to the 2nd upper and lower sidebands, then the wavelengths of the two slave lasers are locked to those sidebands and the optical injection locking is achieved. The two optical wavelengths that beat into the photodetector are then separted four times the frequency (fm) of the RF reference signal that feeds the master laser, thus generating an electrical signal with a frequency equal to $4fm$ [63]. The phases of the locked sidebands are correlated, hence, the resulting electrical signal at the photodetector will have a low-phase noise.

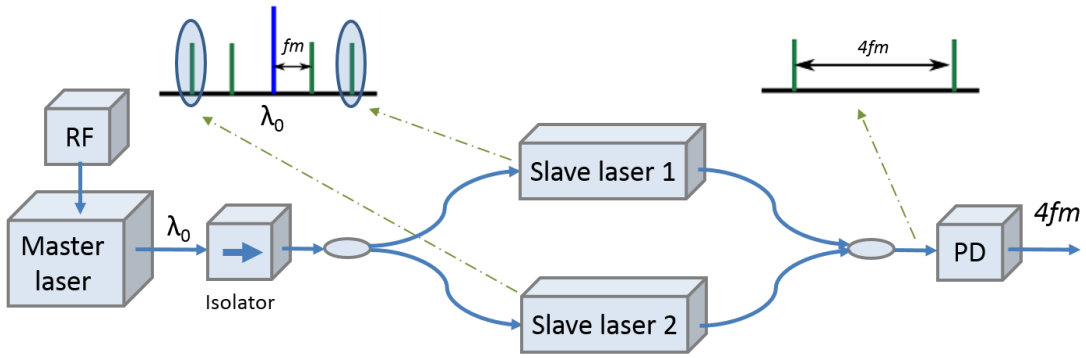

Fig. 6 - Optical injection locking of two slave lasers. Slave lasers are wavelength-locked by the +2nd and -2nd order sidebands.

Another method is optical phase locked loop (OPLL), which is illustrated on Fig. 7 [62]. This method consists of two narrow linewidth lasers that are coupled and photodetected. The phase of photodetected electrical signal is compared with a RF reference signal from a microwave generator. An electrical phase detector, represented by the dotted square, has an output voltage proportional to the phase difference between the photodetected signal and the RF reference. This error voltage is fed to one of the laser sources to control its phase by changing the laser's cavity length or the injection current. The loop makes possible for the phase fluctuation between the lasers to be reduced, and consequently, the photodetected signal are locked to the RF reference. This technique has been widely implemented in different types of laser source [64][65] and microwave frequencies [66].

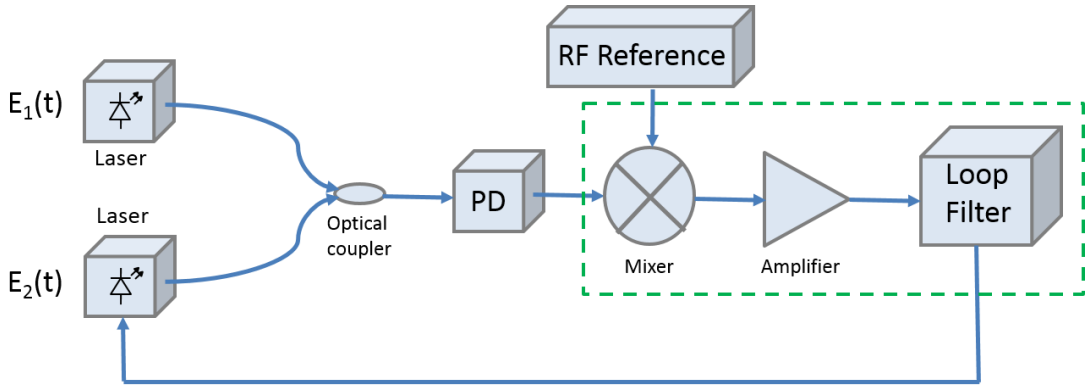

Fig. 7 - Optical Phase Locked Loop. PD: Photodetector.

Optical injection phase locking (OIPL) is another photonics technique developed for further improvement of the signal quality [62][67]. OIPL combines OIL and OPLL in a new optical locking system; the diagram of this technique is shown in Fig. 8. In OIPL the light from a master laser is divided into two channels, one of them coupled into the modulator before being injected into the slave laser. The slave laser is locked to one of the sidebands of the modulated signal (OIL). The other channel is combined with the slave laser output, and then the signals are photodetected. The electrical signal at the output of the photodetector is mixed with a microwave reference signal, and the mixer output passes through a low pass filter to phase-lock the wavelength of the master laser. Experimental results show that using this technique; a lower phase noise is obtained in comparison with OIL or OPLL.

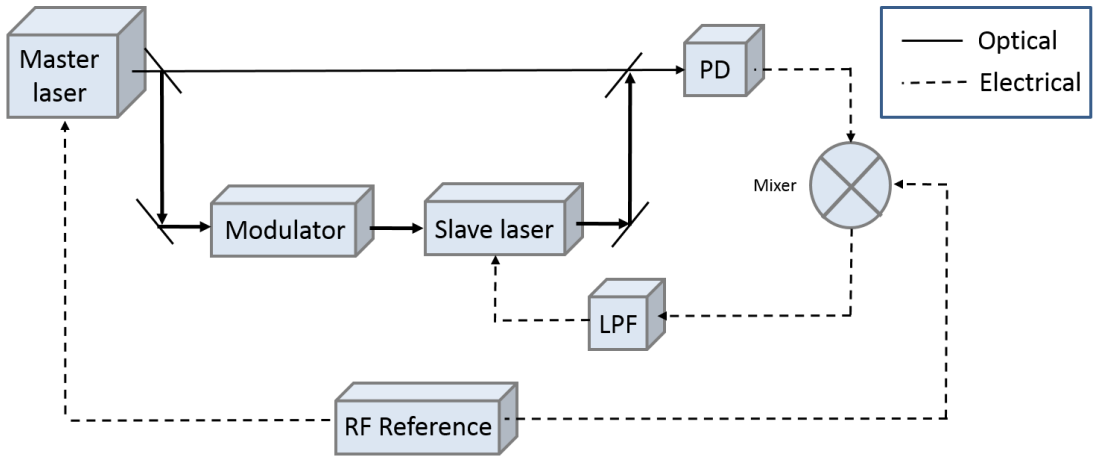

Fig. 8 - Diagram of optical injection phase locking.

Moreover, high quality microwaves are generated using external modulation. In 1992, microwave generation using external modulation was proposed for the first time, where a Mach-Zehnder modulator was biased to suppress the even order sidebands. As a result, the signal generated had twice the frequency of the RF driving the MZM [67]. MZM can also be biased to suppress even order sidebands in addition to a notch filter to filter out the optical carrier [96]. In this way, a signal with four times the frequency of the RF driving the MZM can be obtained. This technique has

been used in different approaches to generate 60 GHz mm-wave signals using 15 GHz drive signals applied to the MZM [68][69].

Frequency tunable microwave and millimeter-wave signals are highly desirable for different applications. Intensity and phase modulation are two approaches that allow generating frequency tunable microwave signals using an optical filter. The intensity modulator based approach shown in Fig. 9a, shows a MZM biased at the maximum transmission point of the transfer function to suppress odd-order sidebands. The notch filter, which can be a fiber Bragg grating (FBG), filters out the optical carrier. As a result, the photodetected electrical signal has four times the frequency of the RF drive signal [70]. In the Phase modulator based approach, the MZM is replaced with an optical phase modulator, which does not require a dc Bias and consequently eliminates the bias drifting problem. Fig. 9b shows the diagram the mentioned approach that consists of an optical carrier generated with a tunable laser source (TLS) that is sent to the optical phase modulator through a polarization controller. The modulated signal and its sidebands pass through a FBG that filters out the optical carrier. Then, the remaining sidebands are amplified using an Erbium Doped Fiber Amplifier (EDFA) and launched to a single mode fiber. SMF chromatic dispersion affects the phase of the sidebands, then the system requires dispersion compensation techniques to eliminate power fluctuation of the generated electrical signals and to maintain the odd-order sidebands suppression [71].

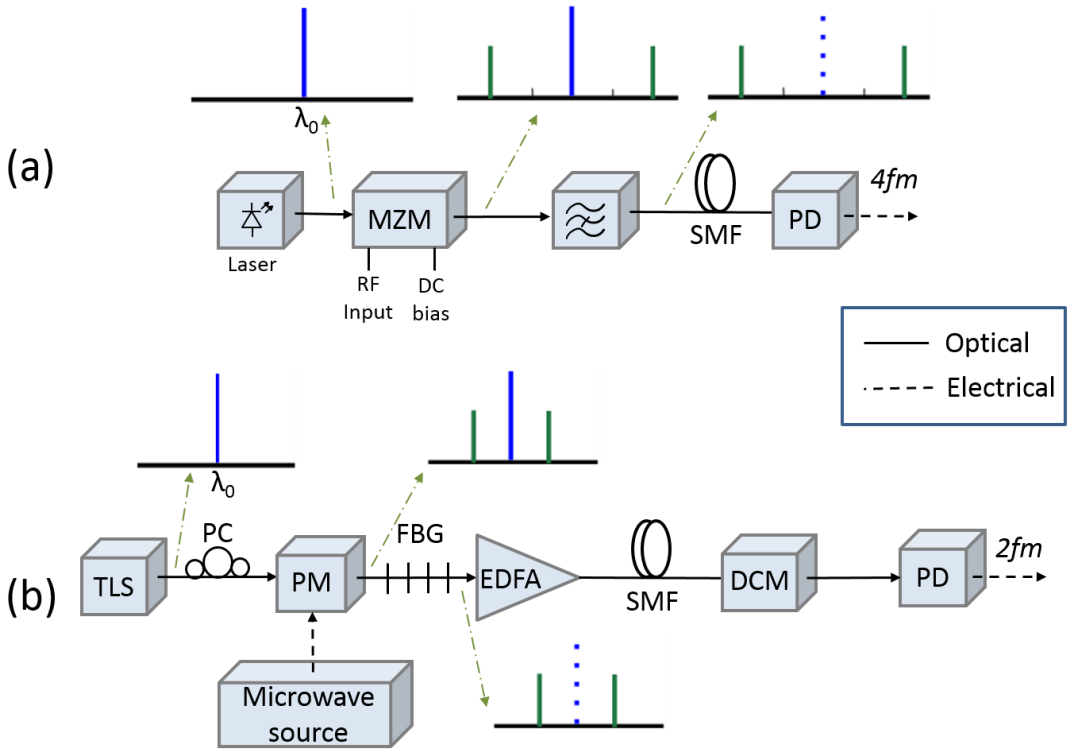

Fig. 9 - External modulation approaches using: (a) *an intensity modulator;* (b) *a phase modulator.*

2.2. Radio over Fiber

A Radio over Fiber (RoF) system is based on the transmission of RF signals using an optical fiber link. The use of RoF systems in telecommunications is possible due to photonic technologies that convert electrical signals into optical though modulation. The conversion from the electrical to the optical domain and vice-versa is ensured, with the purpose of transporting the mentioned RF signal through an optical fiber. RoF provides untethered access to wireless broadband communications and offers a potential solution to the capacity and mobility needs; furthermore, this technology decreases costs in access networks [35]. Moreover, RoF architecture for wireless signal distribution may vary according to the service application; many RoF architectures for both optical intensity and optical phase modulated have been lately reported in the literature [36] [37] [38] [39]. Infrastructure sharing at a centralized location, wide bandwidth operation, and lower data signal attenuation and robustness

to electromagnetic interference can be listed as the main advantages offered by the RoF technology [78].

RoF is a promising candidate in wireless access networks since it combines microwave and optical networks for different applications in a cost efficient way. However, due to its optical nature, nonlinear effects can affect the performance of a RoF system. For instance, the optical power over the fiber could be high enough to excite nonlinear effects such as SBS and four-wave mixing (FWM). The first nonlinear effect affects signals with narrow optical spectrum and limits the power that can be transmitted on a single-mode fiber (SMF) [35], and the second one, four-wave mixing, generates new wavelengths at different frequencies when two or more ligthwaves are transmitted simultaneously. Furthermore, if a Mach-Zehnder modulator (MZM) is used for modulation in the transmission chain of orthogonal frequency division multiplexed subcarriers, the modulator nonlinearity can affect the RoF link resulting in distorted signals [40] and chromatic dispersion due to double-sideband transmission [41].

The versatility of this technology makes RoF to be considered for many communication standards because signals from different technologies can share the same transmission medium [79]. This technology entails the use of optical fiber links to distribute RF signals from a central location to Remote Antenna Units (RAUs). The signal processing of narrowband and wireless Local Area Network (WLAN) communication systems, including coding, multiplexing, RF regeneration, is made in the central station (CS) instead of the base station (BS) [80]. The data signals from the CS are sent through an optical band via a RoF network to the BS. BS may have a simple architecture, they consists mainly from optical-to-electrical (O/E) and electrical-to-optical (E/O) converters, an antenna and microwave circuitry (two amplifiers and a diplexer).

Fig. 10 shows a block diagram of a system that uses a RoF link for central office (CO) and RAU connection. The CO performs switching, routing and network operation administration maintenance, the optical fiber interconnects the BS' antennas responsible for wireless distribution, and the main function of the BS is to convert signals from optical to wireless and vice versa.

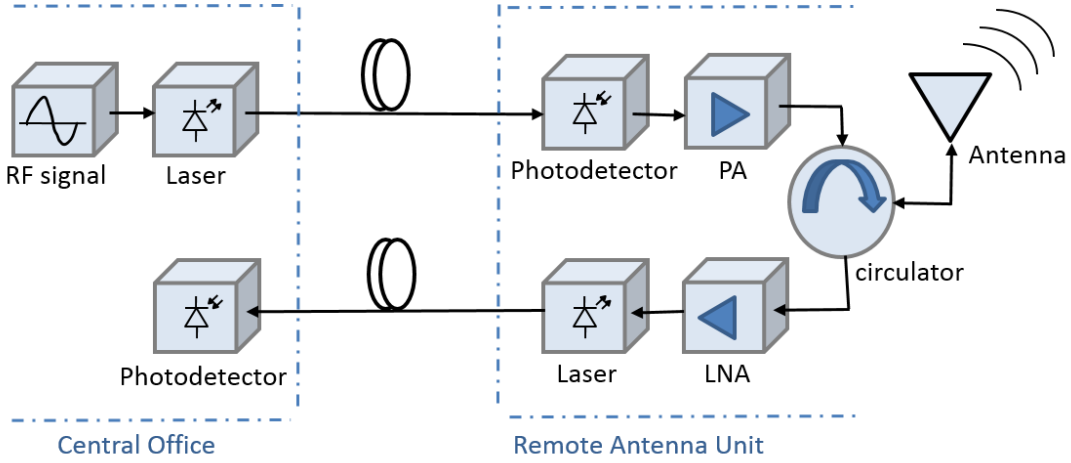

Fig. 10 - RoF system. PA: Power amplifier, LNA: Low Noise Amplifier.

The downlink (from base station to mobile) operation of the RoF system consists on a RF signal that modulates an optical carrier, the modulated signal is transmitted through the optical fiber to the RAU. At the RAU, the RF signal is recovered through photodetection and electrically amplified before antenna transmission. In the uplink (from mobile to base station) operation, a radio signal is received through the antenna and electrically amplified using a low noise amplifier (LNA). The RF amplification is necessary because the power of the user's transmission is low, and consequently, the margin of the SNR is low as well. Then, the amplified signal is used to modulate the optical carrier that will be transmitted through an optical fiber to the CO, where the signal is recovered using a photodetector. In this case, only one antenna is used for both transmission and reception, the RF circulator is used to direct one of the signals at its entrance to be transmitted to one of the other interfaces (antenna or LNA) with only one direction.

Mobile networks is an important application area of the RoF technology. The ever-rising number of mobile subscribers together with the increasing demand for broadband services have kept sustained pressure on mobile networks to offer increased capacity. One method to satisfy capacity demands is using micro-cells and pico-cells, which have a radius from 200 m to 1km, and 10 to 200 m respectively [80]. The goals of microcellular mobile communications systems include service

availability over high demand environments along with the provision of a combination of services including voice, data and video. To provide high quality services, it is necessary to have a high density of remote antennas (BS) per square kilometer, which will allow more subscribers per unit service area. Therefore, the cost of this system architecture might increase due to the higher number of radio base stations required. To make BS more compact and cost effective, RoF systems have been proposed to communicate BS and centralized control stations. Therefore, distributed antenna systems (DAS) using RoF are an efficient solution between central offices and RAUs. Fig. 11 shows a system architecture in which most of the complex pieces of equipment are kept at the CO, and the RAUs are simple; RoF links connect a CO with RAUs that are positioned to provide wide area coverage. It is a potential solution for communication coverage in shopping centers, buildings and tunnels [81].

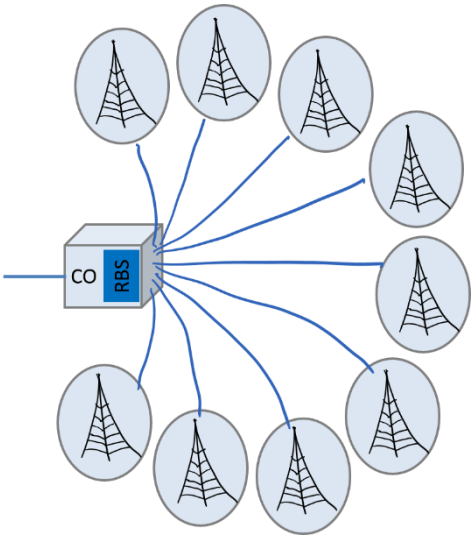

Fig. 11 - RoF system with centralized processing at the central office. CO: Central office. RBS: Radio Base Station.

Moreover, the RoF possibility of sharing infrastructure for different wireless communication patterns has attracted much attention. In [82], a RoF system was proposed and successfully demonstrated for indoor transmission of multi-service multiple input multiple output (MIMO) radio signals from different communication patterns (Long Term Evolution (LTE), GSM (800 MHz), DCS (1.8 GHz), 3G UMTS (2.1 GHz), WLAN (2.4 GHz), future service wireless-VHT (60 GHz) over in-building active DAS. Furthermore, RoF has been also used for the transmission of

Wi-Fi, Wi-Max, and UWB signals simultaneously [83]. For this case, the system employed a Vertical Cavity Surface Emitting Laser (VCSEL) lasers and reflective electro-absorption transceivers to make the system more cost-attractive.

The tendency of an increased number of connected devices inside the home forces telecommunication providers to satisfy high data rates up to multigigabit transmission. Main applications of RoF include Home-Area networks [84], and DAS [38][41]. In-door systems are another application of RoF that has been studied for millimeter-waves distribution and high data rates. In [85], a RoF link was used for the distribution of UWB signals in a fiber to the home (FTTH) network with data rates up to 1.25 Gbps per user. Such systems are potential solutions to provide high capacity connection at high density events in a limited area such as stadiums or auditoriums. In addition, RoF links can be used for RF signal distribution inside tunnels and underground train or metro stations.

RoF systems offer the possibility of integrating wireless and optical networks to provide fixed and mobile users with high capacity, wide coverage, broadband connection and mobility [99]. Different RoF system architectures have been proposed and studied for millimeter-wave (60 GHz) due to the broadband available for the users [86][87][88].

2.2.1. RoF link configurations

There are different configurations to transport RF signals over optical fiber in a RoF system, which are classified depending on the RF frequency bands as follows: RF bands, intermediate frequency (IF) bands, and basebands (BB). These configurations are shown in Fig. 12.

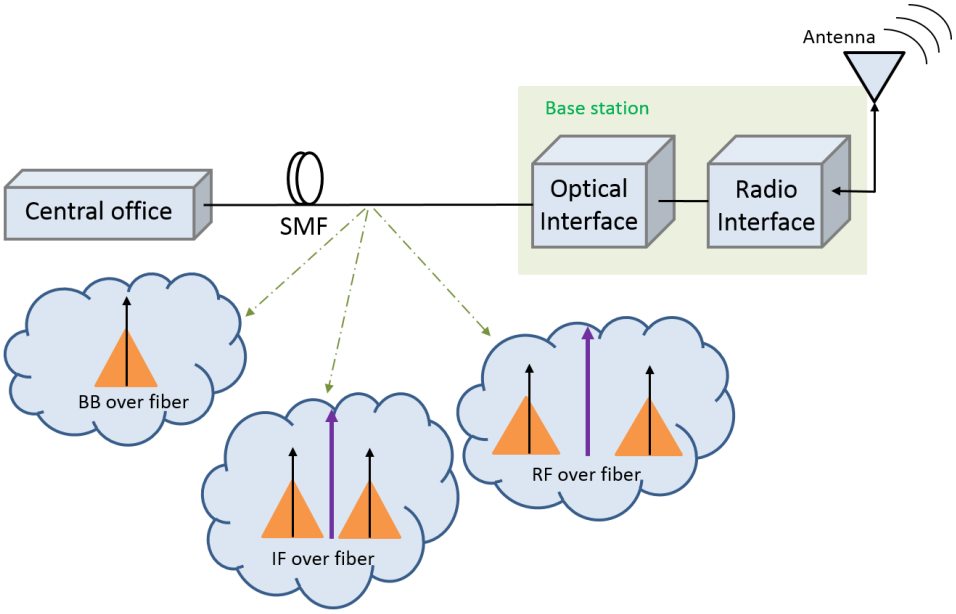

Fig. 12 - RoF transport schemes [61].

The electrical data signal, which can be RF, IF or BB, modulates the optical carrier from a laser diode. RF signals can be directly modulated using laser diodes, or with external modulators. After modulation, the modulated signal is transmitted to the BS through an optical fiber [61]. The electrical signal is recovered at the BS using a photodetector; moreover, it is upconverted if it was transmitted in IF or BB band. IF and BB bands reduce the bandwidth required for optical modulation, even though, IF and BB require additional hardware such as local oscillator and a mixer for RF upconversion at the BS [89].

2.2.2. RoF architectures

RoF architectures may assume different formats depending on the service application. The basic RoF architecture consists of a central office and a remote site connected by an optical fiber. However, this simple system has evolved to supply different services at areas that vary in many characteristics including number of levels and extension. Fig. 13 shows four different RoF architectures.

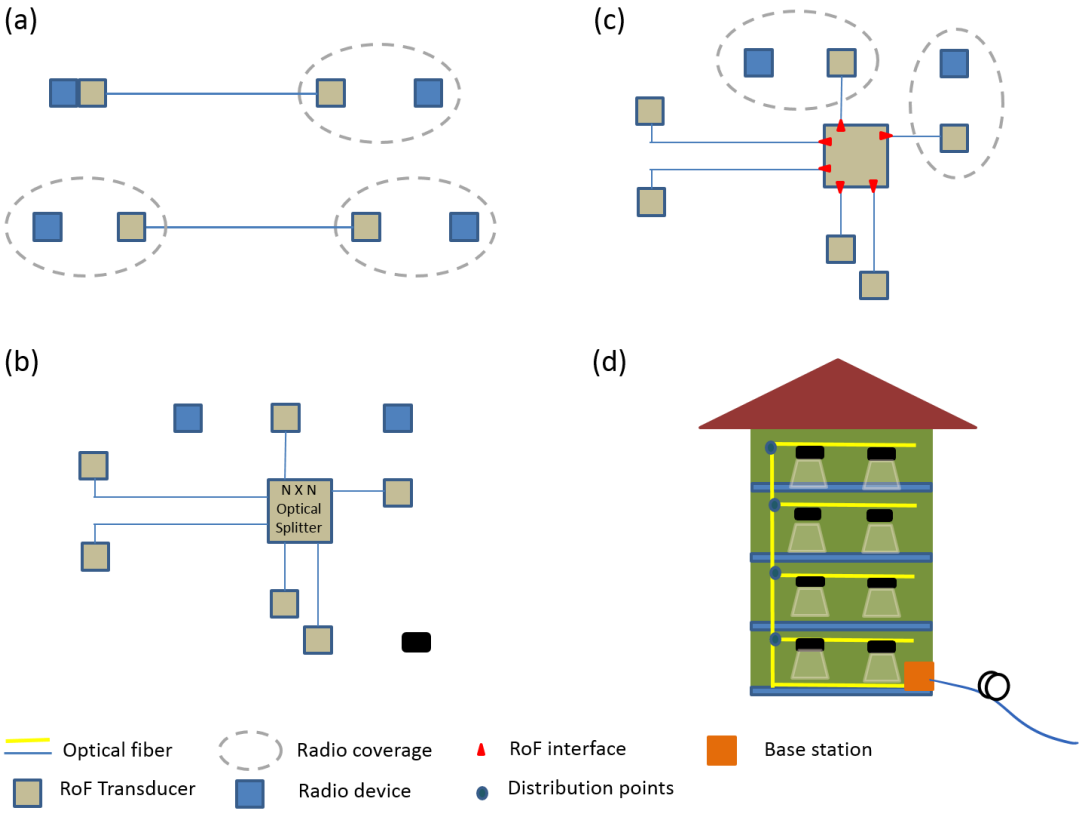

Fig. 13 - RoF architectures. (a) *Point-to-point.* (b) *Point-to-multipoint.* (c) *Active-star.* (d) *Fiber distributed antennas.*

The first and most simple architecture is point-to-point, shown in Fig. 13a. The first type of point-to-point architecture is called remote antenna and consists of a single area covered by a RoF transducer. The transducer is composed by one or two antennas, a laser for transmission, a photodetector for reception and electrical amplifiers for loses induced by the air [90]. The second type of point-to-point RoF architecture has two hops in the air and it is called optical tunnel, this architecture is mainly used in home area networks. The second architecture, Fig. 13b, is called point-to-multipoint. In this architecture the signal is split into different optical links using a 1 x N splitter that shares optical power between all the nodes. The drawback is that the home gateway might be overloaded since there is only one switch to support the whole architecture.

Fig. 13c shows the active-star architecture. This architecture uses several remote antennas that are connected to a switch or multiplexer/demultiplexer; since

the switch is an active component and it is located in the transducer, it requires energy to be powered. If the transducer is powered, the architecture is considered active. Moreover, the active-star architecture is optimal because its significant number of branches offer the best bandwidth x branch [90]. And finally, Fig. 13d shows the architecture for fiber distributed antennas. This configuration is widely used in locations such as stadiums, buildings and subways. In DAS, a base station is in charge of conversion of radio signals to optical signals, and then the signals are transmitted to remote nodes locations, where the signal is converted again to RF domain and directed to the antenna for wireless transmission [81].

2.3. Multiple Four-Wave Mixing

Four-wave mixing is a nonlinear effect caused by the third-order electrical susceptibility ($P_{NL} = \varepsilon_0 \chi^{(3)} : EEE$). This phenomenon occurs when two or more high power optical signals satisfy a phase matching condition and propagate simultaneously through a nonlinear medium, such as optical fiber. As a result, new waves are created at frequencies $\omega_f = \omega_i + \omega_j - \omega_k$, where $\omega_i, \omega_j \neq \omega_k$. Along with the generation of new wavelengths at different frequencies, these can also interact with each other and also with the original pump waves to create more new waves at new frequencies [72]. This process is known as Multiple Four-Wave Mixing (MFWM) [93][94][95].

The dynamics of FWM in optical fibers were investigated in the early 1990's [42], where a mathematical model for FWM was developed that considered the propagation equations of the two pumps and four generated sidebands. This model successfully predicted the exchange of energy between the pumps and FWM sidebands. Moreover, an interesting study in the FWM process is the energy exchange between the pumps and its sidebands [43]. It has been demonstrated that the energy exchange between pumps and the first sidebands of FWM can be solved using Jacobian elliptic functions, which suggests chaotic evolutions in the FWM process. In addition, another research presents a model that describes four-wave

mixing among an arbitrary number of incident waves [44], said model is applied to investigate the behavior of multi-wavelength Erbium-doped fiber lasers exploiting FWM; results showed that a proper value of phase mismatch could accelerate energy exchange among pumps and reduce power of sidebands.

In the FWM process, the energy of three photons can be transferred to a single photon at a frequency $\omega_4 = \omega_1 + \omega_2 + \omega_3$. Some of the phenomena that may arise in this process are third harmonic generation, which occurs when $\omega_1 = \omega_2 = \omega_3$, and frequency conversion, when two of the four frequencies coincide $\omega_1 = \omega_2 \neq \omega_3$. The last mentioned case receives the name of degenerate four wave mixing. Fig. 14 shows the difference between degenerate and non degenerate four-wave mixing.

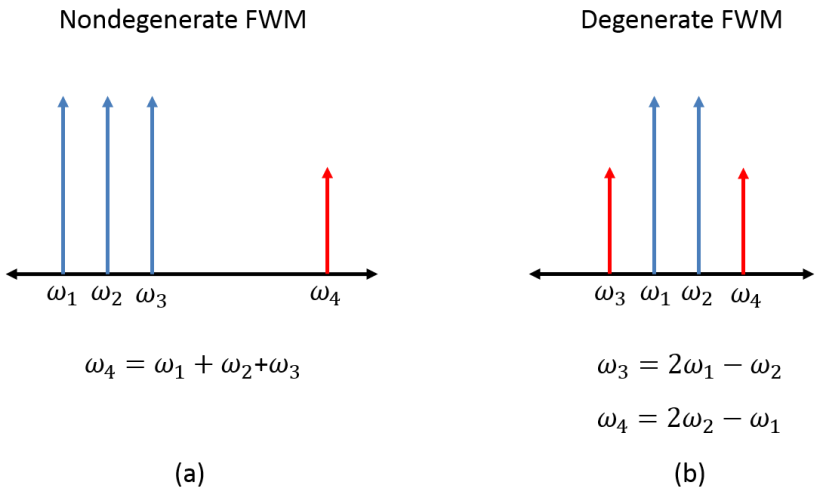

Fig. 14 - Generation of wavelengths in four wave mixing: (a) *Nondegenerate FWM using three pumps;* (b) *Degenerate FWM using two pumps.*

Another case is when two photons of wavelengths at frequencies ω_1 and ω_2 are annihilated along with the creation of two photons at ω_3 and ω_4; it occurs when $\omega_3 + \omega_4 = \omega_1 + \omega_2$. For this particular situation, the phase matching condition is required to meet

$$\Delta k = k_3 + k_4 - k_1 - k_2 \tag{7}$$

The FWM effect happens only if the phase mismatch is approximately zero ($\Delta k = 0$); this condition requires a specific choice of frequencies, which create a

refractive index modulation at the difference frequency [72]. Moreover, in partially degenerate FWM ($\omega_1 = \omega_2$), a pump wave at ω_1 generates two side bands symmetrically located at ω_3 and ω_4 with a frequency shift equal to

$$\Omega_s = \omega_1 - \omega_3 = \omega_4 - \omega_1. \tag{8}$$

considering $\omega_3 < \omega_4$ (see Fig. 15). The energy of the pump wave is transferred to the signal and idler bands ω_3 and ω_4, which are also known as the Stokes and anti-stokes bands respectively. On the other hand, if a second signal at ω_3 is transmitted simultaneously with pump ω_1 through the optical fiber, the signal is amplified, and a new wave ω_4 is generated.

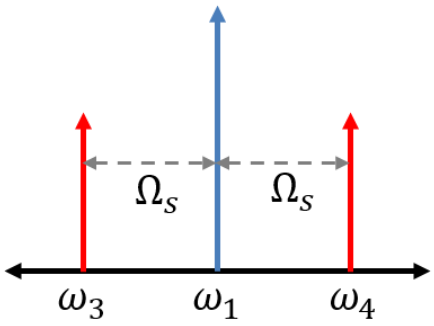

Fig. 15 - Pump wave generating two sidebands.

FWM in optical fibers can be an advantage or disadvantage depending on the application. It can induce crosstalk in WDM systems, which causes a limitation on the performance. In the case of equal channel spacing between the signal frequencies, the frequencies generated through FWM will be overlapped due to equal frequency separation [73]. Another effect of FWM is the noise in the bit pattern, FWM induced noise affects more fibers with low group velocity dispersion (GVD) values. Since FWM depends on the bit pattern of the three generating channels, the signal power fluctuates [74].

Different methods have been reported to overcome impairments due to fiber [46] [47] and external modulator [48][49] nonlinearities. Although nonlinear effects

are most of the times not wanted, research has been carried out to propose the use of nonlinearities with the purpose of using modulation sidebands for data transmission. Regarding the potential applications of FWM, numerous investigations have been conducted for wavelength conversion, new frequency generation [50][51], parametric oscillation [52], and quantum information processing [53][54]. Reported studies demonstrated that Stimulated Brillouin Scattering (SBS) can be used to increase the modulation depth and efficiency of fiber optic links [55][56], and self-phase modulation (SPM) in optical fiber can be used to enhance RF gain of microwave photonic links by over 8 dB [57]. Moreover, in 2012, Wall and Foster proposed the use of partially degenerated four-wave mixing effect to achieve a gain in a microwave link using a highly non-linear fiber (HNLF) [58]. Their study demonstrated that FWM efficiency can be improved using a HNLF, a constant gain of 9 dB along a 14 GHz band was achieved in the first product of FWM.

Furthermore, FWM and MFWM can be efficiently applied to develop nonlinear optical devices [97] [98]. For instance, the efficient generation of broadband MFWM products could be extremely useful for many applications, such as multi-wavelength generation, multiple-channel optical communications, ultra-short pulse generation, generation of frequency combs and optical metrology. One remarkable advantage is that it uses low cost diode lasers. Fig. 16 shows a measurement of an optical spectra of non-degenerate MFWM process at the output of HNLF; two incident wavelengths, λ_1=1556.3 nm and λ_2=1559.6 nm, generate four FWM products.

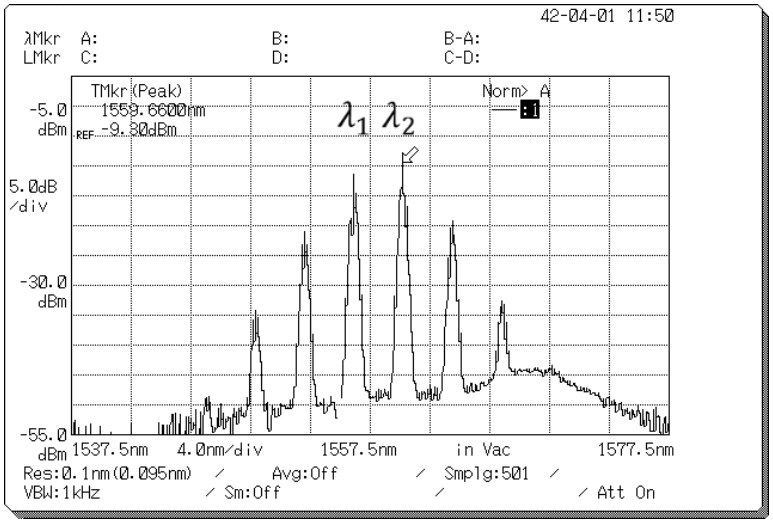

Fig. 16 – Example of a non-degenerate FWM spectra obtained in our experiments.

To analyze the FWM process, we consider four input signals at different frequencies, ω_1, ω_2, ω_3 and ω_4, which are linearly polarized on axis *x*. Their total electric field can be expressed as

$$E = \frac{1}{2}\hat{x}\sum_{j=1}^{4} E_j \exp[i(K_j z - \omega_j t)] + c.c. \tag{9}$$

where $K_j = n_j\omega_j/c$ is the propagation constant, n_j is the refractive index, ω_j is the oscillation frequency of each optical wave, and c is the speed of light in vacuum. The four waves are assumed to propagate in the same direction. Moreover, the optical fiber polarization, which has a linear and a nonlinear component, can be written as

$$\vec{P}(\vec{r},t) = \overrightarrow{P_L}(\vec{r},t) + \overrightarrow{P_{NL}}(\vec{r},t) \tag{10}$$

The linear $\overrightarrow{P_L}(\vec{r},t)$ and nonlinear $\overrightarrow{P_{NL}}(\vec{r},t)$ components are given by

$$\overrightarrow{P_L}(\vec{r},t) = \varepsilon_0 \int_{-\infty}^{\infty} \chi^{(1)}(t-t')dt' \tag{11}$$

$$\overrightarrow{P_{NL}}(\vec{r},t) = \varepsilon_0 \chi^{(3)} \vdots E(r,t)E(r,t)E(r,t) \tag{12}$$

where ε_0 is the permittivity of vacuum, $\chi^{(1)}$ is the linear susceptibility, $\chi^{(3)}$ is the third-order nonlinear susceptibility and $E(r,t)$ is the electric field. If eq. (9) is substituted in eq. (12), we can express nonlinear polarization as

$$P_{NL} = \frac{1}{2}\hat{x}\sum_{j=1}^{4} P_j \exp[i(K_j z - \omega_j t)] + c.c. \quad (13)$$

Eq. (13) contains terms that are responsible for the effects of SPM and cross phase modulation (XPM).

The efficiency of the FWM process depends on different parameters such as channel frequency separation, chromatic dispersion of the fiber, fiber length, and parametric gain, which will be explained in detail further in this chaper. If the phase matching condition is satisfied along with the group velocity, the efficiency of FWM improves [73]. The phase matching condition is based on the mismatch caused by material dispersion Δk_M, waveguide dispersion Δk_W, and nonlinear effects Δk_{NL} as follows

$$\Delta k = \Delta k_M + \Delta k_W + \Delta k_{NL} = 0 \quad (14)$$

If eq. (14) is expressed in terms of the equivalent of the propagation constant, for the case of partially degenerate FWM (when $\omega_1 = \omega_2$), the matching condition can be written as $\Delta k = (n_4\omega_4 + n_3\omega_3 - 2n_1\omega_1)/c$.

G. P. Agrawal (2001) made a detailed vector theory explanation of the non-degenerate FWM process, which is governed by four coupled amplitude equations that can be solved using a numerical approach [91].

By not considering the phase shifts induced by SPM and XPM, [91]. The amplitude A_f inside a multimode fiber of the FWM component at ω_f is defined as

$$\frac{dA_f}{dz} = \frac{\propto}{2}A_f + d_f\gamma A_i A_j A_k^* \exp(-i\Delta kz) \quad (15)$$

where $\propto$ is the power attenuation coefficient of the fiber, $A_m(z) = A_m(0)\exp(-\propto z/2)$ for $m = i, j, k$, $d_f = 2 - \delta_{ij}$ is the degeneracy factor that is equal to 1 when $i = j$, and γ is the nonlinear parameter of the optical fiber. Many nonlinear effects depend on the non linear parameter γ, which is determined by

$$\gamma = \frac{n_2 \omega_j}{c A_{eff}} \tag{16}$$

and $n_2 = \frac{3}{8n} Re\left(\chi^{(3)}\right)$ is nonlinear refraction index of the fiber, and $A_{eff} = \left[\frac{\int_r \int_\theta r dr d\theta I(r,\theta)}{\int_r \int_\theta r dr d\theta I^2(r,\theta)}\right]$ is the effective core area of the fiber, where r and θ denote the polar coordinates. In terms of the nonlinear parameter γ and pump powers P_1 and P_2, the net phase mismatch can be expressed as

$$k = \Delta k + \gamma(P_1 + P_2) \tag{17}$$

where Δk is the phase mismatch given in Eq. (11).

Eq. (17) is considered for two distinct pump waves, even though if there is only one pump, $P_1 = P_2 = P_0$. Therefore

$$k = \Delta k + \gamma(2P_0) \tag{18}$$

The parametric gain is defined as the amplification generated in the optical carriers ω_1, ω_2, ω_3, and ω_4 that take part of the FWM process, and it is expressed in m/W. It depends on the polarization of the pumps, and it has a peak value when the phase mismatch is equal to zero $k = 0$ [72]. When one or two pumps are responsible for the FWM effect, the parametric gain would be defined as

$$g = \sqrt{(\gamma P_0 r)^2 - \left(\frac{k}{2}\right)^2} \tag{19}$$

where $r = \frac{2\sqrt{(P_1 P_2)}}{P_0}$, and $P_0 = \sqrt{P_1 + P_2}$. Where r is the difference between the arithmetic and geometric average mean of the pump powers.

The power transferred to the FWM product at ω_f in a fiber length L is given by

$$P_f = \left|A_f(L)\right|^2 = \eta_f (d_f \gamma L)^2 P_i P_j P_k e^{-\alpha L} \quad (20)$$

where $P_m = |A_m(0)|^2$, for $m = i, j, k$, is the launched power in the m_{th} channel, L is the length of the fiber, $d_f = 2 - \delta_{ij}$ is the degeneracy factor that is equal to 1 when $i = j$ and 2 when $i \neq j$, and η_f is the FWM efficiency, which indicates the power of the FWM process, [72] and it is given by

$$\eta_f = \left|\frac{1-exp[-(\alpha+i\Delta k)L]}{(\alpha+i\Delta k)L}\right|^2 \quad (21)$$

As mentioned before, the FWM efficiency depends on the phase mismatch Δk, and also on the group velocity dispersion of the fiber. If the GVD is large ($|\beta_2| > 5$ ps^2/km) and the dispersion (D) is more than 2 ps/km, η_f is approximately zero for a channel spacing of 50 GHz. However, in low dispersion fibers, and when the pump frequency is close to the zero-dispersion wavelength, $\eta_f \approx 1$; as a result the new FWM component has high power [91].

According to eq. (20), the power of the FWM idler waves, ω_3 and ω_4, depend on the power of the pump waves generating them along with the phase mismatch. The power behavior oscillates and varies according to a $sinc^2(x)$ function. When x takes a value that is an integer multiple of π, the FWM efficiency will be zero [75]. Consequently, it is possible to define a pattern in the fiber length called coherence length, which is defined by

$$L_{coh} = 2\pi/|k| \quad (22)$$

where $k = \Delta k$ is the maximum value of the tolerated wave-vector mismatch. Moreover, it is difficult to maintain the phase mismatch condition due to core diameter variations; thus, a high efficiency FWM occurs when $L < L_{coh}$, and if $\Delta k = 0$, the coherence length would be infinite. This means that the FWM process would be efficient if the fiber has a length L.

2.4. Carrierless Amplitude Phase Modulation

2.4.1. Introduction to CAP

In 1975, Bell Labs originally proposed Carrierless Amplitude Phase (CAP) modulation, originally called Carrierless AM/PM, to be a viable alternative for modulation of high-speed communications in copper wires [31]. This modulation is based on Quadrature Amplitude Modulation (QAM), even though the difference lies in the way the signal is generated. Fig. 17 shows the block diagrams of CAP modulation. In QAM low pass filters shape the information in the modulation and demodulation parts; on the other hand, CAP employs passband filters, a product of square root raise cosine filter (SRRC) and sine/cosine waveforms, which give the data signal a limited bandwidth, zero inter-symbol interference (ISI) and zero cross-channel interference (CCI). These characteristics allow a perfect reconstruction at the receiver [76].

The transmitter block consists of an encoder that divides the bit stream into groups of binary numbers, which will be mapped into CAP symbols. The level of CAP modulation gives the number of positions in the constellation diagram, each different position corresponds to a different symbol. For instance, if CAP-16 is chosen, the constellation will have 16 positions that correspond to the 16 symbols of the constellation diagram. Each symbol has an In-phase and a Quadrature component, which are divided into two different vectors. Both In-phase and Quadrature vectors are up-sampled and shaped using band-pass filters. The shaped digital signals are then added and converted into the digital domain using a Digital Analog converter (DAC). After conversion, the signal can be transmitted.

The inverse process takes place at the receiver. An analog signal is converted to the digital domain using a DAC. The analog signal is divided into two parts, each one has an inverse bandpass filter that will recover the In-phase and Quadrature components of the signal. The recovered component are down-sampled to recover the original datarate. Finally, both components pass through a decoder that converts

the symbol vectors into bits. The received bit stream and the original data message are compared to find out if there are transmission errors.

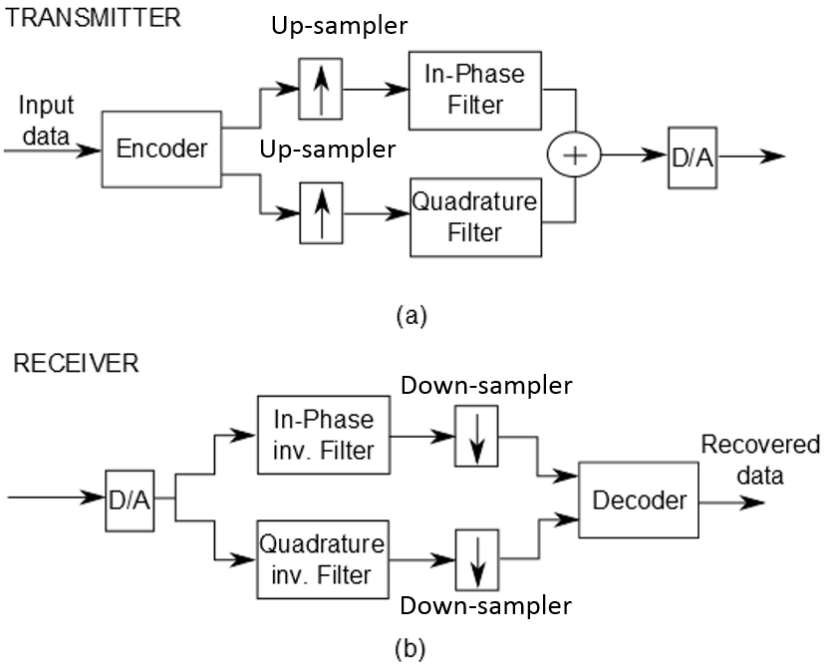

Fig. 17 - Carrierles Amplitude Phase modulation block diagrams: (a) *Transmitter;* (b) *Receiver.*

2.4.2. CAP Modulation: The importance of filter design

CAP is a multilevel, multidimensional modulation format; the incoming data bits are encoded into multilevel symbols. Before filtering the signal components *Q, and I* the symbols have to be up-sampled; if a digital filter is used for pulse shaping, it must be operated at a rate of at least twice the data rate to span. Common up-sampling factors are 3 or 4 [77].

The raised cosine waveform and the square root raised cosine waveform, which are shown in Fig. 18, can be expressed as in eq. (23) and eq. (24).

$$h_{RC}(t) = \frac{sinc\left(\frac{t}{T}\right)cos\left(\frac{\pi\alpha t}{T}\right)}{1-4\left(\frac{\alpha_f t}{T}\right)^2} \tag{23}$$

$$h_{SRRC}(t) = \frac{4\alpha_f}{\pi\sqrt{T}} \frac{cos\left(\frac{(1-\alpha_f)\pi t}{T}\right) + \frac{T}{4\alpha_f t} sin\left(\frac{(1-\alpha_f)\pi t}{T}\right)}{1-4\left(\frac{\alpha_f t}{T}\right)^2} \quad (24)$$

where T represents the period, and α_f is the roll-off factor that is defined by $\alpha_f = \left(\frac{W-\frac{1}{2T}}{\frac{1}{2T}}\right)$. α_f is a measurement of the excess bandwidth; the smaller the roll-off factor, the narrower the bandwidth. However, if a small roll-off factor is chosen, the side lobes of the impulse response increase and the attenuation in the stop band is reduced (see Fig. 19). The roll-off also has a direct influence on the eye diagram: as roll-off increases, the eye diagram opens up [12].

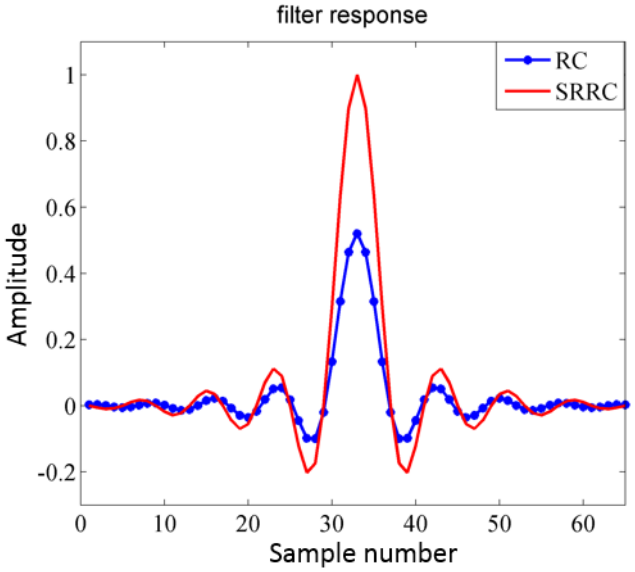

Fig. 18 - Impulse response of the raised cosine (RC) and the square root raised cosine (SRRC) filter. ($\alpha = 0.15$).

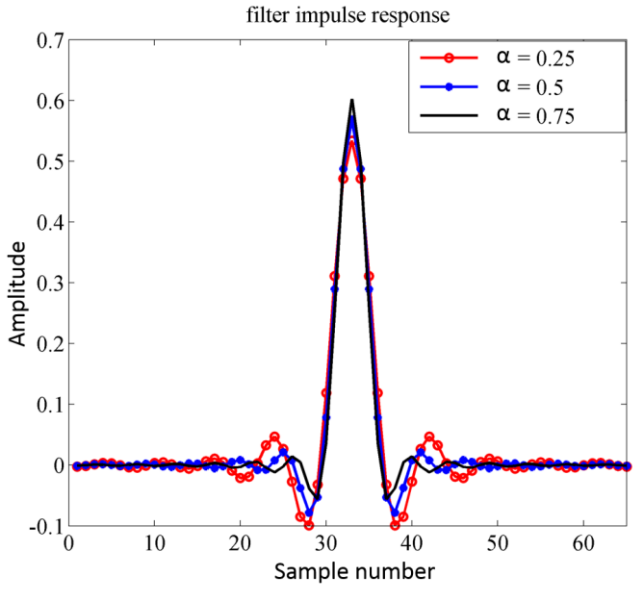

Fig. 19 - Square root raised cosine impulse response for different roll-off factors.

Square-root cosine filtering is adopted in commercial communications, such as cellular technology. A combined response of two SRRC filters, which is generally used to share the pulse shaping between transmitter and receiver, is the same as of a raised cosine filter. The SRRC filters in CAP modulation are very important; in theory, SRRC filters have infinite number of taps in order to have infinite attenuation in the stop band. Therefore in implementation, the response of this type of filter is affected by the tap length, which has to be a finite value. As the tap number increases, the length of the time sequence increases along with the rejection of the filter. Moreover, the number of samples (filter delay) reduces the stopband attenuation [12].

Two signals are used as signature waveforms to modulate data. The passband filters are filters of the transmitter in CAP modulation are given by

$$f_1 = h_{SRRC}(t)\cos(2\pi f_c t) \tag{25}$$

$$f_2 = h_{SRRC}(t)\sin(2\pi f_c t) \tag{26}$$

where f_c is the frequency of the passband filter. The filter f_1 is the in-phase filter, and filter f_2 is the quadrature filter. Fig. 20a. shows the responses of these filters, called the Hilbert pair: two signals with the same magnitude response, but shifted of 90°.

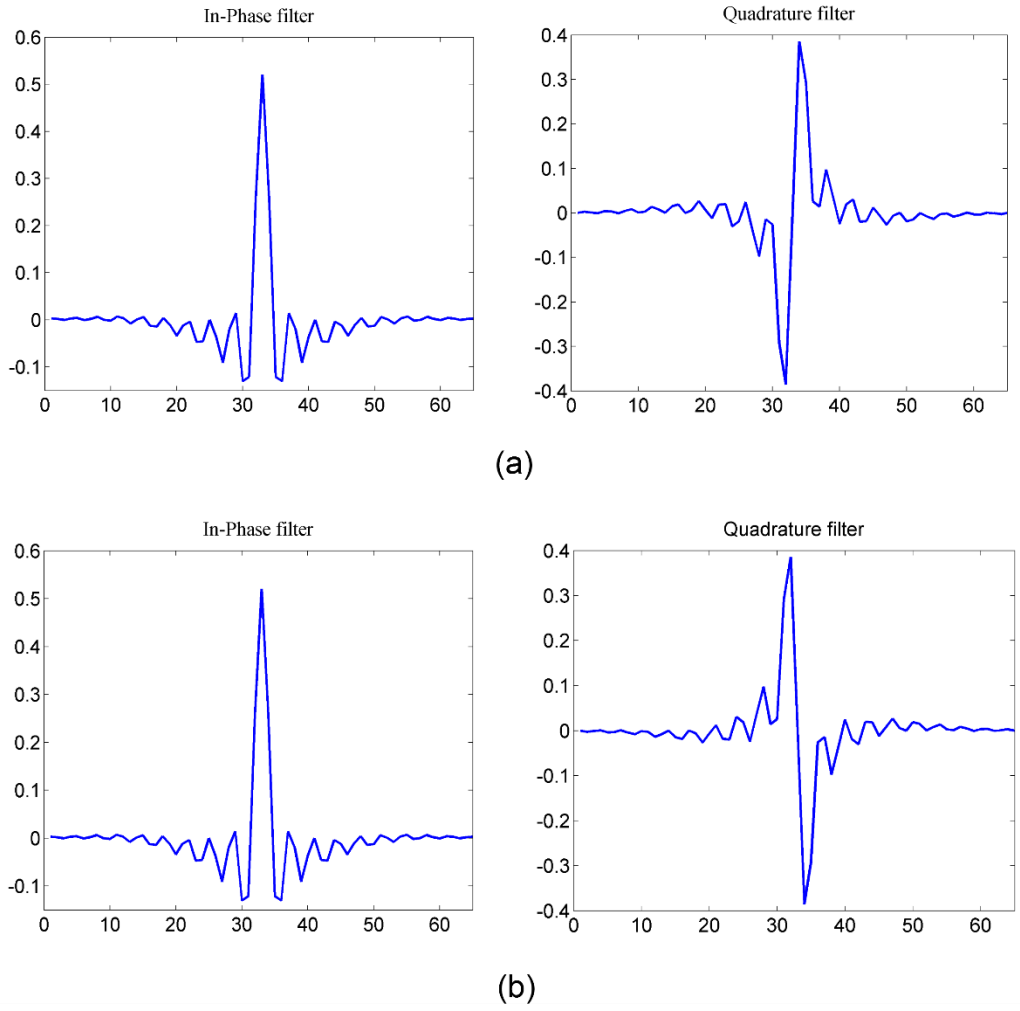

Fig. 20 - Impulse responses of the in-phase and quadrature filters in (a) *Transmision* (b) *Reception.*

At the receiver, the incoming signal passes through two matching filters that have their coefficients reversed (see Fig. 20b). The filtered symbol signals are down-sampled to the original symbol rate. Later, these data streams are decoded, to recover the data bits sent at the transmitter.

2.4.3. CAP System Model

The CAP transmission system has been modeled using algorithms designed in MATLAB. Fig. 21 shows an overview in the form of a block diagram of the model used to achieve CAP modulation. The algorithm was divided into three different blocks: CAP transmitter, which is in charge of data generation, modulation and creation of the signal to be transmitted; channel, which allows to simulate interference by adding white Gaussian noise to the transmitted signal; and CAP receiver, which decodes the incoming data signal and recovers the original sent data stream. Moreover, the transmitter block creates a signal that can be saved as an external variable, which can be accessed from MATLAB; therefore, the receiver input can be loaded from the file that corresponds to the external variable created in MATLAB. The blocks have been designed with the intention of using them not only for simulation, but also for future experimental work in the lab.

Fig. 21 - Overview of the CAP algorithm in MATLAB.

The first part of the transmitter and receiver CAP algorithms contains the initialization functions. Their purpose is to pre-calculate variables that take part of the different processes of the transmitter block. In other words, if you would like to compare the constellation diagrams recovered in the receiver block for different mapping levels, you may need to modify, in this case, the parameter "M". The initialization function of the CAP algorithm is shown in Fig. 22.

```
%% Initialization
Nos = 4; %Upsampling factor

load PRBS_15
PRBS = PRBS';
PRBS = [PRBS ; 0];

%% CAP Mapping
M=16; %Alphabet size (8 QAM, 16 QAM, etc...)

%% Hilbert filter design
roll_off=0.15; %roll-off factor influences amount of the excess
bandwidth
delay=8; %Number of period symbols between start of filter
response and peak of filter
```

Fig. 22 – Initialization function of the CAP algorithm.

The most important parameters of the transmitter and receiver blocks are represented as variables, and all other simulation factors are calculated based on them. The explanation of the initialization variables is given below.

1. Nos – Upsampling factor of the transmitter and receiver.
2. PRBS – The data bit stream is loaded to this variable. *PRBS_15* is the source file, which contains a semi-random binary arrange. This variable is only present in the transmitter block.
3. M – Level of the encoding constellation.
4. roll-off – Parameter for SRRC filter design, takes values between 0 and 1. Measures how much bandwidth is being used over the ideal bandwidth.
5. delay – Delay value used to design the SRRC filter.

Those variables define other variables in the algorithm that should not be modified directly. The first block of the CAP algorithm is the transmitter. As shown in Fig. 23, the transmitter is composed by a data generation block, data to symbol encoder, up-sampling function, filtering block and summation block.

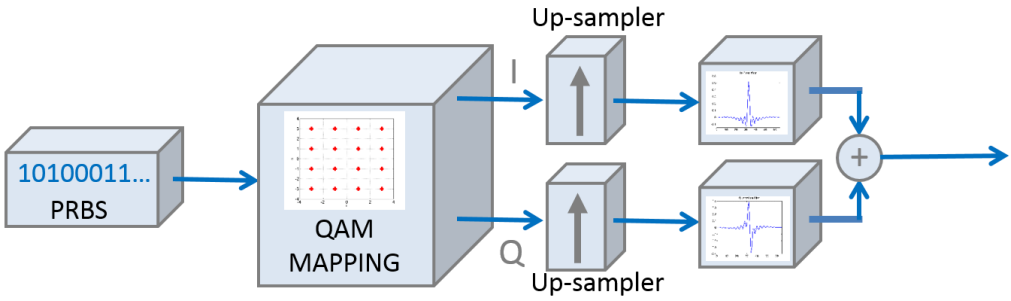

Fig. 23 - Schematic of the CAP transmitter.

At the CAP transmitter, the input data is encoded into a previously defined M-level QAM constellation. The bit stream is divided into groups of binary numbers called symbols. The number of bits on each symbol corresponds to $log_2 M$. Then, the symbols are transformed to decimal; the MATLAB function "*qammod*" is used to encode the decimal numbers into the M-QAM constellation. Each position on the constellation has a real (x axis, in-phase) and an imaginary (y axis, quadrature) component. The real and imaginary components of each mapped symbol are gathered into two different symbol arrays, which are separately up-sampled. The real symbol array is the data that will be filtered with the in-phase filter; therefore, the imaginary symbol array contains the data that will be filtered with the quadrature filter. Later, in-phase and quadrature components are summed up, and the resulting signal can be transmitted through the channel.

The signal generated in the transmitter is passed to the channel. The channel block allows the possibility to add white Gaussian noise to the transmitted signal. The signal to noise ratio per sample in dB can be adjusted to any desired value in order to simulate noise that may affect the signal through the transmitting process.

The signal, after being transmitted and affected by the channel, is passed to the receiver section (Fig. 24). This block is similar to the transmitter block. First, the signal passes through the receiving filters, which are the matched to their equivalent in the transmitter. The filters allow recovering the correct component from the transmitted signal. After recovering in-phase and quadrature components, signals pass through a decoder or de-mapper that makes interprets and makes a decision on

the received symbols. Later, the recovered data can be compared to the sent data for bit error rate (BER) calculation.

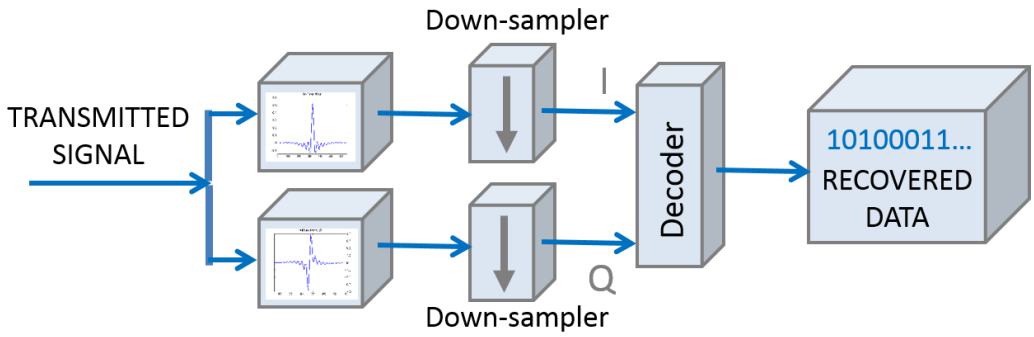

Fig. 24 - Schematic of the CAP receiver.

2.3.4. Simulation results

Several simulation setups have been carried out to test different configurations of CAP signals: different orders of modulation have been tested and the effect of white Gaussian noise through the channel has been studied. In this subsection, the results of those simulations will be presented. The experiments were performed with a data sequence of 32768 bits, and an up-sampling factor of four was used in the CAP transmitter.

a) CAP-16

The first simulation carried out was a transmission of the signal modulated with CAP 16. The received constellations of the CAP 16 modulation for different levels of SNR are in Fig. 25. The presented constellation in Fig. 25a has been obtained from a simulation after the transmission without any noise or other distortions. The spread in the points of constellation, which is barely perceivable, is caused by the limited accuracy of the filter coefficients [12]. The constellations in Fig. 25b, c and d show how the signal to noise ratio increases the distortion of the signal sent. For a SNR above 15 dB, there is a number of errors during each transmission, therefore the bit error rate can be found by comparing the original signal with the recovered signal. A summary of the results obtained in the simulation with CAP-16 is presented in Table 1.

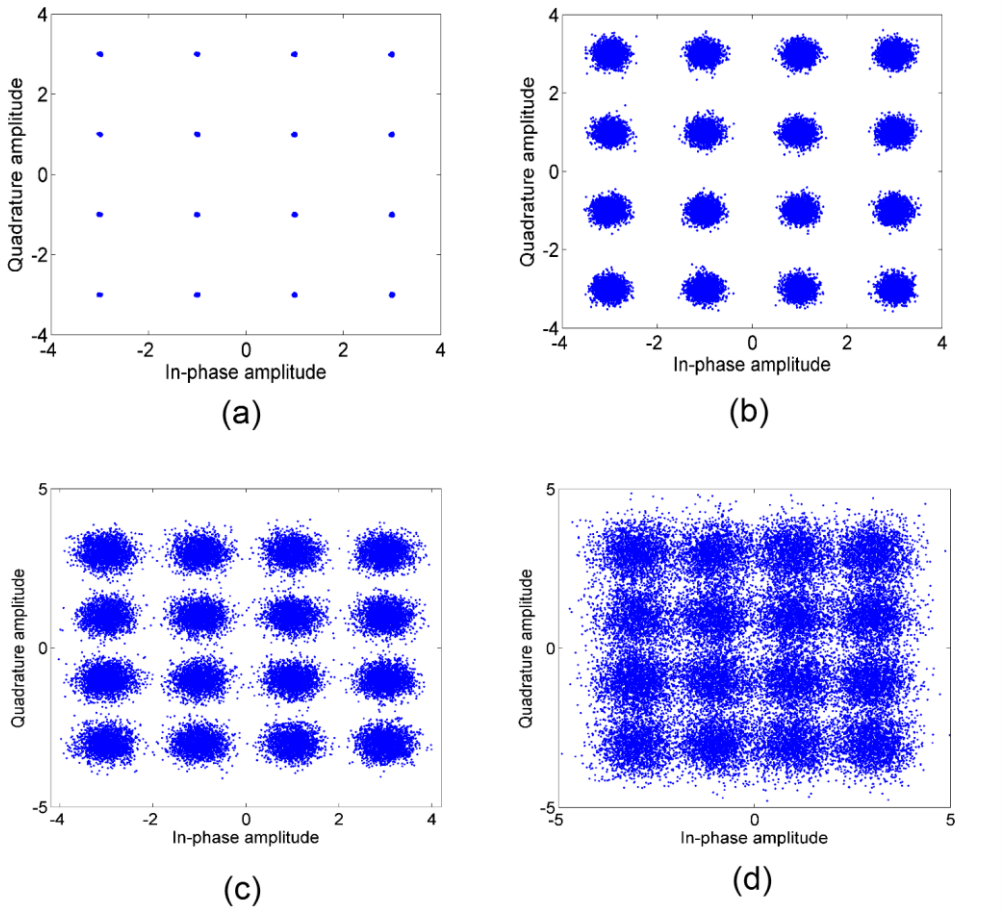

Fig. 25 - Constellation of CAP-16 signal with (a) *no channel distortion* (b) *SNR = 20 dB* (c) *SNR = 15 dB* (d) *SNR = 10 dB.*

Table 1 - BER as a function of SNR for CAP-16.

Signal-to-noise ratio	Bit Error Rate	Number of errors
20 dB	0	0
15 dB	$1{,}524 \times 10^{-4}$	5
10 dB	0,0283	928

b) CAP-32

The second simulation performed was a transmission of the signal modulated with CAP-32. The CAP-32 constellations for different values of signal to noise ratio are shown in Fig. 26. The constellation from Fig. 26a was obtained with a simulation in

which the channel did not have any effect on the signal. It means no distortions or noise were added. The constellations in Fig. 26b and Fig. 26c present a distortion caused by white Gaussian noise added to the transmitted signal. The SNR for each figure is 20 dB and 15 dB, respectively. For this modulation format, no constellation diagram was generated for SNR<15 dB because for a SNR = 15 dB, there is a considerable number of errors, and the BER for this case was 0.0075 as shown in Table 2.

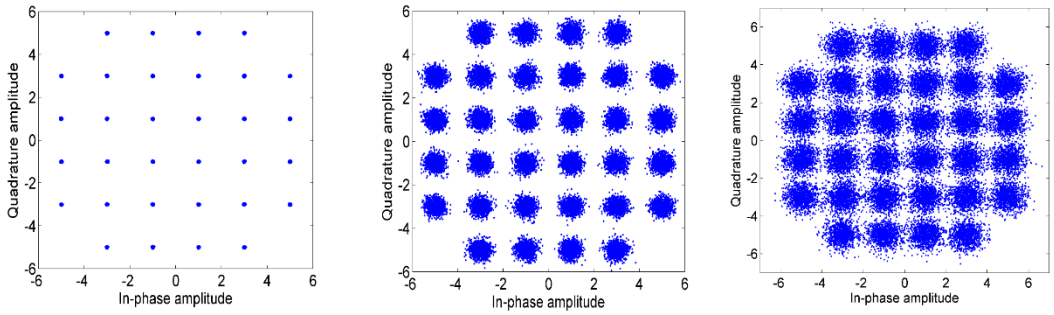

Fig. 26 - Constellation diagrams at the receiver for a signal modulated with CAP-32 for (a) *No distortion* (b) *SNR = 20 dB* (c) *SNR = 15 dB.*

Table 2 - BER as a function of SNR for CAP-32.

Signal-to-noise ratio	Bit Error Rate	Number of errors
20 dB	0	0
15 dB	0.0075	245

c) CAP-64

The third simulation performed was a transmission of the filtered data stream previously modulated with CAP-64. In CAP-64, there is a total of 8 bits per symbol, and 64 points in the constellation where a symbol can be positioned. Fig. 27 shows the effect of the white Gaussian noise on the constellation diagrams.

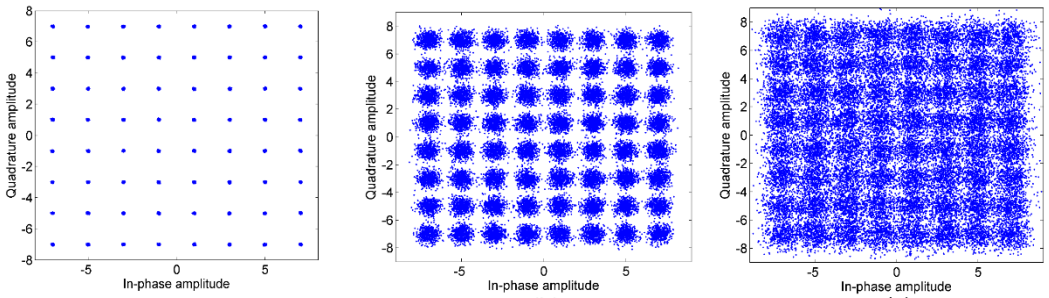

Fig. 27 - Constellation diagrams for the CAP/64 modulated signal with (a) *no distortion* (b) *SNR = 20 dB* (c) *SNR = 15 dB.*

The constellation in Fig. 27a was obtained when a transmission of the data stream was simulated using CAP-64 as the modulation format. In this case, the channel did not have any effect on the signal, which means it was directly send to the receiver as in a Back-to-Back (B2B) scheme. The constellations in Fig. 27b and c present a distortion caused by white Gaussian noise added to the transmitted signal. The signal to noise ratio for each figure is 20 dB and 15 dB, respectively. For this modulation format, as well as for CAP-32, no constellation diagram was generated for SNR<15 dB because for a SNR = 15 dB, the BER was already 0.042. Table 3 contains information regarding the bit error rate and signal to noise ratio of constellations in Fig. 27b and Fig. 27c.

Table 3 - BER as a function of SNR for CAP-64.

Signal-to-noise ratio	Bit Error Rate	Number of errors
20	0.0010	34
15	0.042	1,376

d) CAP-128

Finally, the last simulation to test the CAP algorithm was for CAP-128. The simulation performed was a transmission of a CAP-128 modulated data stream. Fig. 28 shows the effect of the white Gaussian noise on the CAP-128 constellation diagrams.

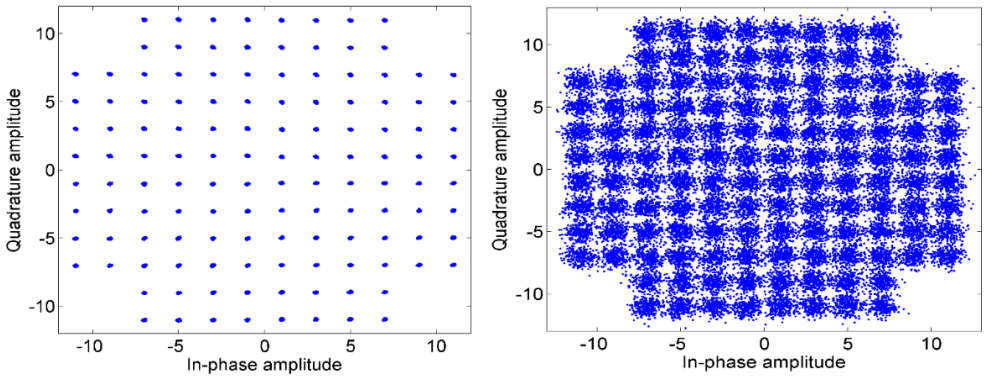

Fig. 28 - Constellation diagrams for the CAP-128 modulated signal with (a) *no distortion* (b) *SNR = 20 dB.*

The constellation from Fig. 28a was obtained with the simulation of a data stream transmission; the data was previously modulated with CAP-128. This constellation shows how the channel did not have any effect on the signal; no white Gaussian noise was added, similar to a B2B connection. The constellation in Fig. 28b presents a distortion caused by white Gaussian noise added to the transmitted signal, the signal to noise ratio is 20 dB and the BER was 0.0145.

One advantage of using higher order modulation forms is that symbols carry more bits of information than other modulation forms, and as a result the data rate of a link increases too. On the other hand, the higher the order of a modulation scheme, the less resilient to noise and interference. As the signal to noise ratio decreases, the errors increase, in some cases requiring a re-send of the data. Those observations reflect what happens in the constellations in Figs. 21 – 24. The transmission is errorless for all the levels of CAP when there is no channel to affect the transmitted signal. However, when white Gaussian noise is added to the signal, the constellation points become more spread for all levels of CAP modulation. The higher order CAP constellations show that there is a higher chance of having errors in the transmission process, therefore higher order modulation formats require a higher signal to noise ratio.

Chapter 3

3. Photonic-assisted microwave amplification in radio over fiber systems

Fig. 29a and Fig. 29b shows the setups of a conventional RoF system and the technique proposed to enable photonic-assisted microwave amplification by taking advantage of multiple FWM process. Based on the radio over fiber architecture, the scheme consists of two continuous wave (CW) lasers, represented by symbols λ_1 and λ_2 respectively, with wavelengths values of 1556.3 nm and 1559.6 nm, and optical power fixed at 16 dBm, which is the maximum power of each laser. The separation between the pumps is 3.3 nm, when optical wavelengths are widely separated it is necessary to increase optical power using and EDFA, which increases the amplified spontaneous emission (ASE) in the optical spectra. Moreover, the separation could not be chosen to be smaller since there is a limitation in the bandwidth of the optical filter. The optical carriers pass through polarization controllers (PC) to adjust the polarization state and maximize the optical power. Then, a 3 dB coupler couples the carriers. The electrical power of the sinusoidal RF signal driving the MZM is set to 14 dBm and the frequency value was set to 17 GHz, which is modulating with the CW optical carriers on a Mach-Zehnder Modulator (Fujitsu FTM 7929, TN00047). The optically amplitude modulated signals are then amplified by EDFA. Then, the high optical power carriers are launched into a highly nonlinear fiber (Zero-dispersion wavelength λ_0 = 1,560 nm; L = 90 m; α = 0.674 dB/km; S_0 = 0.02 ps/nm^2/km; γ = 10 W^{-1}km^{-1}). After passing through 90 m of HNLF, the optical

carriers as well as the optical products generated by the Four-Wave Mixing effect into the optical fiber, are split by a 10/90 optical coupler. The 10% is used to monitor the optical spectra and the nonlinear effect of four-wave mixing using an optical spectrum analyzer (Anritsu MS9720A). On the other hand, the 90% passes through a 3.2nm Band Pass Filter (BPF) that is used to filter out the optical carrier of interest (1552.6 nm) that feeds a 50 GHz photodetector (XPDV1250R u2t). The photodetected signal is then connected to an electrical spectrum analyzer (SDA 830Zi) to monitor the carrier electrical power.

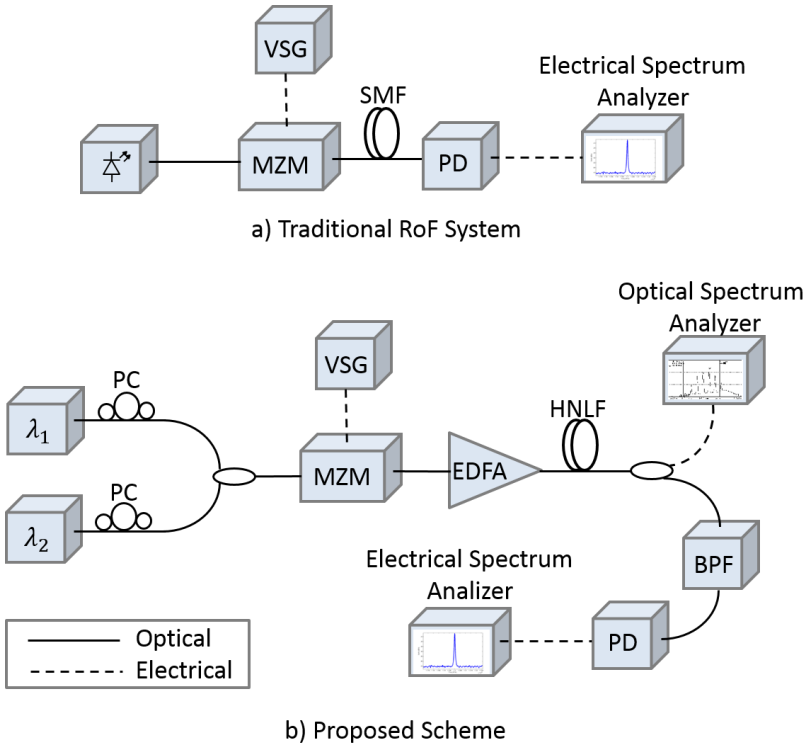

Fig. 29 – (a) *Conventional RoF system* (b) *Photonic-assisted microwave amplification technique: PC, Polarization controller; MZM, Mach-Zehnder Modulator; VSG, Vector Signal Generator; SMF, Single Mode Fiber; HNLF, Highly Non-linear Fiber; EDFA, Erbium Doped Fiber Amplifier; BPF, Band Pass Filter; PD, Photodetector.*

3.1. Simulations using OptiSystem ®

The simulations were carried out to confirm hypotheses regarding the initial idea of using the idler frequencies generated through a FWM process for photonic amplification. The amplified RoF system based on radio over fiber shown in Fig. 58b

was simulated to study and analyze the FWM process response and the system behavior under different system conditions. The system was simulated using the software OptiSystem ® to understand the experiment at each stage. First, the MZM was studied by modulating a signal that was composed by binary ones (1), into the light beam of a CW laser to obtain a figure of the MZM's transfer function. Then, the simulation of the proposed scheme was carried out, paying particular attention to the optical fiber characteristics, which is the component that makes new wavelength creation and optical amplification possible.

3.1.1. MZM characterization

Numerous simulations were carried out to proper understand the MZM behavior and effects of different conditions on the modulation of the input RF signal. To start, the output optical field of the MZM is given by

$$E_0 = E_i(t)\,\frac{e^{i\pi V_1(t)/V_\pi} + e^{i\pi V_2(t)/V_\pi}}{2} \tag{27}$$

where V_π is the pi voltage, V_1 and V_2 are the voltages V_{Bias} at the input of the electrical drives 1 and 2 respectively, and $E_i(t)$ is the input optical field. Since we need to simulate a one single electrical drive MZM, V_2 must be zero. In addition, the V_π value of the MZM in the simulation must match with the one of the MZM used in the experiments at the laboratory (MZM FTM 7929FB, TN00047), which is V_π =1 V. Next, taking into account that $V_2 = 0$, eq. (27) will be

$$E_0 = E_i(t)\,\frac{e^{\frac{i\pi V_1(t)}{V_\pi}} + e^0}{2} = \frac{e^{i\pi V_1(t)/V_\pi} + 1}{2} \tag{28}$$

In eq. (28), if $V_1 = V_\pi$, then $e^{i\pi} = -1$, therefore $E_0(t) = 0$. On the other hand, if $V_1 = 0$, then $e^{i\pi} = 1$, therefore $E_0(t) = E_i(t)$, where $e^{in\pi} = 1$ for $n =$ 0,2,4, ... and $e^{in\pi} = -1$ for $n =$ 1,3,5, ..., where n is the V_1 value.

Fig. 30 shows the simulation diagram used in characterization of the MZM in OptiSystem ®. A LiNb dual drive MZM was used for modulation, and, as mentioned before, the second V_{Bias} and the electrical drive were set to zero to disable this input. It is important to mention that the V_π of the MZM changes with the frequency of the electrical signal [101]. This characterization is carried out with an electrical sine wave with a power of 14 dBm and a frequency of 17 GHz.

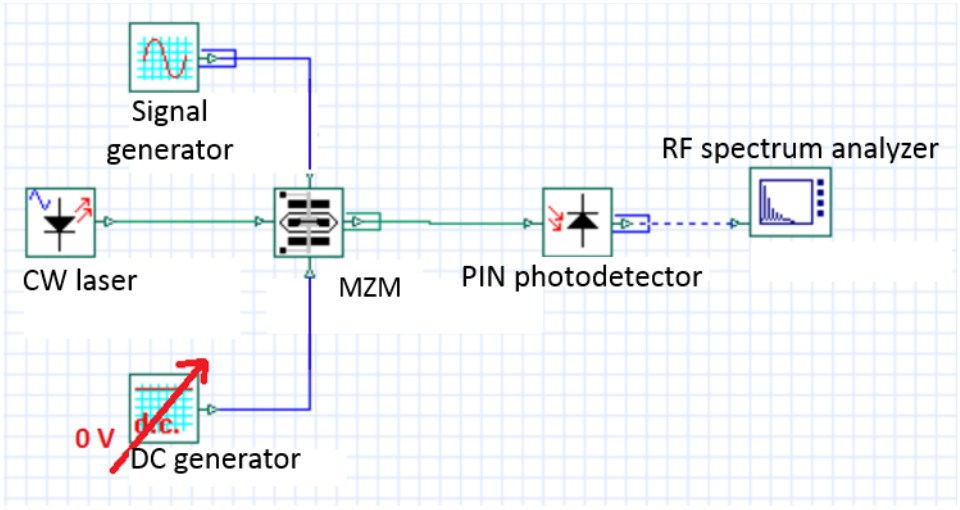

Fig. 30 – Characterization of the MZM in OptiSystem ®.

Fig. 31 shows simulation result of the transfer function of the MZM. To obtain this figure, the bias voltage (V_{Bias}) of the MZM's first electrical drive was swept from 0 to 10 V, and the optical power was measured for each value of V_{Bias}. The highest optical power/optical field is obtained when $V_1 = V_\pi$, and due to the fact the V_{Bias} can be higher, high optical power/field can be obtained when the value of V_1 is a pair integer multiple of V_π.

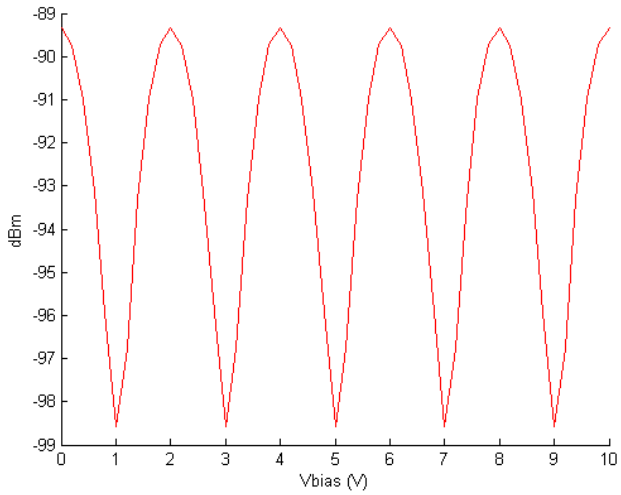

Fig. 31 - Transfer function of the MZM. Optical power as a function of the bias voltage for $V_\pi = 1$.

3.1.2. Numerical Simulations of RoF Systems

Numerical simulations were carried out to evaluate the proposed photonics-assisted amplified RoF system using OptiSystem 13.0 ® by Optiwave. The first purpose is to study the optical and electrical powers that can be reached in several points of the system; these values will be helpful to avoid damages in the experimental setup components at the laboratory. The second purpose is to obtain simulated optical and electrical spectra, which will allow us to modify some parameters in the system to improve results. And third, simulated results provide information regarding the behavior of the setup and the expected results in the experimental work in the laboratory. Fig. 32a shows the block diagram of the traditional RoF system, and Fig. 32b shows the RoF setup employed for simulation using OptiSystem ® software.

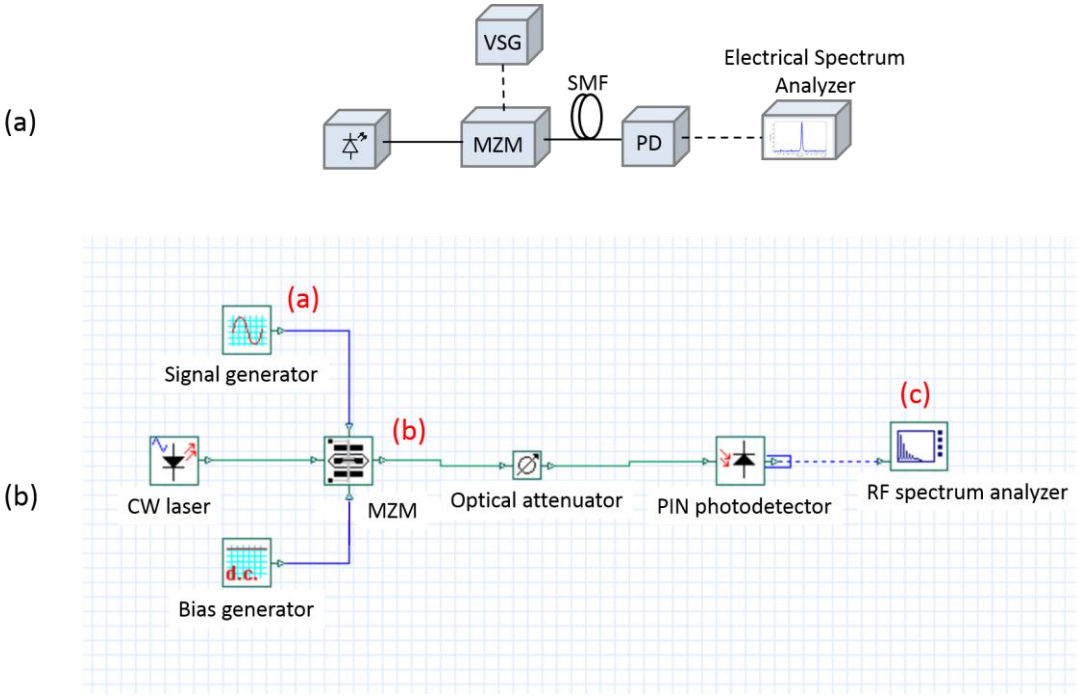

Fig. 32 - Radio over fiber (a) *Traditional setup* (b) *Scheme for simulations.*

The insets in Fig. 32b indicate the points where the three different spectrums of Fig. 30 were taken. Fig. 33a shows the sine wave used as the electrical signal that modulates the optical carrier from the CW laser. In this case, the sine wave has a frequency of 16 GHz and an electrical power of 14 dBm. An optical carrier at 1556.3 nm is modulated by the 16 GHz sine wave using a MZM modulator. Fig. 33b shows the optical spectrum obtained after modulation; the optical carrier and optical sidebands, which are the result of the intensity modulation, are observed. After modulation, an optical attenuator limits the power that feeds the photodetector. The optical signal is photodetected and analyzed using an electrical spectrum analyzer; electrical spectra is shown in Fig. 33c, which is an electrical carrier at the same frequency of the sine wave, which is 16 GHz.

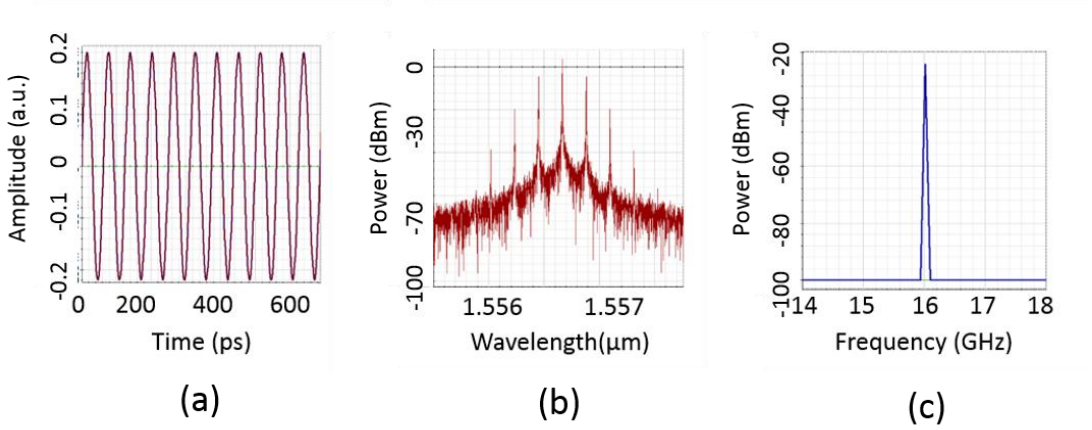

Fig. 33- Spectrum in a radio over fiber system: (a) *Sine wave;* (b) *Modulated signal;* (c) *Photodetected signal.*

Different types of spectra can be obtained depending on the V_{Bias} of the MZM; if the V_{Bias} varies, the modulation index also changes. The modulation index indicates the level of modulation applied to the carrier. If the modulation level is too low, then the modulation does not use the carrier efficiently. On the other hand, if the modulation index is too high the carrier can be over-modulated, which may cause sidebands to extend beyond the allowed bandwidth and interference. Fig. 31 shows three different cases in which the modulation index affects the optical carrier. Fig. 34a shows the spectra for high modulation index. Fig. 34b shows a modulated optical carrier with low modulation index, which occurs when the MZM is biased at the maximum transmission point of the transfer function. Fig. 31c shows an optical carrier with carrier suppression; if the MZM is biased at the minimum transmission point, odd-order optical sidebands are suppressed. Sideband suppression is mainly used for RF frequency multiplication [62]. Moreover, high modulation index allows to obtain a higher FWM efficiency, therefore increasing the FWM product's electrical power, making them more suitable for signal transmission. However, an optical carrier with a low modulation index has been shown to be optimal for data bit transmission, as it will be explained in section 3.1.3.

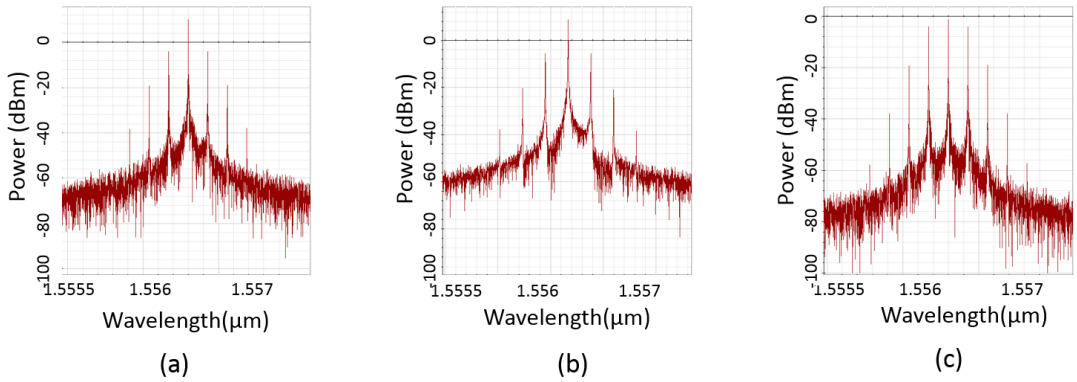

Fig. 34 - Spectrum of the modulated signal: (a) *High modulation index* V_{Bias}*=1.16V* (b) *Low modulation index* V_{Bias} *= 2V* (c) *Carrier supression* V_{Bias} *= 3V.*

3.1.3. Simulation of radio frequency amplification scheme

Fig. 35 shows the proposed scheme for radio frequency amplification using MFWM in OptiSystem ®. The two optical carriers are generated with two CW lasers at 1556.3 nm and 1559.6 nm and an optical power of 16 dBm respectively; then, a 3 dB coupler couples the carriers. A sinusoidal signal with an electrical power of 14 dBm and a frequency that varies between 4 and 19 GHz is modulating the optical carriers with a MZM. The optically amplitude modulated signals are amplified 9.1 dB by and Erbium-doped fiber amplifier and launched into 90 m of HNLF, in which the non-linear phenomena of FWM occurs and generates optical carriers at new frequencies (see Fig. 36). These new optical lightwaves contain the information of the modulated carriers. A 10/90 coupler splits the optical comb obtained at the output of the HNLF. The 10% is used to monitor the optical spectra using a spectrum analyzer. The remaining 90% passes through a 3.3 nm band pass filter that filters out the optical carrier of interest, which is feed to a 50 GHz photodetector. The photodetected signal is connected to an electrical spectrum analyzer to monitor the carrier electrical power.

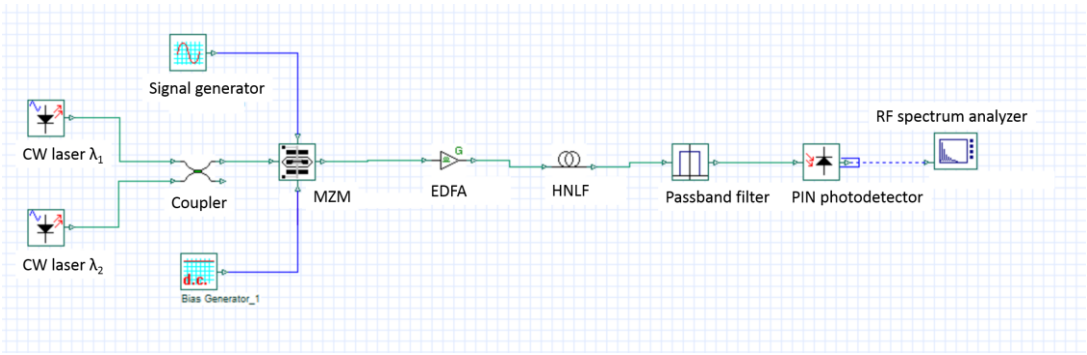

Fig. 35 - Radio over fiber scheme with HNLF for photonic amplification.

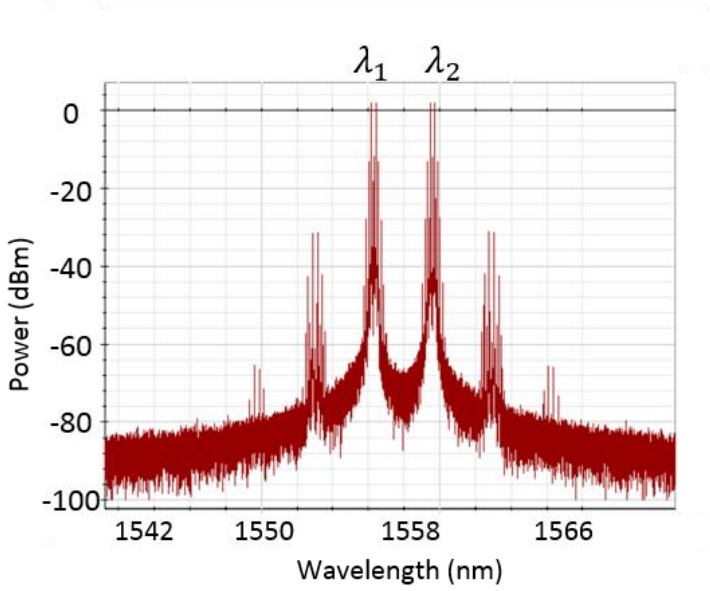

Fig. 36 - Optical spectra of the multiple four-wave mixing effect.

As mentioned in section 3.1.1, the V_{Bias} value directly affects the optical power at the output of the MZM. Simulation results showed that three different optical spectral can be obtained for different V_{Bias} values. Fig. 37 shows the three spectrum where occurs: carrier suppression for V_{Bias}= 1 V, high modulation index for V_{Bias}= 1.5 V, and low modulation index for V_{Bias} = 1.3 V.

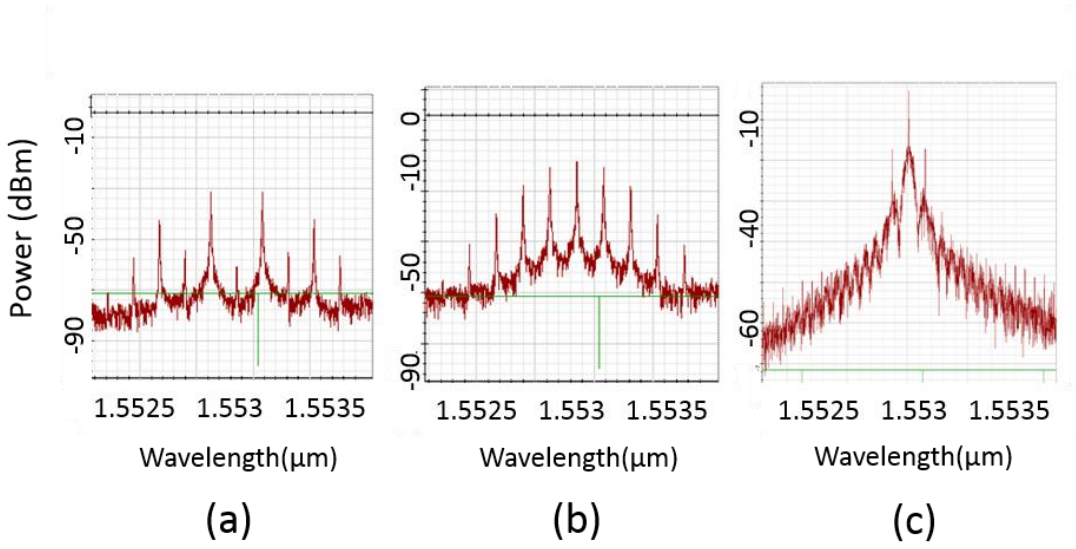

Fig. 37 – Variation V_{Bias} and its effect in optical spectra at the output of the MZM showing different modulation indexes. Left, carrier suppression. Center, high modulation index. Right, low modulation index.

Simulations carried out showed that it is possible to obtain a 29 dB RF gain when the first product of FWM is used for transmission. The optical carriers λ_1 and λ_2 had an optical power of 16 dBm, the MZM's V_{Bias}=1.969696 V, and the EDFA gain was set to 11 dB. Fig. 38 shows the 29 dB achieved amplification with the proposed system.

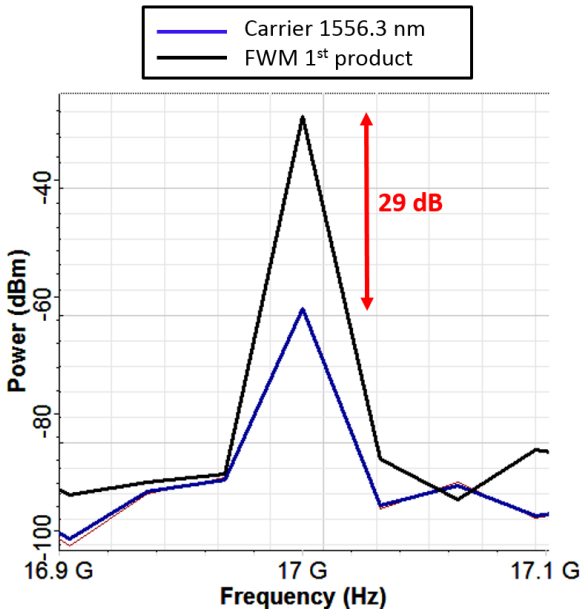

Fig. 38 - Electrical power for the carrier at 1556.3 nm and FWM 1st productat 1552.6 nm.

3.1.4. Simulation of a novel photonically amplified 10Gbit/s radio over fiber system

The photonics-based amplification setup for data transmission is show in Fig. 39a. Simulations were carried out using OptiSystem ®; the simulation setup is shown in Fig. 39b. For data transmission, the photonic assisted RoF system was simulated with an RF input signal generated by a Non-Return to Zero (NRZ) pseudo-random binary sequence combined with a 14 dB sine wave with a frequency of 17 GHz. The resulting signal is modulating the CW optical carriers through the MZM. Once the optical carriers are modulated and carry the data information, they are amplified and launched to a HNLF. The bit rate of the system is 10 Gbit/s is chosen because the purpose of this work is to study the feasibility of using CAP for metro access networks. At the output of the HNLF, an OSA monitors the optical spectra of the optical carriers and FWM products, which carry data as well.

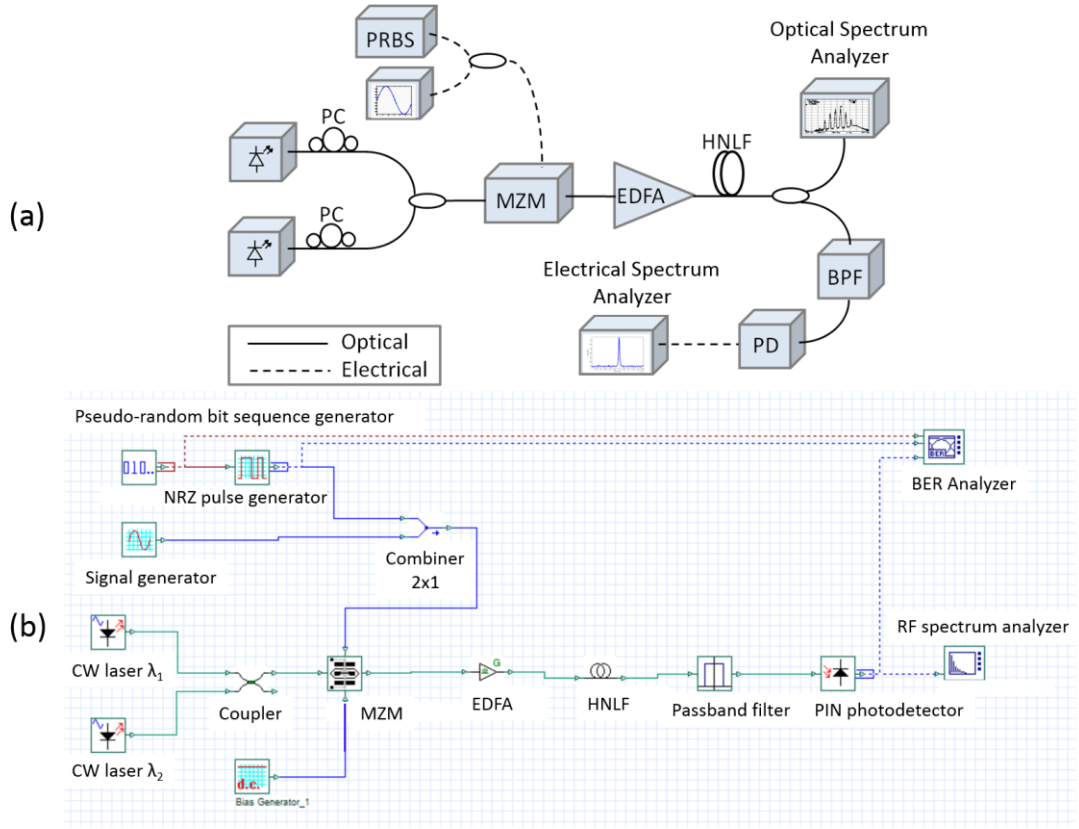

Fig. 39 – Description of the 10 Gbit/s NRZ photonic assisted radio over fiber system. (a) *Block diagram.* (b) *Simulation setup.*

The objective of this section is to compare the transmission system performance using the optical carrier and FWM product, including eye diagrams on different conditions of optical signal-to-noise radio (OSNR) for a 10-Gbit/s data rate. The purpose is to study the advantages of sending information using the FWM first product instead of using an optical carrier. To minimize the BER parameter, the value of the MZM`s V_{Bias} has to been set to V_{π}, which is 1 V for 17 GHz. Experimental and numerical results showed that by making $V_{Bias}= V_{\pi}$, the spectrum of the optical signals λ_1, λ_2, and FWM products are similar in shape and show carrier suppression as shown in Fig. 40. The setup in Fig. 39b is used for simulations. It is under the same conditions and parameter values for numerical analysis when the optical carrier λ_1 and the FWM first product are used for data transmission. In order to study the effect of attenuation in the transmission, an optical attenuator is placed after the HNLF. Attenuation is varied between 0 and 35 dB, eye diagrams and BER

are obtained for the ideal setup with no attenuation and attenuations of 20 dB, 24 dB and 35 dB.

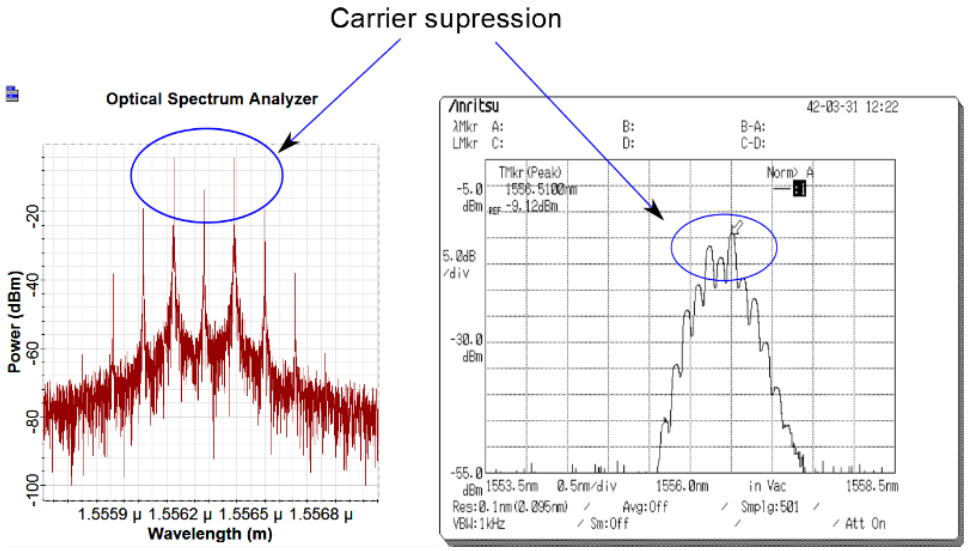

Fig. 40 - Optical spectrum for modulation V_{BIAS} = 1 V showing carrier suppression. (a) *Numerical simulation.* (b) *Experimental result.*

Fig. 41 shows the eye diagrams for different attenuations when the FWM first product and the pump carrier are used for signal transmission. First, it was studied the effect of attenuation when the FWM first product is used for data transmission. When the FWM first product is used for transmission under ideal conditions, the optical power of the filtered wave is -3.76 dBm and the BER=0, which suggests that errors are undetectable for the amount of bits used in the simulation (524,288). The eye diagram obtained for a transmission using the FWM first product with no attenuation in the signal is shown in Fig. 41a. The second case is when the attenuation is 20 dB. The optical power of the filtered carrier is -11.2 dBm, the BER obtained was 1.55×10^{-15} and the eye diagram is shown in Fig. 41b. When the FWM first product is used for data transmission and the attenuation is 24 dB, the optical power is -27.75 dBm, the BER is equal to 2.58×10^{-5} and the eye diagram is shown in Fig. 41c. The results suggest that the attenuation threshold is around 24 dB in order to avoid having a BER higher than the forward error correction (FEC) limit set to 2.7×10^{-3}.

To complete the study, the BER and eye diagrams were obtained for transmission using the optical carrier at 1556.3 nm. The first case was for an ideal transmission with no attenuation. The optical carrier had a power equal to 8.8 dBm, BER= 0 and the eye diagram is shown in Fig. 41d. When transmission has an attenuation of 20 dB, the optical power in the carrier is -11.2 dBm and the BER=0; the eye diagram is shown in Fig. 41e. And finally, to increase the BER an attenuation of 35 dB was set. The optical power in the carrier was -26.15 dBm, BER=$3.29x10^{-6}$ and the eye diagram is shown in Fig. 41f.

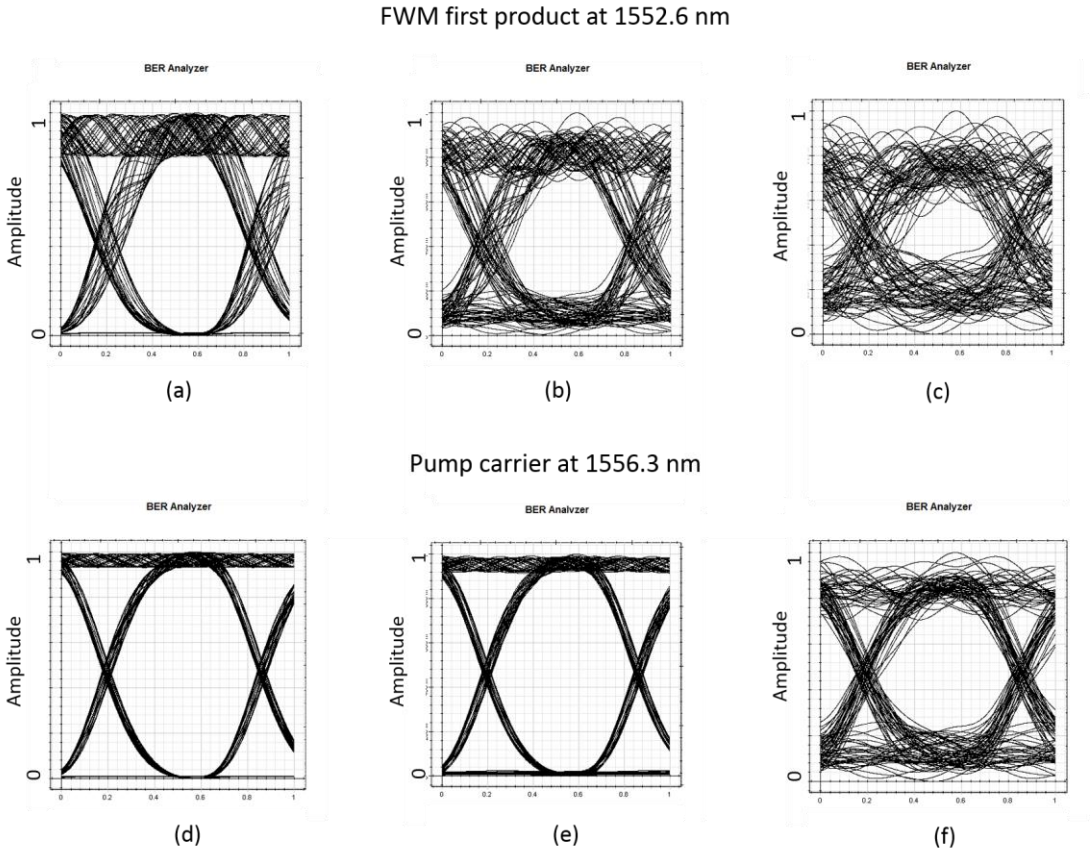

Fig. 41 - Eye diagrams for different values of optical attenuation. Data sent using the first FWM product: (a) *Attenuation= 0 dBm, BER=0;* (b) *Attenuation= 20 dBm, BER=1.55x10^{-15};* (c) *Attenuation= 24 dBm, BER=2.58x10^{-5}. Data sent using the optical carrier at 1556.3 nm:* (d) *Attenuation= 0 dBm, BER=0;* (b) *Attenuation= 20 dBm, BER=0;* c) *Attenuation= 35 dBm, BER=3.29x10^{-6}.*

Fig. 42 presents the BER results as a function of the OSNR at the entrance of the photodetector. Comparing the BER performance of the transmission using the FWM first product and the optical carrier at BER value of 2.7 x10^{-3}, which is defined as FEC limit, results show that using the optical carrier for data transmission has a power penalty of approximately 12 dB.

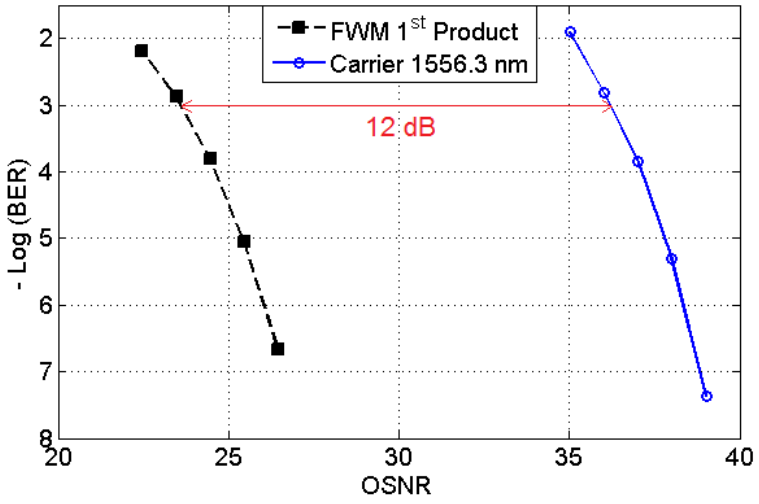

Fig. 42 - BER performance of the system.

3.2. Experimental Results of the photonics-assisted microwave amplification RoF system

Several experiments were carried out to better understand the proposed setup. These essays included optical carrier evaluation, EDFA effect in the optical and electrical power of FWM products, effect of different V_{Bias} values in the electrical power of the photodetected signal, and first FWM product electrical gain in comparison with optical carrier. A photograph of the experimental setup is presented in Fig. 43.

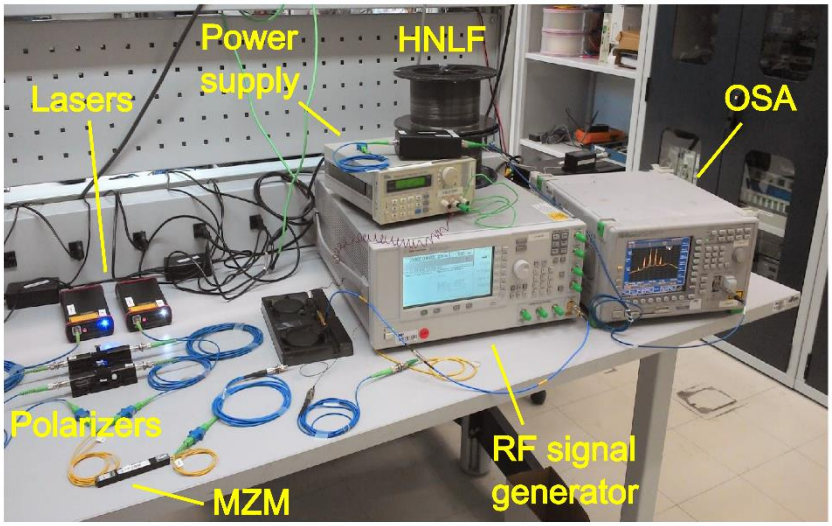

Fig. 43 - Experimental setup of the photonics-based RF amplified RoF system.

3.2.1. Optical carrier evaluation

The experimental work was carried out at the LASOR laboratory at the research and development center, CPqD, in Campinas, Brazil. The first experimental results regarding the optical carrier evaluation were carried out as follows. It consists of a B2B connection between the signal generator and the electrical spectrum analyzer (ESA), as shown in Fig. 44a. The purpose of this first part is to make sure the components that were going to be used for the complete experiment were working adequately. A sine wave was generated with a frequency of 16 GHz and a power of 0 dBm. The photodetected electrical signal is shown in Fig. 44b. The electrical power of the signal generator had to be limited to avoid damages in the ESA, for this reason an attenuator was placed in between both pieces of equipment.

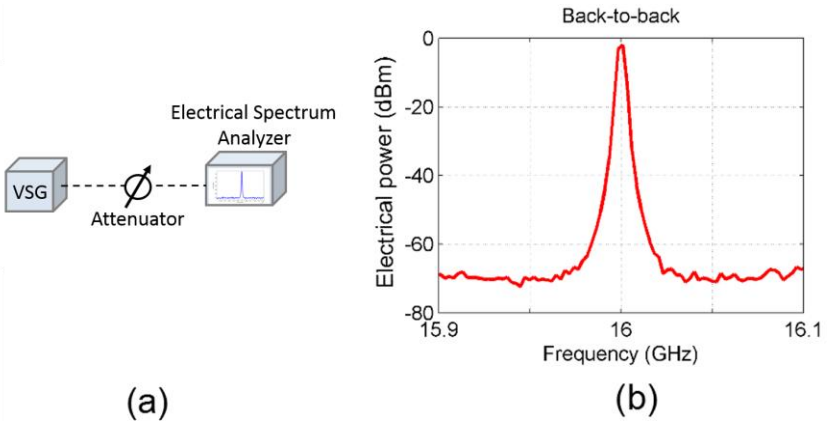

Fig. 44 - Back-to-back. (a) *Experimental setup.* (b) *Photodetected signal.*

The second experimental setup is a Radio over fiber system. The setup, in Fig. 45a, consists of a CW laser at 1556.3 nm with an optical power of 16 dBm. The electrical signal driving the MZM has a power of 0 dBm and a frequency of 16 GHz, it modulates the CW optical carrier. In this setup, the modulated optical carrier is directly connected to the photodetector using a polarization maintaining fiber (PMF). The optical signal is photodetected and the electrical spectra obtained at the ESA can be seen in Fig. 45b.

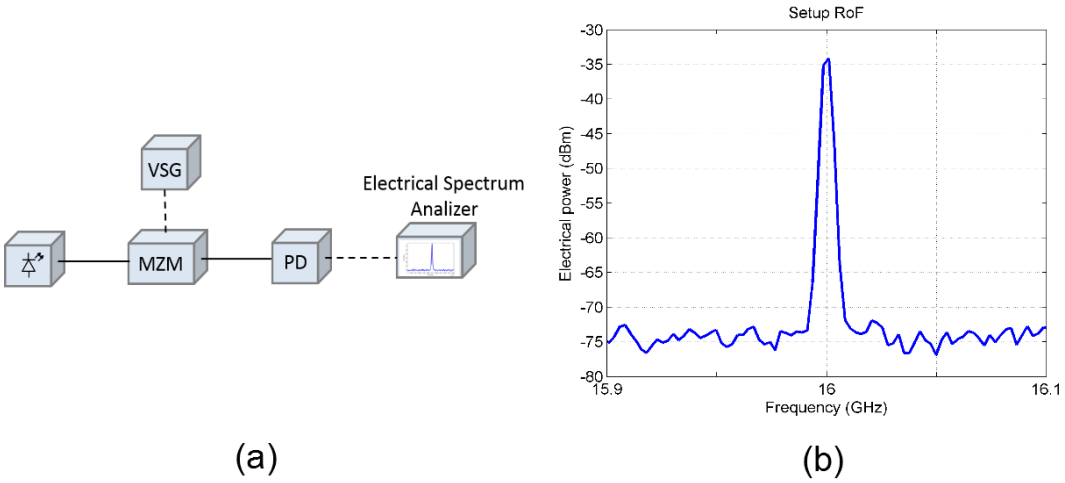

Fig. 45 - Radio over fiber. (a) *Experimental setup.* (b) *Photodetected signal.*

And finally, the third setup of the carrier evaluation, on Fig. 35 (Pag. 51), includes two coupled CW lasers, and a sine wave that modulates the CW laser

optical carriers. In the experimental setup the optical power of the lasers and the electrical power of the RF signal are set 16 dBm and 14 dBm, respectively. For this case, the frequency of the RF signal is 16 GHz. The modulated optical carriers pass through a HNLF, where the non-linear effect of FWM occurs. The high optical power of the launched carriers influence the number of FWM products. The optical spectra at the output of the HNLF is shown in Fig. 46 in which one can clearly observe the two initial pump waves and five FWM products. Then the carrier of interest is filtered out and fed to a photodetector. The optical spectra of the photodetected signal is shown in Fig. 47.

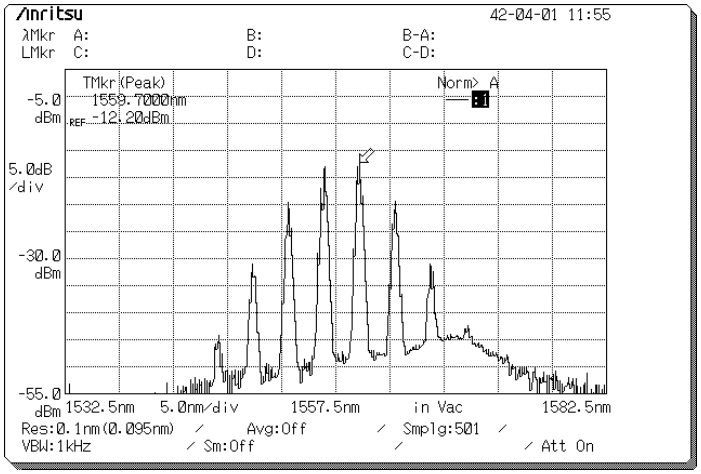

Fig. 46 - Optical frequency comb obtained by Multiple four-wave mixing.

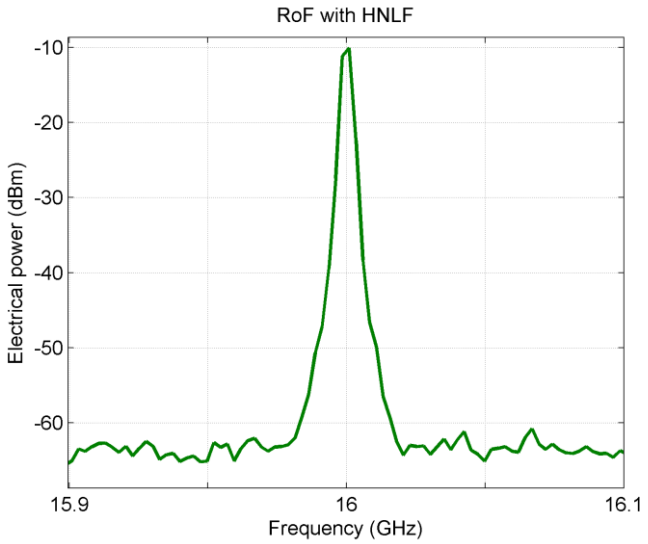

Fig. 47 – Photodetected RF signal obtained by the electrical spectrum analyzer.

3.2.2. Optimizing the RF gain as a function of the electrical and optical parameters

This section contains numerous experimental studies by varying the values of different system parameters of the scheme in Fig. 35, with the purpose of optimizing the photonics-based RF gain. The CW lasers were always at 1556.3 nm and 1559.6 nm, both with an optical power of 16 dBm, and the HNLF is from Sumitomo with the same specifications given at the beginning of this chapter, unless otherwise is stated. First, we start by varying the current of the EDFA.

One of the most important elements of the scheme in Fig. 35 is the EDFA, which controls the carriers' optical amplification. The optical power that the EDFA enhances in the optical carriers affects the FWM process. Not only it increases FWM efficiency, but also high optical power is desired to generate idler sidebands with high optical power, that can generate at the same time more new wavelengths by combining themselves with optical carriers or other products (MFWM). In this particular measurement, the purpose is to analyze the effect of the EDFA amplification in both the electrical and optical power levels of the first products of FWM.

Two different setup scenarios with different V_{Bias} are considered to analyze the influence of the variation of the current that controls the EDFA amplification. The first measure, (a), was taken in the proposed scheme with a sinusoidal RF signal set to 14 dBm, a frequency of 6 GHz, and the V_{Bias} = 6.31 V. The current that controls the EDFA amplification is varied between 0.4 and 0.7 A since the optical power in the wavelengths must be limited to avoid accidents. The relationship between the optical and electrical powers of the first products of FWM (left is stokes, and right is anti-stokes) and different values of the current in the EDFA is shown in Fig. 48a. The second measure, (b), was taken in the proposed scheme of Fig. 35 with a sinusoidal RF signal set to 14 dBm, a frequency of 6 GHz, and the MZM V_{Bias} of 8.3 V. The current that controls EDFA amplification took values starting from 0.35 to 0.9 A. The influence of the different current values in the electrical and optical power of the first products of FWM is reported in Fig. 48b.

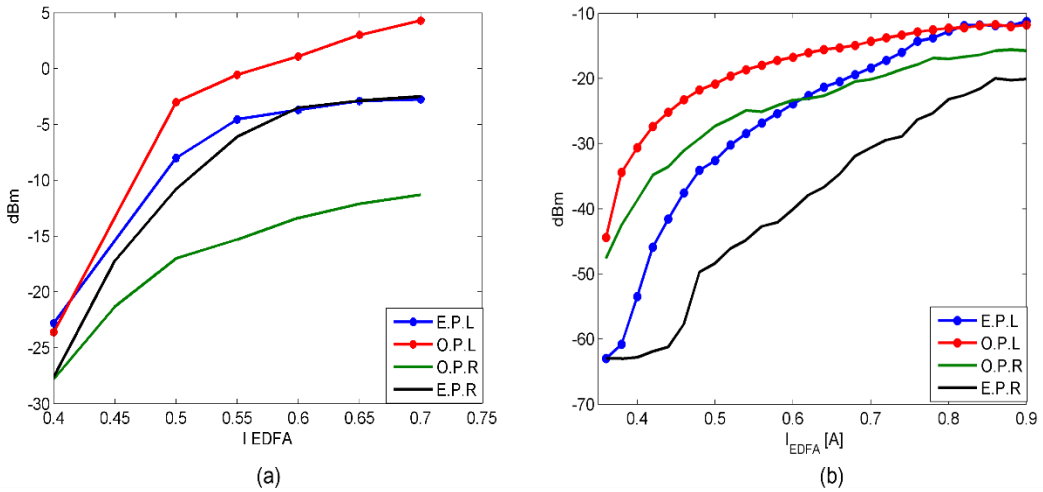

Fig. 48 - Electrical and optical power of the first products of FWM for different EDFA amplification levels: (a) *Setup with an RF signal set to 14 dBm with a frequency of 6 GHz, and* V_{Bias} *= 6.31 V;* (b) *Setup with an RF signal set to 14 dBm with a frequency of 6 GHz, and* V_{Bias} *= 8.3 V. E.P.L: Electrical power first FWM product in the left. O.P.L: Optical power first FWM product in the left E.P.R: Electrical power first FWM product in the right. O.P.R: Optical power first FWM product in the right.*

In Fig. 48a, from an EDFA current from 0.4 to 0.6 A, the electrical power of the stoke band is higher than the anti-stoke band; even though for higher values, the electrical powers of both first products tend to stabilize at the same value, which is approximately 5 dBm. Moreover, it is worth mentioning that the electrical powers of the two first FWM products are higher than their optical power levels. On the other hand, Fig. 48b shows that for the chosen system parameters, the electrical power of the Stokes band is higher than the anti-stokes band for any EDFA current (I_{EDFA}). However, for I_{EDFA} values higher than 0.8 A the electrical and optical power of the stokes band take approximately the same value, which is around -9 dBm. In addition, the anti-stokes band had a higher optical power, approximately 15 dB higher than the electrical power for an I_{EDFA} starting in 0.35 to 0.6 A. For higher I_{EDFA} values, this difference decreases but the optical power maintains a higher level. These measures were taken to analyze the feasibility of data transmission using FWM products. Consequently, results show that the Stokes band is more suitable due to its higher electrical power for different I_{EDFA} and MZM values.

Fig. 49 shows how the optical and electrical powers are related; for this case of study, the RF power and frequency were 14 dBm and 6 GHz, and I_{EDFA} = 0.8 A

and a V_{Bias} = 8.3 V. Moreover, the behavior of the optical and electrical power was measured. It is the same for different wavelengths, results were obtained measuring the anti-stokes band (first product of FWM at 1663.3 nm). According to Fig. 48b, the optical power must be higher than the electrical power of the anti-stokes band, which is confirmed in Fig. 49. In addition, it is possible to observe that the optical power is affected as well by the V_{Bias} of the MZM. Optical power presents a shape similar to the one of the electrical power, the peak and valley values occur for the same V_{Bias} in both types of powers. Moreover, the difference between the minimum and maximum optical power measured is of 10 dB. The maximum difference between the maximum and minimum point of the electrical power is approximately 40 dB.

Another parameter studied was the variation of V_{Bias} and its influence in the RF power gain; even changes as small as 0.02 V in the V_{Bias}, influence the electrical power of the wavelengths. The microwave gain is defined as the difference between the electrical power photodetected using a FWM product and that from the conventional RoF system at the same optical power level. Fig. 50 reports a comparison of the measured electrical power as a function of the modulator Bias voltage for the conventional (Fig. 45a) and photonic-assisted amplified (Fig. 29) RoF system. The RF power and RF frequency driving the MZM have been set to 14 dBm and 17 GHz respectively. An RF power gain around 24 dB and 15 dB of the FWM first product is observed for values of V_{Bias} of 1.1 and 8.6 V respectively, demonstrating the microwave amplification targeted at this work. Fig. 51 shows measured optical spectra before photo-detection associated to the three inset labels a, b and c in Fig. 50, illustrating the variation of the modulation index as a function of the V_{Bias} at the MZM.

Fig. 49 and Fig. 50 show a similar pattern in the behavior of the optical power, the maximum and minimum values are placed for the same V_{Bias} values. The minimum values occur when there is carrier suppression as shown in Fig. 51a and maximum values occur when there is a high modulation index as shown in Fig. 51b. This behavior occurs in all the optical carriers that take part of the FWM spectrum, meaning that the pump carriers and the MFWM products show a similar behavior.

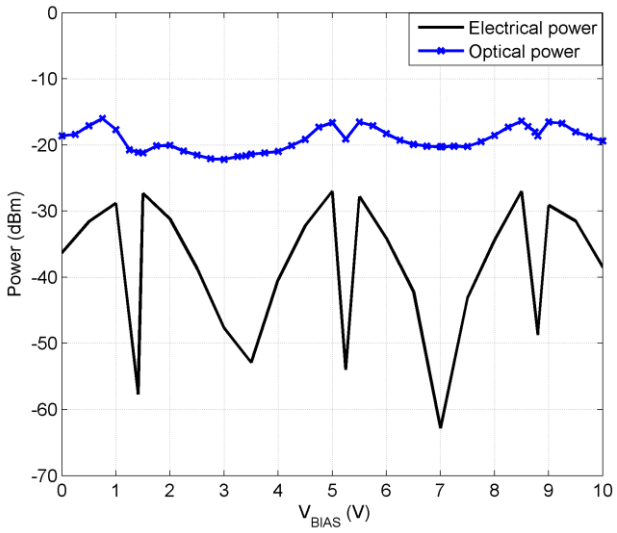

Fig. 49 - Optical and electrical power of the first product of FWM.

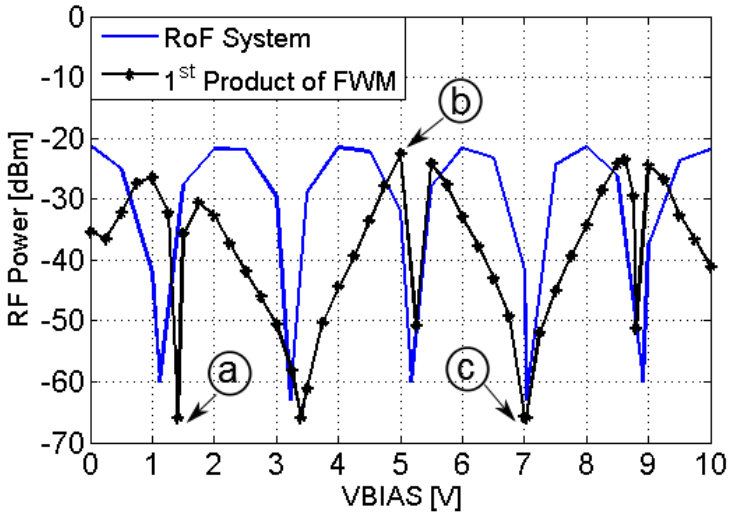

Fig. 50 – RF power as a function of modulator bias: conventional RoF system vs the first FWM product.

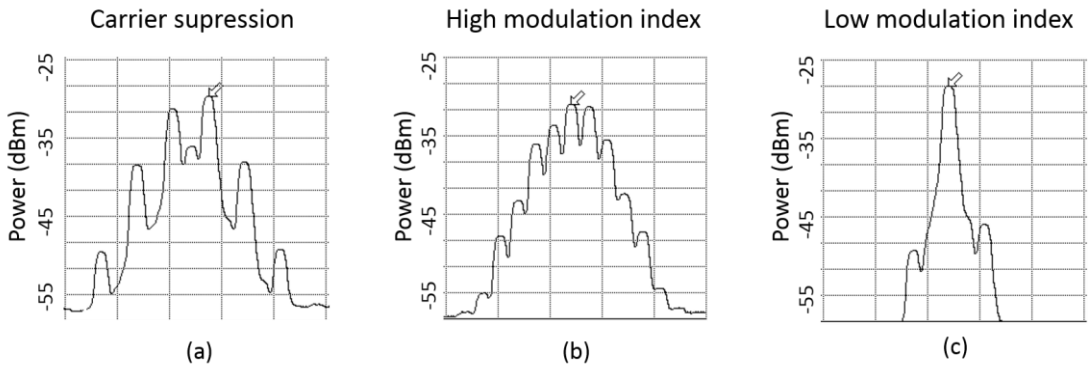

Fig. 51 - *Optical spectrum for three different conditions of modulation bias:* (a) *carrier suppression;* (b) *high modulation index;* (c) *low modulation index.*

To support obtained results related to microwave electrical gain, we proceed to obtain the electrical power spectrum of the optical carrier at λ=1556.3 nm and the first product of FWM at λ=1552.6 nm. It is worth mentioning that that the optical and electrical power levels are affected by different interferences such as dirty connectors or changes of the light polarization in the nonlinear optical fiber. Thus, Fig. 52 shows an example of the measured electrical spectra at 16 GHz for an optical power of -2.2 dBm. The measured microwave gain for this case was 24 dB.

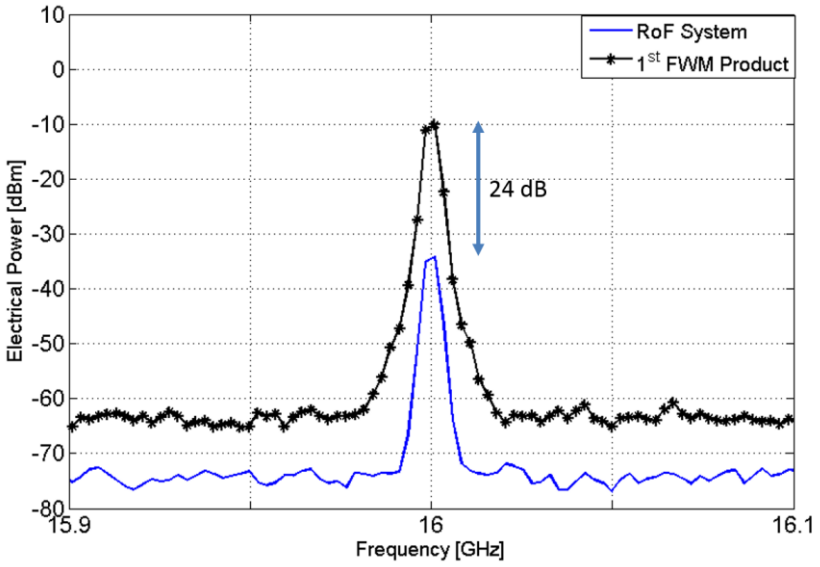

Fig. 52 - Measurement of the photonic-assisted microwave gain at 16 GHz.

Similar to the microwave gain obtained by comparing the photodetected electrical spectra of the RoF conventional system and that of the photonic-assisted amplified RoF system, there is also a microwave gain obtained when comparing the electrical power of the first FWM product to the electrical power of one of the pump carriers. Fig. 53 shows a comparison of the measured electrical power of FWM first product and optical carrier (pump) when the V_{Bias} varies. The RF power and frequency were of 14 dBm and 17 GHz, respectively. The difference in electrical power between pump and first product of FWM can be noticed specially for a V_{Bias} of 1.4, 1.7 and 3.4 V, where the electrical power of the pump exceeds the electrical power of the first product of FWM in approximately 9, 7 and 16 dB. Nevertheless, at a V_{Bias} of 1.25 and 8.75 V the first product of FWM has a gain of 17 and 19 dB, respectively over the pump`s electrical power. Moreover, a gain around 5 dB can be obtained for a V_{Bias} of 5.0, 5.5, 8.5 and 9 V.

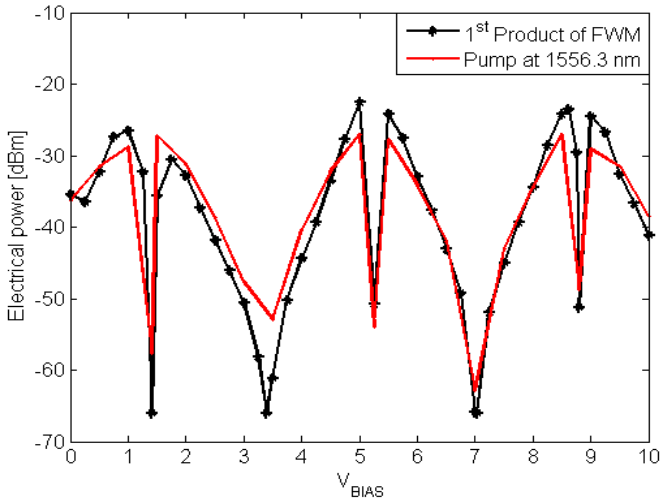

Fig. 53 - Gain analysis as a function of modulator bias comparing first product of FWM and optical carrier at 1556.3 nm.

Measures presented in Fig. 53 demonstrate that electrical gains of up to 19 dB can be obtained when electrical power of the pump and the first FWM product are compared. The electrical spectra that demonstrate that the optical power of the first product of FWM is enhanced by 6 dB in comparison to the electrical power of the

optical carrier are shown in Fig. 54. The conditions of the setup were: RF power and frequency was 14 dBm and 17 GHz, respectively. The MZM V_{BIAS} was 5 V.

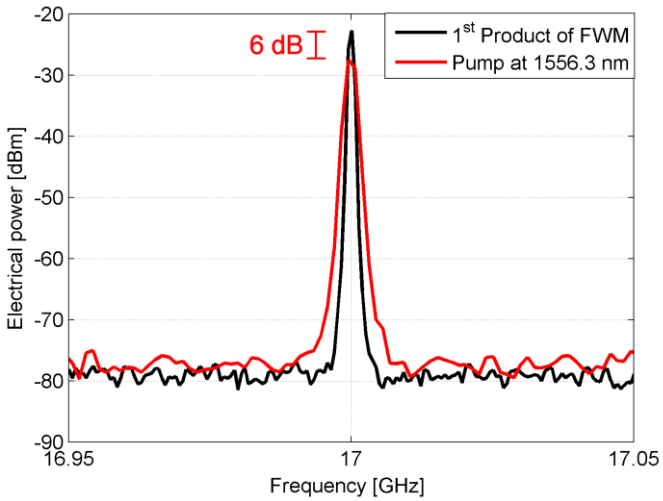

Fig. 54 –Measured electrical power at the first FWM product and optical carrier.

Microwave gain measurements were performed from 4 to 19 GHz. Fig. 55 shows the measured maximum electrical power after photo-detection of both the optical carrier at λ=1556.3 nm and the first product of FWM of the proposed scheme at λ=1552.6 nm, as a function of the RF frequency driving the MZM. The input power at the input of the MZM was set to 14 dBm and the V_{Bias} was set to 8,6 V. An electrical power gain of the FWM first product of approximately 26 dB is observed for a frequency value of 17 GHz. The highest RF gain is obtained for a frequency of 17 GHz because the polarization controllers were optimized for this frequency.

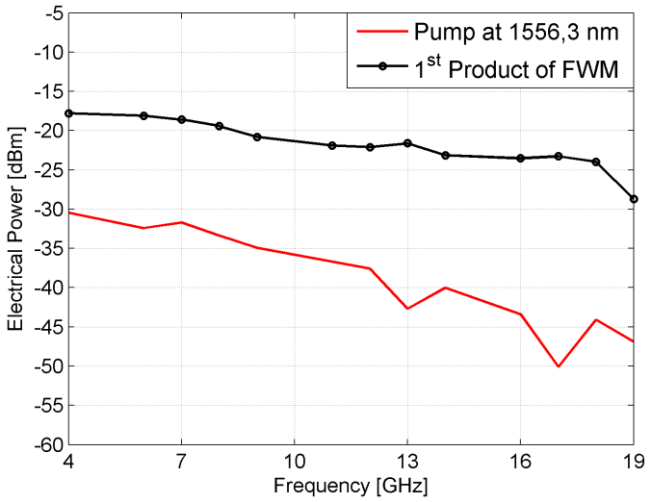

Fig. 55 - Measured gain as a function of microwave frequency.

Chapter 4

4. Photonics-based RF amplification system used for wavelength generation for a RoF system with CAP modulation

4.1. Radio over Fiber using CAP

A RoF setup with CAP modulation is shown in Fig. 56. This numerical setup consists of a CAP transmission block that creates the electrical signal that drives an electro-absorption (EA) modulator and modulates the optical carrier. The modulated optical signal is launched to a single mode optical fiber and then photodetected. The photodetected electrical signal is demodulated using the CAP reception block and data bits are recovered. Simulations were carried out to test different system configurations using OptiSystem ®. CAP modulation of different orders and bit rates have been tested and analyzed.

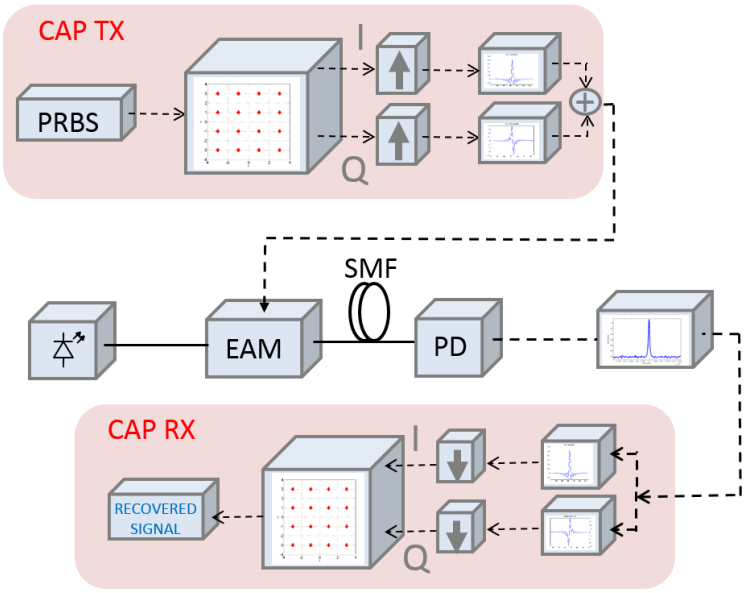

Fig. 56 - Radio over fiber system with CAP modulation. PRBS: Pseudo random bit sequence. MZM: Mach-Zehnder modulator. SMF: Single-mode fiber.

3.1.1. Co-simulation MATLAB – OptiSystem

The strategy for simulating a RoF with CAP modulation is based on the following procedure: OptiSystem ® as the main software for simulating the optical system; MATLAB for CAP modulation and demodulation. The MATLAB algorithm used in subsection 2.4.3 was slightly modified and divided into two different algorithms so that each one could be called at different moments of the simulation: transmission and reception. The first step in co-simulation is to establish a B2B connection in OptiSystem ® between the MATLAB blocks of CAP transmission and reception. A pseudo random bit generator from the transmitters/Bit sequence generator's library is used to generate the data bits that are going to be modulated; the number of bits, sample frequency, and other parameters can be modified. Then, the bit array enters into the MATLAB block along with an electrical signal, which in this case is a sine wave generator that will be used as a base for the signal at the output of the first MATLAB block (transmission), which is electrical as well. The output of the CAP transmission block is connected to the input of the MATLAB block diagram that represents CAP reception as seen in Fig. 57.

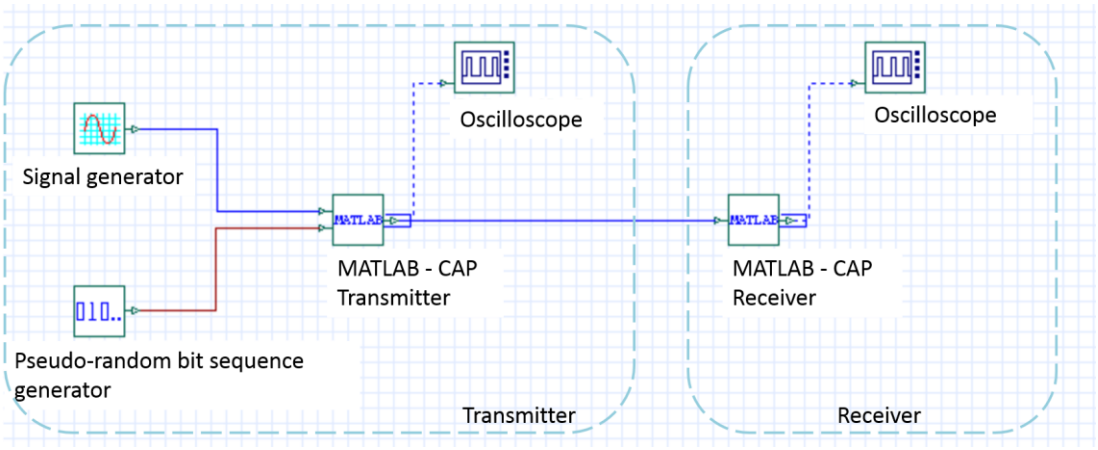

Fig. 57 - Co-simulation MATLAB-OptiSystem ®. CAP transmitter and receiver connected in Back-to-Back.

The purpose of this first simulation setup is to confirm that the algorithm works properly and therefore a low BER can be obtained. This simulation setup was designed in such a way that results could be obtained in OptiSystem ® and MATLAB. Fig. 58 shows the first bits of the data sent array, the first bits of the recovered data (both obtained using OptiSystem ®), and a figure of the overlaid first bits of sent and recovered data (obtained with MATLAB). For this first simulation, CAP-16 was the modulation format and no errors were obtained. The transmission and reception algorithms were successfully designed. The next step is to prove this algorithm on a RoF system.

(a)

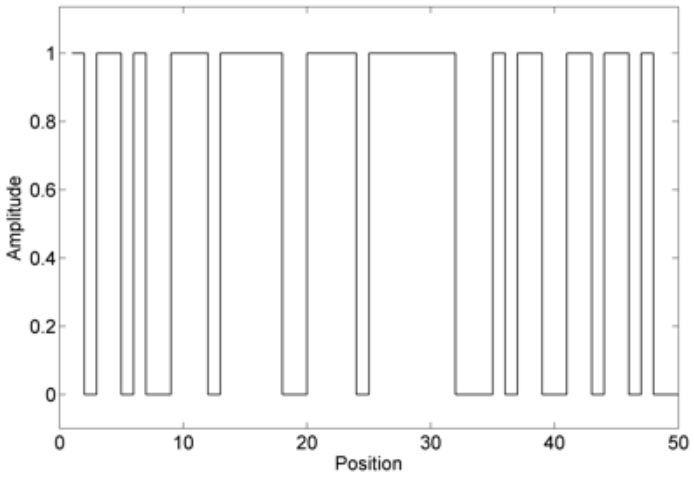

(b)

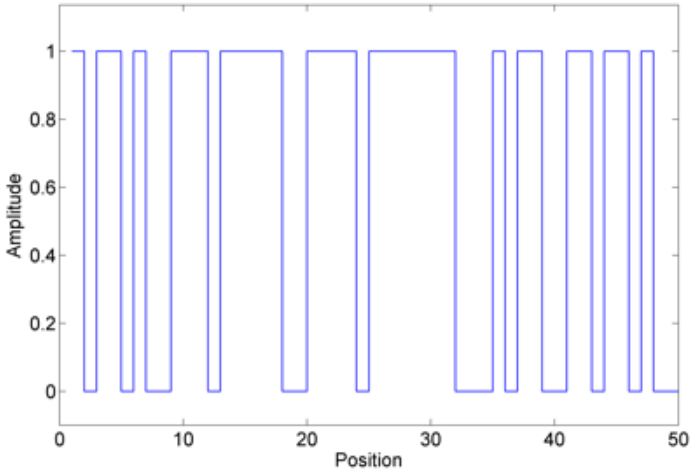

(c)

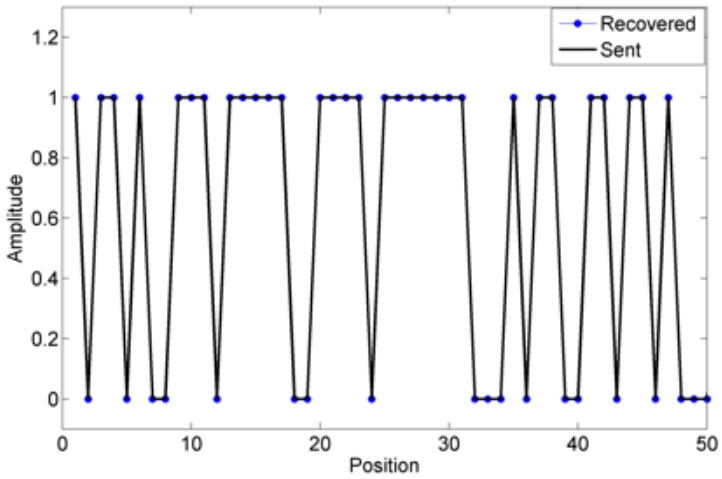

Fig. 58 - Data bits sent (a) *and recived* (b) *using OptiSystem ®, and* (c) *MATLAB.*

Different system configurations varying bit rate and M-CAP modulation format have been simulated for a data array of 16384 bits. Results are found in Table 4. Since this is an evaluation setup to prove co-simulation between MATLAB and OptiSystem ®, it is expected to have a BER=0 for the different system configurations; no noise is affecting the connection between transmission and reception blocks.

Table 4 – Simulation results of different system configurations varying CAP level and bit rate, B2B configuration.

Modulation format	Bit rate (Gbit/s)	BER
8-CAP	10	0
	20	0
	30	0
16-CAP	10	0
	20	0
	30	0
32-CAP	10	0
	20	0
	30	0
64-CAP	10	0
	20	0
	30	0
128-CAP	10	0
	20	0
	30	0

a) Radio over Fiber with CAP modulation

Once it is proven that the co-simulation between MATLAB and OptiSystem ® is working properly, CAP modulation is simulated on a conventional RoF system. The first simulation setup is the optical B2B shown in Fig. 59, which is a RoF system with intensity modulation direct detection (IM/DD). It consists of an electrical signal generated through CAP modulation that modulates the optical carrier of a CW laser (λ=1556.3 nm and optical power of 10 dB) using the analytical model of an electro-absorption (EA) modulator. EA modulator was chosen due to its low insertion loss,

broad modulation bandwidth, large extinct ratio and low wavelength chirp; this component maps electrical signals into the optical domain [92]. The modulated optical signal is launched to a SMF that is connected to a photodetector. The optical signal is photodetected and processed by the CAP reception block for bit recovery and BER calculation.

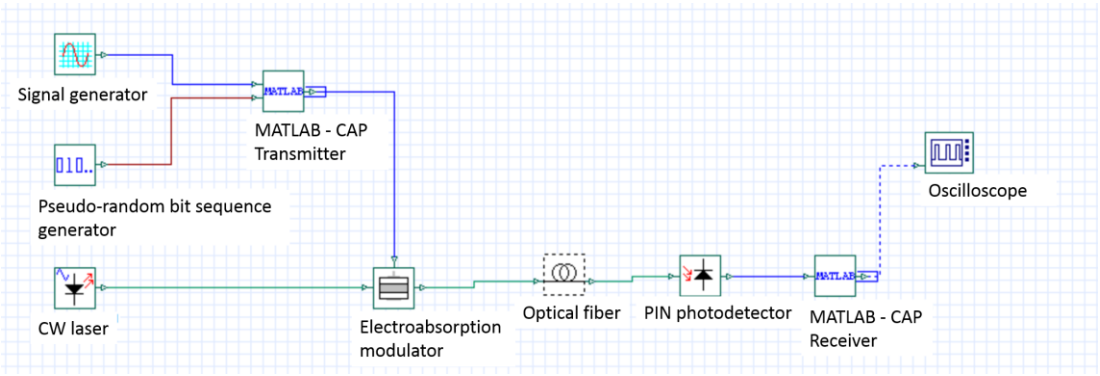

Fig. 59 - Simulation setup. Radio over Fiber with CAP modulation.

Fig. 60a shows the CAP electrical signal that drives the EA modulator, which modulates the optical carrier from a CW laser using an intensity modulator. At the output of the modulator, the optical carrier intensity varies depending on the values of the received electrical signal. Optical spectra of the modulated signal are shown in Fig. 60b. The modulated signal is launched to an optical fiber at a data rate of 10 Gbit/s; for this study, the fiber length is 0 Km since we are first establishing an optical B2B connection. Later, the optical signal is photodetected, and an RF signal is obtained, which is shown in Fig. 60c. The signal spectrum at different points of the system varies in domain (optical/electrical) and amplitude, even though its shape is maintained. At the CAP receiver block, a normalization function is used to give the original values to the incoming data. This function measures the highest and lowest symbol in the received data stream and normalizes its values according to the maximum and minimum values of the transmitted data stream. Once symbols have their original amplitude, the data stream passes through a de-mapping process to recover the bits. Finally, recovered and sent bits arrays are compared (Fig. 60d) to find the number of errors and the BER.

Different simulations were carried out varying the bit rate and the CAP level. Results showed that independent of the level of the CAP modulation format and the bit rate used in the system simulations, a BER = 0 is achieved for system with an optical B2B connection. Table 5 shows a summary of the simulations: the level of CAP modulation and the bit rate were varied.

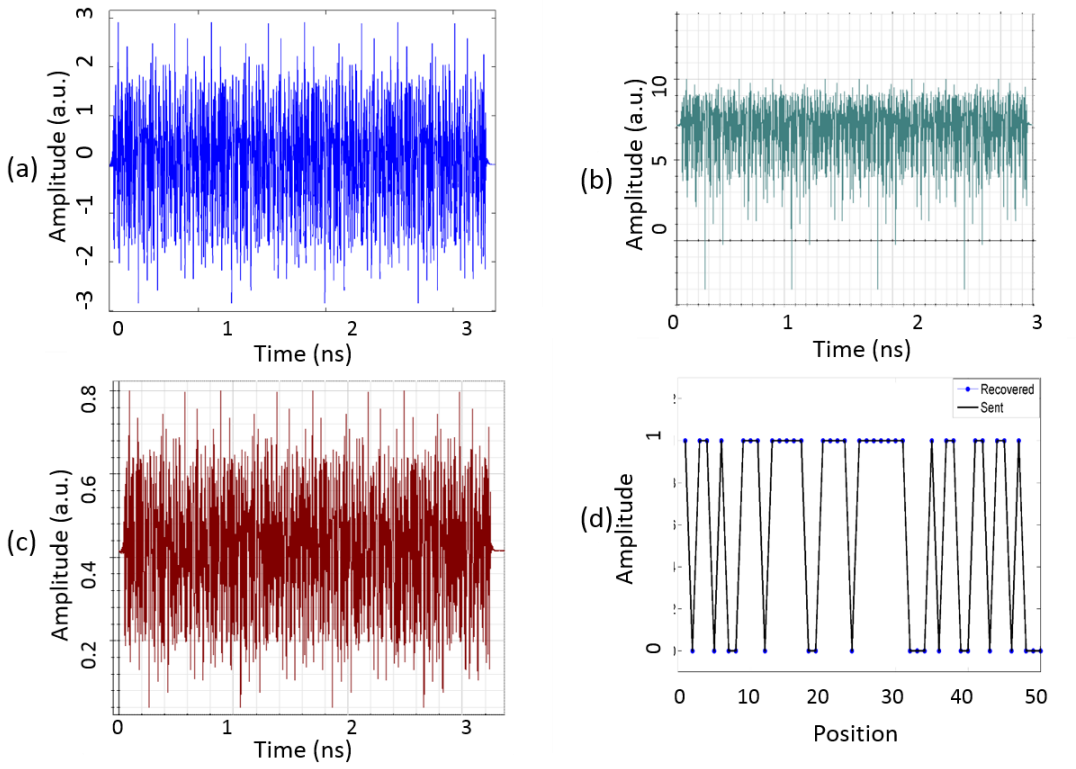

Fig. 60 - Electrical and optical spectra in the RoF system with CAP modulation: (a) *CAP generated electrical signal;* (b) *Optical spectra after modulation;* (c) *Photodetected electrical signal;* (d) *Sent and recovered bits* (BER=0).

Table 5 - Simulation results of different system configurations varying CAP level and bit rate for a RoF system with an optical B2B connection.

Modulation format	Bit rate (Gbit/s)	BER
8-CAP	10	0
	20	0
	30	0
16-CAP	10	0
	20	0

	30	0
32-CAP	10	0
	20	0
	30	0
64-CAP	10	0
	20	0
	30	0
128-CAP	10	0
	20	0
	30	0

4.2. Photonics-based RF amplification system used for wavelength generation for a RoF system with CAP modulation

The photonic-assisted microwave amplification system is used to generate the optical wavelength of a RoF system with CAP modulation. The main advantage of using this setup is the possibility to use carriers at different frequencies to transmit data; the bandpass filter filters out the optical carrier of interest that will be modulated with the CAP signal using an EA modulator. Fig. 61 shows the block diagram of the proposed scheme.

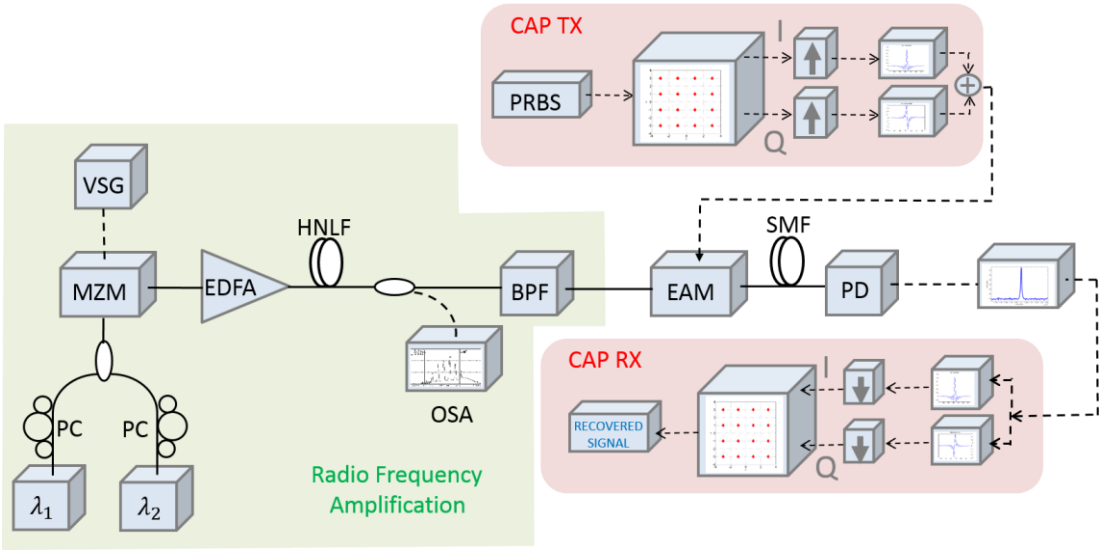

Fig. 61 - RF amplification system used for wavelength generation for data transmission using a RoF system.

To prove this scheme we carried out numerical simulations in OptiSystem ®, and Fig. 62 shows the block diagram of the simulation. The left part of the system corresponds to the photonic-based RF amplification stage. The optical carriers λ_1 and λ_2, with wavelengths values of 1556.3 nm and 1559.6 nm respectively, had an optical power fixed at 16 dBm; a 17 GHz sine-wave with a power of 14 dBm drives the MZM, which is biased at 1.969696 V. The EDFA amplifies the optical signal in 11 dB, which passes a Sumitomo HNLF (Zero-dispersion wavelength λ_0 = 1560 nm; L = 90 m; α = 0.674 dB/km; S_0 = 0.02 ps/nm^2/km; γ = 10 W^{-1}km^{-1}) and an optical filter with a bandwidth of 3.45 nm that filters the optical carrier of interest. A sequence of 16,384 bits CAP signal modulates the filtered wavelength, the bit rate was set to 10, 20 and 30 Gbit/s. Different levels of CAP are studied for each filtered wavelength and bit rate. The filtered optical wavelengths,1556.3 nm and 1552.6 nm, are fixed to have an optical power of 12.25 dBm before CAP modulation; an optical attenuator is used to adjust optical power.

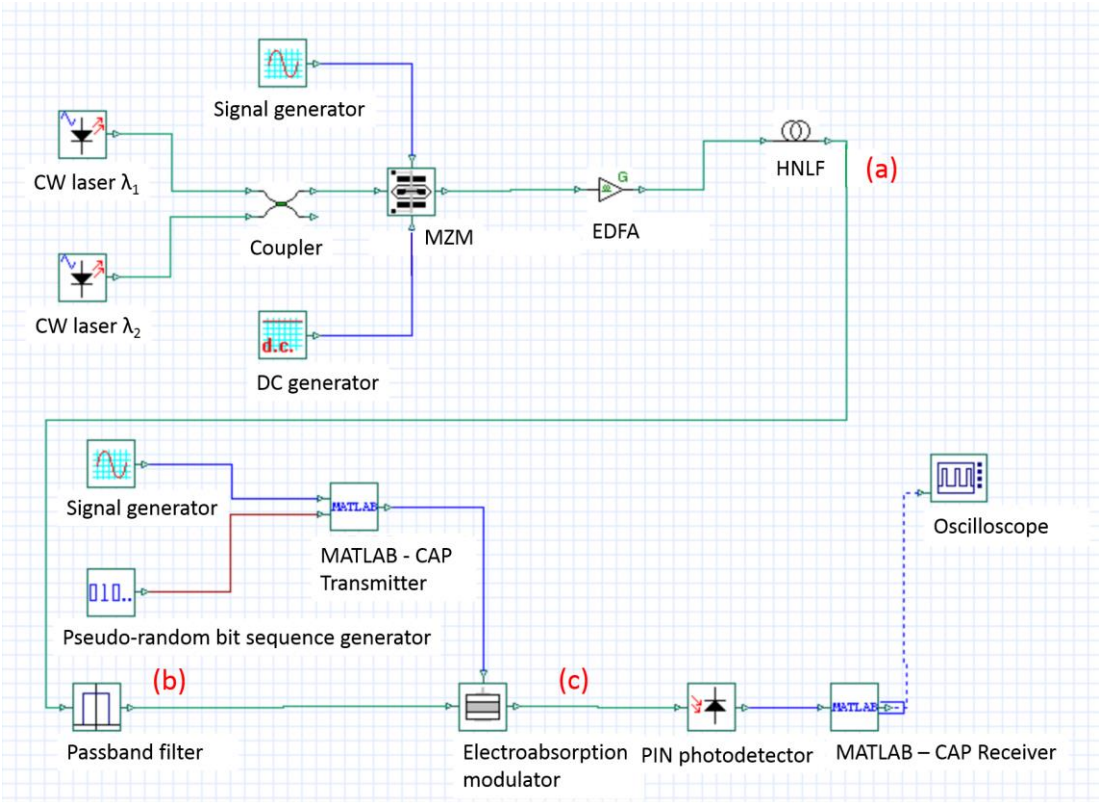

Fig. 62 - Setup for simulations; Wavelength generation and CAP modulation.

The spectra at different points of the simulation setup are shown in Fig. 63. First, Fig. 63a shows the FWM effect on the HNLF, which corresponds to point marked as (a). Then, the optical carrier chosen for modulation is filtered out using a bandpass filter, and its optical spectra is shown in Fig. 63b, spectrum taken at point marked with inset (b) on the simulation setup (Fig. 62). Once the optical carrier is modulated with the CAP signal (Fig. 63c, spectrum obtained at point marked with inset (c) in Fig. 62), it is photodetected and the data bits are recovered. Fig. 63d shows that the bit recovery is successful, the first 100 sent and recovered bits are overlaid in this figure as a proof of this result.

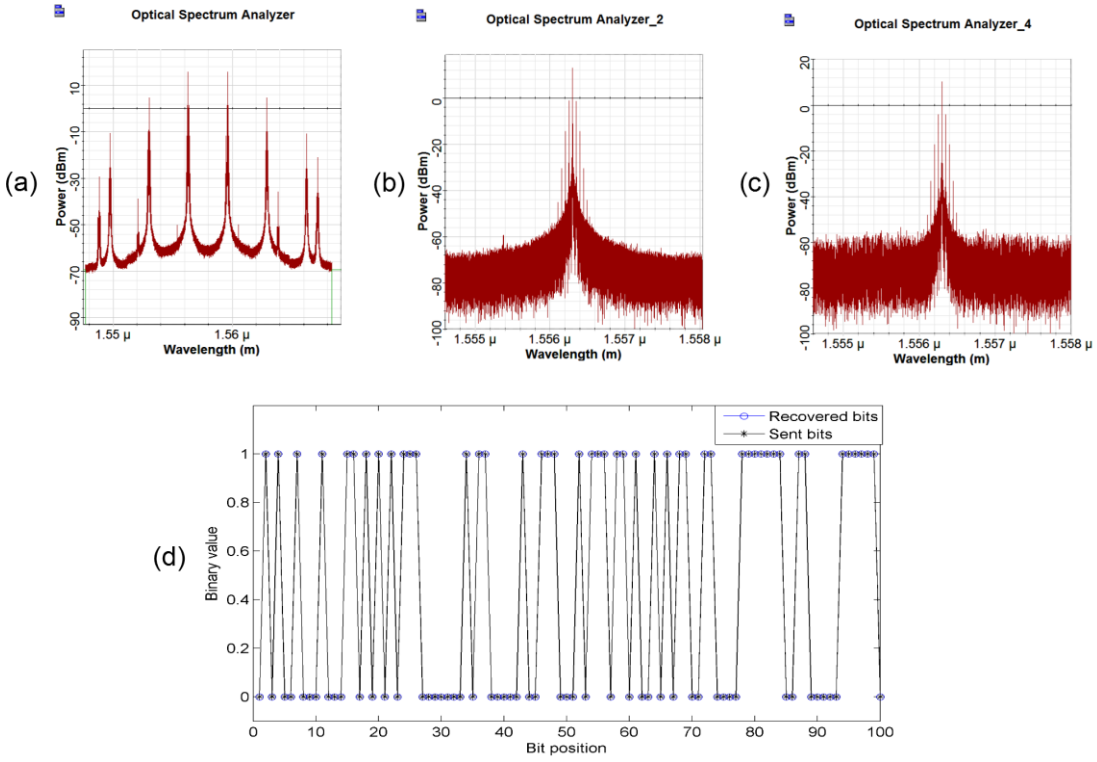

Fig. 63 - Optical spectra at different points of the simulation setup: (a) FWM at the end of the HNLF; (b) Filtered optical carrier; (c) Optical carrier modulated by a CAP signal; (d) Recovered bits Vs. Sent bits.

Table 6 contains the results obtained from the simulations carried out for CAP transmission on a RoF system with an optical B2B connection.

Table 6 - Results obtained for CAP modulation using optical carrier at 1556.3 nm

Modulation format	Bit rate (Gbit/s)	BER	Electrical power (dBm)
	10	0	-24,110
8-CAP	20	0	-25,030
	30	0	-25,230
	10	0,00134277	-24,311
16-CAP	20	0	-25,760
	30	0	-25,210
	10	0,03302002	-24,111
32-CAP	20	0	-26,420
	30	0	-26,310

	10	0,08654785	-24,532
64-CAP	20	0	-24,620
	30	0	-24,612
	10	0,14324951	-24,123
128-CAP	20	0	-26,123
	30	0,00018311	-26,932

Simulations carried out using the first FWM product for signal transmission show that a higher amount of errors can occur in transmission at lower bit rates; in this case, errors were obtained for data transmission at 10 Gbps. Results that show a BER=0 indicate that the number of errors is undetectable for the amount of bits that were used in the simulation, which were a total of 16384 and 128 samples per bit.

Table 7 - Results obtained for CAP modulation using FWM product at 1552.6 nm.

Modulation format	Bit rate (Gbit/s)	BER	Electrical power (dBm)
	10	0,16168213	5,102
8-CAP	20	0,03173828	4,956
	30	0,03308105	4,732
	10	0,25305176	4,012
16-CAP	20	0,05285645	3,670
	30	0,05554199	3,990
	10	0,31170654	3,876
32-CAP	20	0,13134766	3,923
	30	0,13470459	3,982
	10	0,3460083	3,290
64-CAP	20	0,16534424	3,901
	30	0,15496826	4,012
	10	0,36090088	3,787
128-CAP	20	0,20947266	3,125
	30	0,20269775	3,120

Simulations carried out using the FWM first product for data transmission show that data is received with a higher BER in comparison to the BER of the data received when the optical carrier at 1556.3 nm was used for transmission. Moreover,

results show that the BER increases as the level of CAP used in the modulation, and also as the bit rate decreases. Similar BER were obtained for 20 and 30 Gbps, as well as a similar value in the optical power before photodetection.

In general, simulations show that sending data using the optical carrier has a lower BER, and results indicate that data will be successfully recovered. Moreover, simulation results show that the number of errors increases with the level of CAP modulation used. Furthermore, the number of errors is lower at the highest bit rate, 30 Gbps. Since the optical power of both the wavelengths at 1556.3 nm and 1552.6 nm is the same, it is possible that the BER is higher when the information is sent using the first product of FWM due to interference caused in the CAP modulation stage. The effect of a higher optical power in the source signal was studied, however the noise increment caused by optic amplification decreased the signal quality, which did not benefit the BER. It is worth mentioning that the RF gain between the FWM first product and the optical carrier, which were used as a source for data transmission, was approximately 29 dB. This RF gain maintained after CAP modulation, the electrical power was higher but the difference between the electrical peak powers of the carriers at 1556.3 n and 1552.6 nm was 29 dB.

In addition, the effect of higher optical power in the laser sources was studied. Results show that an increased optical power in the sources only affects the number of products of FWM; the higher the power of the optical carriers, the more FWM products in the comb optical spectra. Therefore, the optical power of the filtered carrier is limited to a power around 16 dBm, because for higher optical powers, it will be distributed to the new wavelengths generated through FWM, and not in the optical power of the FWM first products.

Chapter 5

5. Conclusions and Future Works

This work is based on the study and development of a novel radio over fiber based approach for photonics-based amplification of radio frequency signals using four-wave mixing. Its main objective was to evaluate the proposed system feasibility for data transmission in convergent networks based on optical backhauls. Moreover, the aim of the study had other two principal purposes: i) analysis of the proposed scheme for data transmission using the first product of FWM, ii) feasibility of including CAP modulation for high capacity transmission.

Chapter 1 included an overview of the subscribers increasing demand for higher internet data rates due to current services requirements, the need of optical wireless networks for mobile communications, and the need of new modulation formats to meet the bandwidth capacity and speed requirements. In addition, this chapter includes a bibliographic review of the main works in the areas of broadband communications, radio over fiber, and four-wave mixing. This state-of-the-art allowed understanding not only the radio over fiber development over the years, but also it was the key to find a gap in the research area in which it could be possible to make a contribution.

Chapter 2 presented the main technologies studied during the development of this work. A theory study was carried out in microwave photonic generation, multiple four-wave mixing and carrierless amplitude phase modulation; mathematical equations and simulation results included. Whereas Chapter 3 included the simulation study of a radio over fiber system with CAP modulation. First, the

radio over fiber technology was briefly explained, and an introduction to RoF systems with CAP modulation was included to justify our efforts in this area. Numerical simulations and experimental results are presented in Chapter 4 with the purpose of proving the feasibility of the proposed RF amplification system. Numerical simulations were carried out using the OptiSystem ® software by Optiwave Inc. Experimental results were carried out at the LASOR laboratory of the Research and development center CPqD in Campinas, Brazil.

We proved experimentally that photonic amplification of RF signals could be achieved using the first FWM product. Experimental results showed gains up to 24 dB could be achieved when comparing the photodetected signal spectra of the first product of FWM and that of a traditional RoF system. Moreover, if the first FWM product is compared to one of the optical carriers, a RF gain of up to 26 dB can be achieved. We could experimentally demonstrate that photonic-based amplification using the first product of FWM can be accomplished for frequencies between 4 and 19 GHz. These results motivated us to study through simulations the possibility of data transmission using the proposed photonic amplification RoF system. We proved that data transmission at 10 Gbit/s is possible, even though there is a 12 dB penalty for transmission when the first product of FWM wavelength is chosen.

Furthermore, we wanted to use an advanced modulation format in our proposed scheme, and we chose CAP due to the low complexity of its transmitter and receiver blocks. On the one hand, we successfully implemented a photonics-based RoF amplification scheme that generates optical carriers at different frequencies with high electrical power. On the other hand, we study CAP as data modulation format to improve the transmission bit rate. Finally, we simulated a traditional RoF system with CAP modulation, achieving a BER = 0 for a B2B connection. Then, we include the photonics-based amplification setup to generate an optical carrier that is modulated with the CAP signal in a radio over fiber system. Simulation results show a BER = 0 when using an optical carrier for data transmission and 8-CAP to 32-CAP modulation formats. The use of the first product of FWM as the optical carrier that is modulated by the CAP signal has been proven to be inadequate due to its lower optical power when compared to the power of the optical carrier.

Future works

The novel photonically amplified RoF system opens the door to new high capacity and longer reach fiber wireless systems compared to conventional RoF architectures. Further experimental evaluations are strongly recommended as next steps to identify system design challenges and improvements.

Moreover, we propose to carry out more experiments to validate CAP modulation including a traditional RoF scheme to continue research in this area including transmission with antennas designed at the Laboratory WOCA from Inatel. Another interesting effect to be studied in the RoF with CAP modulation setup is the fiber length. RoF systems are commonly used in FTTH, therefore the effect that different fiber lengths may have on signal transmission and recovery is useful for future applications. Furthermore, we propose the implementation of a RoF system with CAP modulation using a field programmable gate array (FPGA). The FPGA will allow us to enable or disable photonic amplification and transmission using optical carrier or FWM product.

We also encourage studying ways of compensating nonlinearities in optical fibers to ensure a successful data recovery. In addition, it would be interesting to see how the photonic amplification scheme proposed can be used to generate optical carriers at different frequencies for different purposes.

References

[1] International Telecommunication Union, "*Measuring the information society 2014",* Geneva, November 2014.

[2] C. A. Brackett, "*Dense wavelength division multiplexing networks> principles and applications"*, IEEE journal on selected areas in communications, vol. 8, No. 6, 1990, pages 948-964.

[3] C. C. Davis, I. I. Smolyaninov, and S. D. Milner, "*Flexible optical wireless links and networks"*, IEEE Communications magazine, Vol. 31, No. 3, March 2003, pages 51-57.

[4] D. J. T. Heatley et al., "*Optical Wireless: The story so far*", IEEE communications magazine, December 1998.

[5] D.K. Borah et al. "*A Review of Communication-oriented Optical Wireless Systems"*, EURASIP Journal on Wireless Communications and Networking, 2012, pages 1-28.

[6] V. Garg, "Wireless communications & Networking", Morgan Kaufmann, 2010.

[7] D. P. Agrawal, and Q. Zeng, "*Introduction to wireless and mobile systems",* 4th edition, Cengage Learning, 2014.

[8] D. J. Goodman, "*Trends in cellular and cordless communications"*, IEEE communications magazine, Vol. 29, No. 6, 1991, pages 31-40

[9] Q. Bi, G. I. Zysman, H. Menkes, "*Wireless Mobile communications at the start of the 21st century"*

[10] S. Ohmori, Y. Yamao, N. Nakajima, "*The future generations of mobile communications based on broadband access technologies", IEEE* communications magazine, vol. 38, No. 12, 2000, pages 134-142

[11] P. J. Winzer, and R. J. Essiambre, "*Advanced Optical Modulation Formats"*, Procedings of the IEEE, vol. 94, No. 5, 2006, pages 952-985.

[12] J. Proakis, "*Digital Communications*", 3rd edition, McGraw-Hill Inc., 1995

[13] R. Gitlin, J. F. Hayes, and S. B. Weinstein, "*Data communications principles*", New York: Plenum, 1992.

[14] C. E. Shannon, "*A mathematical theory of communication",* Bell System Technical Journal, vol. 27, 1948, pages 379-423, 623-656.

[15] R. J. Essiambre, G. Kramer, P. J. Winzer, G. J. Foschini, and B. Goebel "*Capacity limits of optical fiber networks*", Journal of Lightwave technology, vol. 28, No. 4, 2010, pages 662-701.

[16] J. Conradi, I. Kaminow and T. Li, "*Bandwidth-efficient modulation formats for digital fiber transmission systems",* in *Optical Fiber Telecommunications IV*-B, Academic Press, 2002, pages 862-901.

[17] P. J. Winzer, R. J. Essiambre, and S. Chandrasekhar, *"Dispersion-tolerant optical communication systems"*, in Procedings of European conference of Optical Communication (ECOC), 2004, We2.4.1.

[18] R. A. Griffin, and A. C. Carter, "*Optical differential quadrature shift key (oDPSK) for high-capacity optical transmission",* Procedings Optical Fiber Communications conference (OFC), 2002, WX6

[19] M. Ohm, "*Optical 8-DPSK and receiver with direct direction and multilevel electrical signals"*, IEEE/LEOS Workshop of advanced modulation formats, 2004, pages 44-46

[20] M. Ohm, and J. Speidel, "*Quaternary optical ASK-DPSK and receivers with direct detection"*, IEEE Photonics Technology Letters, Vol. 15, No. 1, 2003, pages 159-161

[21] S. Hayase, N. Kikuchi, K. Sekine, and S. Sasaki, *"Proposal of 8-state per symbol (binary ASK and QPSK) 30-Gbit/s optical modulation/demodulation scheme"*, Procedings European conference of Optical Communication (ECOC), 2003, Th2.6.4.

[22] S. Randel, F. Breyer, S. C. J. Lee, "*High-speed transmission over multimode optical fibers",* Optical communications conference/National fiber optic Engineers conference, 2008, paper OWR.2

[23] I. Kalet, "*The multitoned channel"*, IEEE Transactions in communications, vol. 37, No. 2, 1989, pages 119-124

[24] T. Tanaka, and M. Nishihara, "*Experimental investigation of 100-Gbps transmission over 80-km single mode fiber using discrete.multitone modulation"*, Procedings SPIE 8646, Optical metro networks and short-haul systems, 2013, vol. 8646.

[25] K. Szczerba, B. E. Olsson, P. Westbergh, A. Rhodin, J. S. Gustavsson, A. Haglund, M. Karlsson, A. Larsson, P. A. Andrekson, "*37 Gbps transmission over 200m of MMF using single cycle subcarrier modulation and a VCSEL with 20 GHz modulation bandwidth"*, European Conference on Optical Communication (ECOC), 2010, paper We.7.B.2

[26] A. S. Karar, and J. C. Cartledge, "*Generation and detection of a 112-Gb/s dual polarization signal using a directly modulated laser and half-cycle 16-QAM Nyquist-subcarrier-modulation"*, European conference on optical communication (ECOC), 2012, paper Th.3.A.4

[27] J. L. Wei, D. G. Cunningham, R. V. Penty, and I. H. White, "*Study of 100Gigabit Ethernet using carrierless amplitude/phase modulation and optical OFDM"*, Journal of lightwave technology, vol. 31, No. 9, 2013, pages 1367-1373

[28] L. Tao, Y. Wang, Y. Gao, N. Chi, and C. Lu, " *Experimental demonstration of 10 Gb/s multi-level carrier-less amplitude and phase modulation for short range optical communication systems"*, Optics express, vol. 21, No. 5, 2013, pages 6459-6465.

[29] J. D. Ingham, R. V. Penty, and I. H. White, "*40 Gb/s carrierless amplitude and phase modulation for low cost optical datacommunication links",* Procedings Optical Fiber Communications conference (OFC), 2011, paper OThZ3

[30] J. Zhang, J. Yu, F. Li, N. Chi, Z. Dong, and X. Li, "*11x5x9.3Gb/s WDM-CAP-PON based on optical single-side band multi-level multi-band carrier-less amplitude and phase modulation with direct detection"*, Optics express, Vol. 21, No. 16, 2013, pages 18842-18848

[31] D. D. Falconer, "*Carrierless AM/PM*" in Bell Laboratories Technical Memorandum, 1975

[32] The ATM Forum, Technical Committee, "155.52 Mb/s Physical Layer Specification for Category-3 Unshielded Twisted Pair", 1995

[33] International Telecommunication Union, Telecommunication Standardization Sector; "G.991.1 : High bit rate digital subscriber line (HDSL) transceivers", 1998

[34] A. Shalash, and K. K. Parhi, "*Comparison of discrete multitoned and carrierless AM/PM techniques for line equalization"*, IEEE International symposium on circuits and systems, vol. 2, 1996, pages 560-563.

[35] A. K. Vyas, N. Agrawal, "*Radio over fiber: future technology of communication"*, International Journal of Emerging Trends & Technology in Computer Science IJETTCS, Vol. 1, No. 2, 2012.

[36] L. Zhang, X. Hu, P. Cao, T. W., and Y. Su, "*A multiband radio over fiber system using one single-drive MachZehnder modulator*," Communications and Photonics Conference and Exhibition (ACP), 2010, pages 449,450

[37] D. Wake, A. Nkansah, N. J. Gomez, G. de Valicourt, R. Brenot, M. Violas, Z. Liu, F. Ferreira, and S. Pato, "*A comparison of Radio over Fiber Link types for the Support of Wideband Radio Channels",* IEEE Journal of Lightwave Technology, Vol. 28, No. 16, 2010.

[38] D. Wake, M. Webster, G. Wimpenny, K. Beacham, L. Crawford, "*Radio over fiber for mobile communications"*, IEEE international Topical Meeting, 2004, pages 157-160

[39] L. Noel, D. Wake, D. G. Moodie, D.D. Marcenac, L.D. Westbrook, D. Nesset, "*Novel techniques for high capacity 60-GHz fiber-radio transmission systems, Microwave theory and techniques"*, IEEE transactions, Vol.45, No. 8, part 2, 1997, pages 1416-1423

[40] P. Horváth, I. Frigyes, "*Effects of the nonlinearity of a mach-zehnder modulator on OFDM Radio-over-fiber transmission"*, IEEE communications letters, Vol. 9, No. 10, 2005, pages 921-923

[41] R. Abdolee, R. Ngah, V. Vakilian, T. A. Rahman, *"Application of Radio-over-Fiber (ROF) in mobile communication"*, Asia-Pacific conference on applied electromagnetics procedings APACE2007, December 2007.

[42] J.R. Thompson and R. Roy, "*Nonlinear dynamics of multiple four-wave mixing processes in a single-mode fiber*", Physical Review A, Vol. 43, No. 9, May 1991, pages 4987-4996.

[43] S. Trillo, S. Wabnitz, and T.A.B. Kennedy, "*Nonlinear dynamics of dual-frequency-pumped multiwave mixing in optical fibers*," Physical Review A, Vol. 50, No. 2, Aug. 1994, pages 1732–1747.

[44] X. Xu, Y. Yao, X. Zhao, and D. Chen, "*Multiple Four-Wave-Mixing Processes and Their Application to Multiwavelength Erbium-Doped Fiber Lasers*", Journal of Lightwave Technology, Vol. 27, No. 14, Jul. 2009, pages 2876-2885.

[45] K. Inoue, "*Four-Wave Mixing in an Optical Fiber in the Zero-Dispersion Wavelength Region*", Journal of Lightwave Technology, Vol. 10, No. 11, 1992, pages 1553-1561.

[46] K. Nakajima, M. Ohashi, K. Shiraki, T. Hiroguchi, and Y. Miyajima, "*Four-wave mixing suppression effect of dispersion distributed fibers"*, Journal of Lightwave Technology, Vol. 17, No. 10, 1999, pages 1814-1822

[47] M. Sauer, A. Kobyakov, A. B, Ruffin, "*Radio-over-fiber transmission with mitigated stimulated Brillouin scaterring"*, IEEE Photonics Technology Letters, Vol. 19, No. 17, 2007, page 1487.

[48] G. H. Smith, D. Novak, Z. Ahmed, *"Overcoming chromatic-dispersion effects in fiber-wireless Systems Incorporating External Modulators"*, IEEE transactions on Microwave theory and techniques, Vol. 45, No. 8, 1997, pages 1410-1416.

[49] G. H. Smith, D. Novak, Z. Ahmed, *"Technique for optical SSB generation to overcome dispersion penalties in fiber-radio systems",* IEEE Electronics Letters, *Vol. 33, No. 1, 1997, pages 74-75*

[50] K. Washio, K. Inoue, S. Kishida, "*Efficient large-frequency-shifetd three-wave mixing in low dispersion wavelength region in single mode optical fibers"*, Electronic Letters, Vol. 16, No. 17, 1980 pages 650-680.

[51] C. Lin, W. A. Reed, A. D. Pearson, and H. T. Shang, "*Designing single-mode fibers for near-IR (1.1µm-1.7 µm) frequency generation bu phase matched*

four-wave mixing in the minimum chromatic dispersion region", Electronic Letters, Vol. 18, No. 2, 1982, pages 87-88.

[52] J. E. Sharping, M. Fiorentino, P. Kumar, and R. S. Windeler, "*Optical parametric oscillator based on four-wave mixing in microstructure fiber"*, Optic Letters, Vol.27, No.19, 2002, pages 1675-1677.

[53] J. Fulconis, O. Alibart, J. L. O'Brien, W. J. Wadsworth, and J. G. Rarity, "*Nonclassical interference and entanglement generation using a photonic crystal fiber pair photon source*", Physical Review Letters, Vol. 99, 2007, p. 120501.

[54] T. Ozeki, "*High-fidelity transmission of quantum polarization states through birefringent optical fibers*", Physical Review Letters, Vol.74, 2006, p. 024302.

[55] K.J. Williams and R.D. Esman, "Stimulated Brillouin Scattering for Improvement of Microwave Fibre-Optic Link Efficiency," Electronics Letters, Vol. 30, No. 23, Nov. 1994, pp. 1965-1966.

[56] S. Tonda-Goldstein et al, "*40 dB Dynamic Enhancement of Modulation Depth for Optically Carried Microwave Signals*," Electronics Letters, Vol. 39, No. 10, May 2003, pages 790-792.

[57] M.R. Phillips and M.D. Regan, "*Enhancement of Microwave Optical Link Gain by Self-Phase Modulation in a Fiber Interferometer*," IEEE Photonics Technology Letters, Vol. 20, No. 24, Dec. 2008, pages 2174-2176.

[58] W.S. Wall and M.A. Foster, "*Ultra-Wideband Gain in Microwave Photonic Links using Four-Wave Mixing*", Proc. of Conference on Lasers and Electro-Optics CLEO, 2012, CTu3A.4.

[59] J. Yao, "*Microwave photonics*," Journal of Lightwave Technologies, vol. 27, No. 3, February 2009, pp. 314-335.

[60] R. Minasian, E. Chan, and X. Yi, "*Microwave photonic signal processing*," Optics Express, Vol. 21, September 2013, pages 22918-22936.

[61] J. Capmany, and D. Novak, "*Microwave photonics combines two worlds*," Nature Photonics, vol.1, no.6, September 2007, pages 319-330.

[62] J. Yao, "*Microwave photonics: Photonic generation of microwave and millimeter-wave signals*", International Journal of Microwave and Optical Technology, Vol.5, No.1, January 2010, pages 16-21.

[63] L. Goldberg, H. F. Taylor, J. F. Wellner, and D. M. Bloom, "*Microwave signal generation with injection locked laser diodes",* Electronic letters, vol.19, No. 13, 1983, pages 491-493.

[64] J. Harrison, and A. Mooradian, "*Linewidth and offset frequency locking of external cavitiy GaAlAs lasers"*, IEEE Journal of quantum electronics, vol. 25, no. 1, 1989, pages 1252-1255

[65] R. T. Ramos, and A. J. Seeds, "*fast heterodyne optical phase-lock loop using double quantum well laser diodes"*, Electronic letters, vol. 28, no. 1, 1992, pages 82-83

[66] U. Gliese, T. N. Nielsen, M. Bruun, E. L. Christensen, K. E. Stubkjaer, S. Lindgren, and B. Broberg, "*A wideband heterodyne optical phase-locked loop for generation of 3-18 GHz microwave carriers"*, IEEE photonic technology letters, vol. 4, no. 8, 1992, pages 936-938.

[67] J. J. O'Reilly, P. M. Lane, R. Heideman, and R. Hofstetter, "*Optical generation of very narrow linewidth millimeter wave signals"*, Electronic letters, vol. 17, no. 2, 1999, pages 2309-2311.

[68] J. J. O'Reilly, and P. M. Lane, "*Fiber-supported optical generation and delivery of 60 GHz signals"*, Electronic letters, vol.30, no. 16, 1994, pages 1329-1330

[69] P. Shen, N. J. Gomez, P. A. Davies, W. P. Shillue, P. G. Huggard, and B. N. Ellison, "*High-purity millimeter-wave photonic local oscillator generation and delivery"*, Proceeding of international microwave photonics tropical meeting, 2003, pages 189-192.

[70] G. Qi, J. P. Yao, J. Seregelyi, C. Belisle, and S. Paquet, "*Generation and distribution of a wide-band continuously tunable mm-wave signal with an optical external modulation technique"*, IEEE transactions on microwave theory technologies, vol.53, no.10, 2005, pages 3090-3097

[71] G. Qi, J. P. Yao, J. Seregelyi, C. Belisle, and S. Paquet, "*Optical generation and distribution of continuously tunable millimeter-wave signals using an optical phase modulator"*, Journal of lightwave technology, vol. 23, no.9, 2005, pages 2687-2695

[72] G. P. Agrawal, *Nonlinear Fiber Optics*, 2nd Edition, Academic Press Inc., 1995, Chapter 10.

[73] N. Shibata, R.P. Braun, and R.G. Waarts, "*Phase-Mismatch Dependence of Efficiency of Wave Generation Trough Four-Wave Mixing in a Single- Mode Optical Fiber"*, IEEE Journal of Quantum Electronics, Vol. 23, No. 7, July 1987, pages 1205-1210

[74] Ivan Kaminow and Thomas Koch, "Optical Fiber Telecommunications IIIA", Academic press, 2012

[75] T.V. Higgins, "*Nonlinear Optical Effects are Revolutionizing Electro-optics*", Laser Focus World, August 1994.

[76] A. H. Abdolhamid, and D. A. Johns, "*A comparison of CAP/QAM architectures*", IEEE International symposium on Circuits and Systems, June 1998, p. IV-316

[77] J. Kurzweil, "*An Introduction to Digital Communications*", 1st edition, John Wiley & Sons Inc, 1999

[78] A. J. Cooper, "'*Fibre/Radio' for the provision of cordless/mobile telephony services in the access network"*, Electronic Letters, Vol. 26, No. 24, 2010, pages 2054-2056

[79] M. J. Crisp, S. Li, A. Wonfor, R. V. Penty, and I. H. White, "*Demonstration of radio over fibre distributed antenna network for combined in-building WLAN and 3G coverage"*, Optical Fiber Communication conference (OFC), paper JThA81, 2007.

[80] H. Al-Raweshidy and S. Komaki, "*Radio over Fiber Technologies for Mobile Communications Network*s", Artech House, 2002.

[81] A. Attar, H. Li, and V. C. Leung, "*Applications of fiber-connected distributed antenna systems in broadband wireless access"*, IEEE International conference on Computing, Networking and Communications (ICNC), 2012, pages 623-627

[82] A. Chowdhury, H. C. Chien, S. H. Fan, J. Yu, and G. K. Chang, "*Multi-band transport technologies for in-building host-neutral wireless over fiber access systems"*, Journal of lightwave technology, vol. 28, No. 16, 2010, pages 2406-2415.

[83] M. P. Thakur, T. Quinlan, S. B. Ahmad Anas, D. K. Hunter, S. D. Walker, D. W. Smith, and D. Moodie, "*Triple-format, UWB-Wi-Fi-WiMax, Radio-over-fiber co-existence demonstration featuring low-cost 1308/1564 nm VCSELs and a reflective Electro-absorption transceiver"*, IEEE Conference on Optical Fiber Communications OFC, 2009, pages 1-3

[84] J. Guillory, S. Meyer, I. Siaud, A. M. Ulmer-Moll, B. Charbonnier, A. Pizzinat, and C. Algani, "*Future multigigabit wireless systems in the Home-Area network"*, IEEE vehicular technology magazine, 2010, pages 30-38

[85] R. Llorente, T. Alves, M. Morant, M. Beltran, J. Perez, A. Cartaxo, and J. Marti, "*Ultra-wideband radio signals distribution in FTTH networks"*, IEEE Photonics technologies letters, Vol. 20, No. 11, 2008, pages 945-947

[86] J. Guillory, E. Tanguy, A. Pizzinat, B. Charbonnier, S. Meyer, H. W. Li, C. Algani, "*Radio over fiber tunnel for 60 GHz wireless Home Network"*, Optical Fiber Communication Conference (OFC), 2011, paper OWT6

[87] J. Guillory, Y. Ait Yahia, A. Pizzinat, B. Charbonnier, C. Algani, M. D. Rosales, and J. L. Polleux, "*Comparison between two 60GHz multipoint RoF architectures for the Home Area Network"*, IEEE 17th European conference on Netoworks and Optical Communications (NOC), 2012, pages 1-5

[88] J. Guillory, E. Tanguy, A. Pizzinat, B. Charbonnier, S. Meyer, C. Algani, and H. Li, "*A 60 GHz wireless home area network with radio over fiber repeaters"*, Journal of lightwave and technology, vol. 29, no. 16, 2011, pages 2482-2488

[89] E. I. Ackerman, and C. H. Cox, "*RF fiber optic link performance"*, IEEE microwave, 2001, pages 50-58

[90] J. Guillory, S. Meyer, I. Siaud, A. M. Ulmer-Moll, B. Charbonnier, A. Pizzinat, and C. Algani, "*Radio-over-fiber architectures for the future home area networks"*, 2012

[91] G. P. Agrawal, "Applications of nonlinear fiber optics", Academic press, 2001.

[92] H. Fukano, T. Yamanaka, M. Tamura, and Y. Kondo, "*Very-Low-Driving-Voltage Electroabsorption Modulators Operating at 40 Gb/s"*, Journal of lightwave technology, vol. 24, no. 5, 2006, pages 2219 – 2224.

[93] S. A.de S. Melo, Arismar Cerqueira S. Jr., A. R. do Nascimento Jr., L. H. H. de Carvalho, R. da Silva, and J. C. R. F. de Oliveira, "*Optical Frequency Comb*

based on Multiple Four-Wave Mixing and Erbium Doped Fiber", Revista Telecomunicações, v. 15, p. 43, 2013.

[94] Arismar Cerqueira S. Jr**.** . "*Beyond efficient generation of multiple four-wave mixing products*", Workshop on Specialty Optical Fibers, 2008.

[95] Arismar Cerqueira S. Jr., J. D. Marconi, A. A. Rieznik, H. E. Hernandez Figueroa, H. L. Fragnito., J. C. Knight, "*Multiple four-wave mixing in ultra-flattened dispersion photonic crystal fibers*", Optical Fiber Communication Conference and Exposition (OFC) and The National Fiber Optic Engineers Conference (NFOEC), 2008, v. OtuB2.

[96] R. M. Borges, Arismar Cerqueira S. Jr., "*Convergent and reconfigurable optical-wireless network for LTE and Wi-Fi offloading applications*," IEEE Latin-American Conference on Communications LATINCOM, 2014.

[97] K. Kikuchi, and C. Lorattanasane, "*Design of Highly efficient four-wave mixing devices using optical fibers"*, IEEE Photonics technology letters, vol. 6, no. 8, pages 992-994.

[98] Y. M. Fang, Z. Qin, H. Wang, L. Cao, J. Xin, J. Feng, and J. Jing, "*Quantum optical devices based on four-wave mixing in hot rubidium vapor"*, Science China Physics, Mechanics and Astronomy, 2015, pages 1-8

[99] E. Raimundo-Neto, J. R. G. Rosa, M. A. F. Casaroli, I. F. da Costa, A. M. Alberti, Arismar Cerqueira S. Jr. "*Implementation of an Optical-Wireless Network with Spectrum Sensing and Dynamic Resource Allocation Using Optically Controlled Reconfigurable Antennas*", International Journal of antennas and Propagation, 2014, pages 1-11.

[100] I. Stavros, "*Microwave photonics: devices and applications"*. Vol. 3. John Wiley & Sons, 2009.

[101] I. G. Insua, "*Optical generation of mm-wave signals for use in broadband radio over fiber systems"*. Jörg Vogt Verla, 2010.